ISSN 2074-272X

науково-практичний журнал 2019/5

Електротехніка і Електромеханіка

Electrical Engineering & Electromechanics

Електротехніка. Визначні події. Славетні імена
Електричні машини та апарати
Електротехнічні комплекси та системи. Силова електроніка
Теоретична електротехніка та електрофізика
Техніка сильних електричних та магнітних полів. Кабельна техніка
Електричний транспорт
Електричні станції, мережі і системи

З 2015 р. журнал індексується у міжнародній наукометричній базі Web of Science Core Collection: Emerging Sources Citation Index

«ELECTRICAL ENGINEERING & ELECTROMECHANICS»

SCIENTIFIC & PRACTICAL JOURNAL

Journal was founded in 2002

Founders:

National Technical University «Kharkiv Polytechnic Institute» (Kharkiv, Ukraine)

State Institution «Institute of Technical Problems of Magnetism of the NAS of Ukraine» (Kharkiv, Ukraine)

ISSUE 5 / 2019

TABLE OF CONTENTS

Editorial office address: Dept. of Electrical Apparatus, NTU «KhPI», Kyrpychova Str., 2, Kharkiv, 61002, Ukraine
phones: +380 57 7076281, +380 67 3594696, **e-mail:** a.m.grechko@gmail.com (**Grechko O.M.)**

ISSN (print) 2074-272X
ISSN (online) 2309-3404

Printed 18 October 2019. Format 60 x 90 ⅛. Paper – offset. Laser printing. Edition 200 copies.
Printed by Printing house «Madrid Ltd» (11, Maksymilianivska Str., Kharkiv, 61024, Ukraine)

UDC 629.7:930.1 **doi: 10.20998/2074-272X.2019.5.01**

M.I. Baranov

AN ANTHOLOGY OF THE DISTINGUISHED ACHIEVEMENTS IN SCIENCE AND TECHNIQUE. PART 51: ROCKET-SPACE TECHNOLOGY DESIGNER SERGEY KOROLEV AND HIS ACCOMPLISHMENTS IN MISSILE DESIGN

Purpose. ***Preparation of short scientifically-historical essay about one of founders of domestic rocket production and practical cosmonautics, distinguished Soviet designer of space-rocket technology Sergey Pavlovich Korolev.*** ***Methodology.*** ***Known scientific methods of collection, analysis and analytical treatment of scientific and technical information, touching becoming and development in the world of space-rocket technique and resulted in scientific monographs, journals and internet-reports.*** ***Results.*** ***A short scientifically-historical essay is presented about the distinguished Soviet designer of space-rocket technique S.P. Korolev, becoming one of founders of domestic rocket production and practical cosmonautics. The important deposit of former German people, creating rockets, workings in the USSR after completion of the World War II is marked, in development of the first Soviet ballistic rockets. Basic scientific and technical achievements of talented and purposeful scientist and practical worker, becoming in 1950 a Chief Designer of the Special Design Bureau No. 1 (SDB-1), S.P. Korolev in area of creation of Soviet strategic rocket weapon (rocket-nuclear «shield») and modern space-rocket technique for mastering of near and distant space tellurians. It is pointed out that under the direction of the Chief Designer of SDB-1 S.P. Korolev in the USSR was developed and accepted on the armament of Soviet Army consisting of two stages intercontinental ballistic rocket (ICBR) of type P-7 (1956, military index 8K71, by power of thermonuclear war-head in 5 Mt and distance of its flight in 8 thousands km) with the liquid rocket engines (LRE) of type РД-107 and РД-108 of design of distinguished Soviet designer in area of rocket engines V.P. Glushko. It is indicated that the Chief Designer S.P. Korolev is the «father» of domestic space-rocket technique, providing by powerful launch vehicles, created in the USSR on the basis of ICBR with LRE of РД-7 type (military index 8K71), start of first in the world of Soviet space satellite (on Octobers, 4, 1957) and start on the circumterrestrial space orbit of the first in history humanity of Soviet cosmonaut Yu.A. Gagarin (on April, 12, 1961).*** ***Originality.*** ***Certain systematization is executed of known from mass medias of scientific and technical materials, touching becoming and development in the USSR of rocket production, at the sources of which the talented scientist-practical worker and distinguished Soviet designer of space-rocket technique S.P. Korolev.*** ***Practical value.*** ***Scientific popularization and deepening for the students of higher school, engineer and technical and scientific workers of physical and technical knowledge in area of history of becoming and development in the former USSR of modern rocket production, extending their scientific and technical range of interests and further development of scientific and technical progress in society.*** References 25, figures 10.

Key words: **space-rocket technology, distinguished Soviet designer of space-rocket technology Sergey Korolev, achievements in modern rocket production, cosmonautics, scientifically-historical essay.**

Наведено короткий науково-історичний нарис про видатного радянського конструктора ракетно-космічної техніки Сергія Павловича Корольова, що став одним з основоположників вітчизняного ракетобудування і практичної космонавтики. Відмічений важливий внесок колишніх німецьких ракетників, що працювали в СРСР після закінчення Другої світової війни, в розробку перших радянських балістичних ракет. Описані основні науково-технічні досягнення С.П. Корольова в галузі створення радянської стратегічної ракетної зброї і сучасної ракетно-космічної техніки для освоєння землянами ближнього і дальнього космічного простору. Показано, що головний конструктор С.П. Корольов є «батьком» вітчизняної ракетно-космічної техніки, що забезпечила запуск першого в світі радянського штучного супутника Землі (1957 р.) і перебування на навколоземній космічній орбіті першого в історії людства радянського космонавта Ю.О. Гагаріна (1961 р.). Бібл. 25, рис. 10.

Ключові слова: **ракетно-космічна техніка, видатний радянський конструктор ракетно-космічної техніки Сергій Корольов, досягнення у сучасному ракетобудуванні, космонавтика, науково-історичний нарис.**

Приведен краткий научно-исторический очерк о выдающемся советском конструкторе ракетно-космической техники Сергее Павловиче Королеве, ставшем одним из основоположников отечественного ракетостроения и практической космонавтики. Отмечен важный вклад бывших немецких ракетчиков, работавших в СССР после окончания Второй мировой войны, в разработку первых советских баллистических ракет. Описаны основные научно-технические достижения С.П. Королева в области создания советского стратегического ракетного оружия и современной ракетно-космической техники для освоения землянами ближнего и дальнего космического пространства. Показано, что главный конструктор С.П. Королев является «отцом» отечественной ракетно-космической техники, обеспечившей запуск первого в мире советского искусственного спутника Земли (1957 г.) и пребывание на околоземной космической орбите первого в истории человечества советского космонавта Ю.А. Гагарина (1961 г.). Библ. 25, рис. 10.

Ключевые слова: **ракетно-космическая техника, выдающийся советский конструктор ракетно-космической техники Сергей Королев, достижения в современном ракетостроении, космонавтика, научно-исторический очерк.**

Introduction. When you get acquainted with biographies of prominent scientists and engineers of the world from various fields of knowledge, you often «catch» yourself thinking that what an often difficult fate these people had for the great deeds, the mysterious cosmos of people for us. By their years of suffering and conscious goals, they had to «get through» incredible life difficulties, including betrayal of cruel and selfish colleagues, far-fetched accusations of wrecking in the service, arrests, court sentences and imprisonment in harsh conditions in prisons and camps. This is especially true of such people who were the best representatives of

the true intelligentsia, whose life fell on the period of revolutions and rampant political dogmas and repressions in their homeland. Often, the objective laws of the development of human society, and sometimes fateful cases, led these spiritually strong people from life's «dead ends» to the main paths for the development of scientific and technological progress in it. Such stoic people include the outstanding Soviet designer of rocket and space technology, twice Hero of Labor (1956; 1961), Academician of the Academy of Sciences of the USSR (since 1958) Sergey Pavlovich Korolev [1] (Fig. 1), to whom this essay is dedicated.

The goal of the paper is preparation of a brief scientific and historical essay about one of the founders of domestic rocket science and practical cosmonautics, an outstanding Soviet designer of rocket and space technology S.P. Korolev.

1. The beginning of the life and career of S.P. Korolev. He was born on January 12, 1907 in the city of Zhitomir in the family of Pavel Yakovlevich Korolev, a teacher of Russian literature [1]. His mother, Maria Nikolayevna Moskalenko, soon broke up with his father (because of which Sergey was brought up from his mother's parents in the city of Nizhyn, now Chernihiv Oblast, from two to ten years old) and in 1916 moved to Odessa to the place of work of the new husband – mechanical engineer Grigory Mikhailovich Balanin (Sergey's stepfather). In September 1917, he begins to study in the first class of the 3rd Odessa Men's Gymnasium [1]. The turbulent events of the civil war made adjustments to his studies.

Fig. 1. Outstanding Soviet designer of Space-rocket technology, twice Hero of Labor, Lenin Prize Laureate, Academician of the Academy of Sciences of the USSR Sergey Pavlovich Korolev (12.01.1907-14.01.1966) [1]

Young Sergey had to take a seven-year school program at his parents' home. Further, in the period 1922-1924 his studies at the construction school No. 1 of Odessa followed, after which he received secondary education and a mason specialty [2]. At this time, he «fell ill» with aviation. In 1924, Sergey entered the Kyiv Polytechnic Institute in the field of aviation technology. Here he became a glider athlete. In 1926, he transferred to the N.E. Bauman Moscow Higher Technical School (MHTS) at the Aeromechanical Faculty. In February 1930, S.P. Korolev successfully defended his graduation project at MHTS related to the design of a light aircraft of the CK-4 type (the diploma project supervisor is a future outstanding Soviet aircraft designer, three times Hero of Labor, Academician of the Academy of Sciences the USSR A.N. Tupolev [3]) [4]. So under the «wing» of A.N. Tupolev he became an aeromechanical engineer. As it turned out in the future, this person will fulfill in his life an even larger and actually fateful role – he will «pull» him into the design world in the winter of 1939 to develop new military aircrafts (even of prison character, but with clean bed and enhanced nutrition) from the prison camp, which was murderous in harsh conditions at the distant gold mine «Maldyak» of the Soviet Kolyma and thereby actually will save him from the cold and starvation death of a prisoner [4, 5].

2. The main events of the pre-war and military periods of the work of S.P. Korolev in rocket and aviation technology (1930-1945). In September 1931, S.P. Korolev and talented rocket engine enthusiast F.A. Zander achieved with the help of the Soviet Osoaviahim the creation in Moscow of a new public organization – the Jet Propulsion Research Group (JPRG) [6]. In August 1933, the JPRG successfully launched the first in the USSR small ballistic missile with a liquid rocket engine (LRE) [6]. In the same 1933, on the basis of the Moscow JPRG and the Leningrad Gas-Dynamic Laboratory, the Reactive Scientific Research Institute (RSRI) was created under the leadership of I.T. Kleimenov, whose deputy became S.P. Korolev (Fig. 2) [6].

Fig. 2. Young S.P. Korolev while working at the RSRI (1933, Moscow) [6]

In the years 1934-1935, he was the Head of the Departments of cruise missiles and rocket aircrafts at the RSRI. By 1938, projects of liquid cruise missiles and long-range ballistic missiles, as well as aviation missiles for firing at air (ground) targets and anti-aircraft solid-fuel missiles were developed in these Departments of the RSRI. We indicate that for the period 1937-1938 there were arrests of prominent specialists of the RSRI, which since 1937 became known as SRI-3 [7, 8]: I.T. Kleimenov, G.E. Langemak (the Deputy Director of the Institute for science, the main co-author of the development of a new type of weapon in the world – the Soviet «Katyusha» multiple rocket launcher (MRL) [8]), S.P. Korolev, V.P. Glushko, and other. At present, it is

believed that these arrests, which caused great harm to domestic science and rocketry, were directly related to the Head of the Rocket Engine Development Department (since 1936) A.G. Kostikov (30.10.1899 – 05.12.1950), who became on September 15, 1938 (after the arrest of these employees of the SRI-3) the Chief Engineer of the leading Institute in the USSR, engaged in the development and testing of missile shells, and installations for launching them from the ground and from airplanes [7-9]. It is known that A.G. Kostikov on June 20, 1938 headed the expert commission of SRI-3, which gave an opinion to the bodies of the People's Commissariat of Internal Affairs of the USSR on the harmful character of the activities of engineers V.P. Glushko (in the future, an outstanding Soviet specialist in the field of rocket engine technology, twice Hero of Labor, Academician of the Academy of Sciences of the USSR [10]) and S.P. Korolev [7]. Note that A.G. Kostikov, taking advantage of his official position, actually appropriated co-authorship (to mask his thieves' plans, he filed it together with the Institute's designer I.I. Gvay, and the Deputy Head of the Main Artillery Directorate of the Red Army of the country V.V. Aborenkov) of the development at the SRI-3 of the «Katyusha» guards rocket mortar (БМ-13 combat vehicle), which they presented in the USSR Copyright Certificate No. 3338 of February 19, 1940 for the invention «*Mechanized installation for firing rocket shells of various calibers*» [7]. It is also interesting that on June 17, 1941 (literally on the eve of the beginning of World War II in the USSR [3]) A.G. Kostikov demonstrated the firepower of the «Katyusha» MRL based on the domestic three-axle ЗИС-6 car to the leadership of the CPSU and the USSR Government [7, 8]. The success of the «Katyusha» demonstration was overwhelming! Immediately, on June 21, 1941, personally I.V. Stalin, as the Head of the Government of the USSR, made an urgent decision to deploy mass production of M-13 rocket missiles and БМ-13 launchers for them developed by the SRI-3, and also to begin the formation of the corresponding military units in the Red Army [7]. Despite the terrible military events for the USSR at the beginning of the war, on July 28, 1941, two Decrees of the Supreme Soviet of the USSR on awarding «*For outstanding services in the invention and design of one of the types of weapons that enhance the combat power of the Red Army*» were issued: Chief Engineer of SRI-3 A.G. Kostikov was awarded the title of Hero of Labor by the first of the Decrees) and 12 employees of this Institute were awarded by orders by the second Decree [7]. In addition, the «false father» of the legendary «Katyusha» was soon awarded the military rank of Major General of the Engineering and Aviation Service. Career «starfall» for A.G. Kostikov continued further: from the beginning of 1942 to February 18, 1944, having a degree of Candidate of Technical Sciences, was the Director of the SRI-3, and on September 29, 1943 he was elected a Corresponding Member of the Academy of Sciences of the USSR (Department of Mechanics). But, as they say among our people, «God marks the witchcraft». For «deceiving the Soviet Government and disrupting its important task» A.G. Kostikov was dismissed on February 18, 1944 and arrested on March 15, 1944 (he was in prison till February 28, 1945) [7]. Suspicions of his espionage and betrayal were not confirmed. After his release, he was restored to his rights and from August 1, 1945 until the end of his life he worked as the Head of the Bureau of the SRI-24, engaged in the development of missile shells [7, 8].

The true role of the employees of the RSRI (SRI-3) illegally repressed in the 1930s in the creation of the domestic jet weapon of the «Katyusha» MRL (БМ-13 combat vehicle) was nevertheless restored [7]: by Decree of the President of the USSR of June 21, 1991 I.T. Kleimenov, G.E. Langemak, V.N. Luzhin, B.S. Petropavlovsky, B.M. Slonimer and N.I. Tikhomirov were awarded the high title of Hero of Labor (posthumous), and their names were rehabilitated.

After such quite large in volume, but important for completeness of the representation of the history of the creation of rocketry in the USSR by the example of the legendary» Katyusha» (БМ-13 combat rocket launcher, which did so much for our Victory during the war) retreat, we return to the pre-war events directly related with the specified SRI-3 and the person of S.P. Korolev. On June 27, 1938, on the basis of the above conclusion of the SRI-3 expert commission headed by the notorious A.G. Kostikov, he was arrested as a member of the Trotskyist counter-revolutionary organization [5]. Then, on September 27, 1938, he was sentenced to 10 years of imprisonment in labor camps by the Military College of the Supreme Court of the USSR. He spent a year in Butyrka prison (Moscow), where he was brutally tortured and beaten during interrogations [11]. In April 1939, S.P. Korolev found himself in the distant Kolyma in a prison camp mining gold at the Maldyak mine. In the first year of his camp in Kolyma, he miraculously survived scurvy and half-starved existence. From the «paws» of death, former Director of the Moscow Aviation Plant No. 156 M.A. Usachev (by the way, a master of sports in boxing, who had a strong physique), who personally knew S.P. Korolev and undeservedly sentenced to 15 years for the death on December 15, 1938 of the legendary pilot V.P. Chkalov, the new И-180 fighter designed by N.N. Polikarpov which was being prepared for flight tests just at the said plant, saved him [12]. M.A. Usachev, as a «guardian angel», ended up in the camp hut of the Maldyak mine at a critical moment for the life of S.P. Korolev near him. It was he who provided him with the urgently needed camp medical assistance and an additional food ration, which put the inmate-goner S.P. Korolev «on his feet» [11].

In December 1939, the prisoner S.P. Korolev as a military specialist, included in the list of 100 people needed by the aircraft designer A.N. Tupolev, who was arrested in 1938 to work in prison on a new Soviet bomber, and was sent from the Kolyma mine «Maldyak» to Moscow [1, 4]. An interesting fact is that, upon the arrival of the stage in Magadan (the capital of the Kolyma region), he was late for the «Indigirka» steamer, bound to Vladivostok and sunk (as it became known later) during a storm in the Okhotsk Sea [4]. Well, it's a sign of fate for our hero! Apparently, he was needed on Earth to do something important in the near future. Upon arrival on

March 2, 1940 in Moscow, a camp prisoner S.P. Korolev by a special meeting was convicted a second time and sentenced to eight years in prison [11]. After which he was transferred to a new place of detention – Central Design Bureau No. 29 (CDB-29) of the People's Commissariat of Internal Affairs of the USSR, where in the conditions of the prison «sharashka» under the guidance of aircraft designer A.N. Tupolev he took an active part in the creation and production of one of the best during the period of the Second World War front-line bomber of the Ty-2 type [3] and at the same time proactively developed projects of guided aerial torpedo and a new version of the missile interceptor [4, 6]. The latter, probably, was the reason for his transfer in 1942 to another prison-type design bureau – Special Design Bureau No. 16 (SDB-16) at the Kazan Aircraft Plant No. 16, where work was carried out on new types of rocket engines with a view to their use in aviation [1]. In this institution, he, with his characteristic enthusiasm, devotes himself to the idea of using jet engines in practice to improve the aircrafts: reducing the take-off run of the aircraft during take-off and increasing the dynamic characteristics of the aircraft during air combat. In early 1943, S.P. Korolev in the framework of SDB-16 was appointed the Chief designer of the group of rocket installations used on aircraft [1]. According to the results of work on the development of an aircraft rocket installation, in July 1944 he was prematurely released from prison with release a criminal record, but without rehabilitation. In 1945, S.P. Korolev S.P. awarded for valiant work by the Order of the Badge of Honor [5]. Until the end of the Second World War, he actively worked as a civilian in SDB-16 at the Kazan Aircraft Plant.

3. On the contribution of former German rocket experts to the creation of the first Soviet ballistic missiles. For many years, the work of German rocket experts in the USSR, invited, as we say, by the voluntary-forced order by the security services of the victorious country of World War II to transfer their experience in creating rocket technology to Soviet specialists, was hushed up. As for the United States, the Americans never hid the fact that their initial successes in creating ballistic missiles and in space missions included a «German rocket foundation» which included 765 leading German rocket engineers who had been working for the United States Army from September 1945 [10, 13]. As we know, in September 1944, Germany created the first-ever combat ballistic single-stage medium-range missile with a liquid-propellant rocket engine of the V-2 type (the Chief Designer of the rocket is the outstanding German designer of rocket technology Wernher von Braun [10]), capable of delivering by air at speed of up to 1.5 km/s ordinary chemical explosives (for example, trinitrotoluene) weighing up to 1 ton at distance of up to 300 km [10, 14]. In September 1945, S.P. Korolev was sent to Germany, where he was acquainted with German captured missile technology as part of the Soviet Technical Commission for almost a year [13]. It should be noted that due to the restoration of one of the underground plants for the production of the V-2 rocket near the city of Nordhausen [10] in post-war Germany, which ended up in the Soviet zone of occupation, 10 sets of this rocket were sent to the USSR [13]. A great contribution to this work was made by the long-lived missile engineer B.E. Chertok (1912 - 2011), who stood at the «source» of rocket science in the USSR and later became Deputy to the Chief Designer of rocket and space technology S.P. Korolev and who left behind invaluable memoirs of the development of rocketry in the USSR [14-17]. The wise B.E. Chertok, while still in Germany as part of the mentioned Technical Commission, managed to attract the talented assistant and ally of Wernher von Braun Helmut Gröttrup (1916 - 1981) to work in the field of the formation of Soviet rocket science. In turn, H. Gröttrup, thanks to his vast knowledge, talent as a leader, decency, wide views on technical problems and a benevolent character, managed to interest many German rocket experts in work on rocketry in the interests of the USSR. As a result, in the summer of 1946, about 500 German experts, headed by H. Gröttrup, were sent to the USSR to raise the Soviet missile industry [13]. Some of them (up to 150 people) were placed in complete isolation from people on Gorodomlya Island in the middle of the picturesque Seliger Lake (Tver Region) [13].

In the USSR, on May 16, 1946, to manage rocket development, on the basis of the Artillery Plant No. 88, the lead SRI-88 (Podlipki station, Moscow Region) was created under the guidance of a major Soviet military production organizer, Major General L.R. Honor [18, 19]. In the structure of the Soviet SRI-88, which had 25 Departments, the German rocket experts have the modest role of Branch No. 1. It should be noted that those who worked in the USSR in excellent living conditions with high salaries became «Soviet» German rocket engineers, ahead of the number of achievements of «American» German experts (Wernher von Braun group [10]), in the projects of ballistic missiles developed they became world pioneers. It was they who first proposed for these missiles [13]: detachable warheads, bearing tanks, intermediate bottoms, hot pressurization of fuel tanks, flat nozzle heads of rocket engines, rocket thrust vector control using engines, etc. They included rocket scientists with world-famous [13]: Hoh (control systems), Magnus (gyroscopes), Umpfenbah, Albring, Müller and Rudolf (Rudolf). They, as part of the creation of the USSR missile «shield», completed ballistic missile projects for 600, 800, 2500 and 3000 km. They also proposed a project for an intercontinental ballistic missile (an analogue of the future famous Soviet strategic missile P-7) [13]. In 1953, the «exodus» of Russified German rocket experts from the USSR began. As the saying goes, «the Moor has done his job, the Moor may retire». As befits a leader, H. Gröttrup was the last to leave the USSR. Famous Soviet rocket engineer B.E. Chertok in his memoirs notes that at the station at farewell of this German rocket expert «*he couldn't look H. Gröttrup in the eyes with shame*» [13, 14].

4. Key achievements of S.P. Korolev in space and rocket technology in the post-war period of his work (1946-1966). To begin with, on May 13, 1946, a secret Resolution of the Council of Ministers of the USSR No. 1017-419 cc «Issues of Jet Arms» (now declassified) was issued, aimed at creating a new military industry in the

USSR for the development and production of strategic missiles [6]. In accordance with this directive document in August 1946 S.P. Korolev was appointed Head of Department No. 3 of the Special Design Bureau (SDB) at the SRI-88 for the development of medium and long-range ballistic missiles. The initial task for S.P. Korolev, set for SRI-88 personally by I.V. Stalin, was the development and creation of a domestic analogue of the German ballistic missile V-2, called «Product No. 1» (P-1 rocket) [6]. In October 1948, S.P. Korolev (Fig. 3) begins flight design tests of the Soviet single-stage ballistic missile P-1 (analogue of V-2) and in 1950 it was successfully put into service in the Soviet Army [20].

Fig. 3. Soviet designer of rocket technology S.P. Korolev in field tests of a ballistic missile created under his command (1948, Kapustin Yar training ground) [4]

This missile with a range of 300 km in comparison with the German V-2 missile was significantly more reliable in storage and operation [20]. Further, under the leadership of S.P. Korolev a ballistic missile P-2 was created with flight range of 600 km [20]. The P-2 rocket with a liquid-propellant rocket engine had a carrying fuel tank, a more convenient layout for operation in military units and a warhead detaching in flight. The new autonomous control system for the P-2 missile had twice the accuracy of firing at targets as compared to the P-1 missile [20].

By the beginning of 1950, the framework of Department No. 3 at the SRI-88 had become tight for the rapidly growing team of rocket designers led by S.P. Korolev. On April 30, 1950, an order was issued by the Minister of Arms of the USSR, Colonel General D.F. Ustinov on the transformation of the SDB of the SRI-88 into the Special Design Bureau No. 1 (SDB-1) at the SRI-88 for the development of ballistic long-range missiles with LRE, which since 1956 has become an independent enterprise, and S.P. Korolev was appointed its Head and Chief Designer (Kaliningrad, Moscow region, now the city of Korolev) [6]. Then, in 1953, the implementation of the P-3A ballistic missile project of an unstabilizing scheme with a flight range of 1200 km followed [6]. During 1954, SDB-1 of S.P. Korolev on the basis of this missile completed work on the development of the P-5M missile with a range of up to 1200 km carrying a nuclear warhead [6]. Successful flight tests at the Semipalatinsk test site of the USSR (South-East Kazakhstan) of this missile gave the foundation of the Ministry of Defense of the USSR to take it into service in 1956. This was the first domestic strategic missile, which became the basis of the nuclear missile «shield» of our country [5]. Based on the P-11 rocket S.P. Korolev in 1957 developed and put into service in the Soviet Army a strategic ballistic missile P-11M with a nuclear warhead, transported in the refueling form on a tank chassis [20]. After a certain modification of this missile to the marine conditions of combat alert of Soviet atomic submarines in SDB-1 of S.P. Korolev a sea-based ballistic missile P-11ФМ was created [20]. This missile was equipped with a new control and aiming system, which makes it possible to fire when the sea is quite rough from the surface position of the atomic submarine. To finalize this combat vehicle, the documentation for it was transferred to SDB-385 (Miass, Chelyabinsk Region). Together with the P-11ФМ missile, the talented designer V.P. Makeev, who later became its Chief Designer [20, 21], was sent to this now world-famous Russian Center for the development of sea-based ballistic missiles. In this regard, we can say that S.P. Korolev laid the foundations for the establishment in the Urals of this unique in the USSR rocket science center. Soviet liquid ballistic missiles lost a number of parameters to American solid-fuel rockets. Therefore, in SDB-1 under the leadership of S.P. Korolev experimental solid-fuel ballistic missiles PT-1 and PT-2 were developed [5]. Note that modern missile systems are mainly equipped with solid-fuel intercontinental ballistic missiles (ICBMs), which are based on the PT-2 ICBM, created by the Chief Designer of SDB-1 S.P. Korolev [5, 6].

The main direction in the scientific and technical activities of the Academician of the Academy of Sciences of the USSR S.P. Korolev in the field of rocketry was the development and creation of ICBMs operating on LRE [1]. A special place among the achievements of SDB-1 and its Chief Designer S.P. Korolev takes the development and creation of a two-stage ICBM type P-7 (8K71) with LRE. In 1956, this strategic ICBM was developed. It had a detachable warhead (5 Mt warhead) weighing up to 5.5 tons and a flight range of 8,000 km (Fig. 4) [1, 20].

This rocket was successfully tested in 1957 at the specially built missile training ground No. 5 (Southwest Kazakhstan), better known to the general reader as the southern Baikonur Cosmodrome (near city of Leninsk) [1, 15]. We also point out that for combat duty of these ICBMs in the USSR, a launch station was built (the «Angara» facility) in the area of the village Plesetsk (Arkhangelsk region), currently known as the northern Plesetsk Cosmodrome (Russia) [1, 16]. Note that the modification of this ICBM called P-7A (8K74) had a 3 Mt warhead with a mass of 3 tons and a flight range of 12,000 km [1, 22]. The P-7A ICBM was in service with the Strategic Missile Forces of the USSR in the period 1960-1968 [1, 15]. Later on, SDB-1 developed a more advanced design of a two-stage ICBM with a LRE of the P-9 type, launched from an open starting position (Chief Designer – S.P. Korolev) [20]. In this rocket, supercooled liquid oxygen began to be used as an oxidizing agent. In 1962, the Strategic Missile Forces of the USSR started service of a modification of this P-9A missile launched from a closed launch position (a mine version of ICBM)

[20]. On this, SDB-1, led by S.P. Korolev, ceased to engage in combat missile-related topics and concentrated its design forces and creative capabilities on the development and creation of launch vehicles and systems designed for the peaceful development of near and deep space.

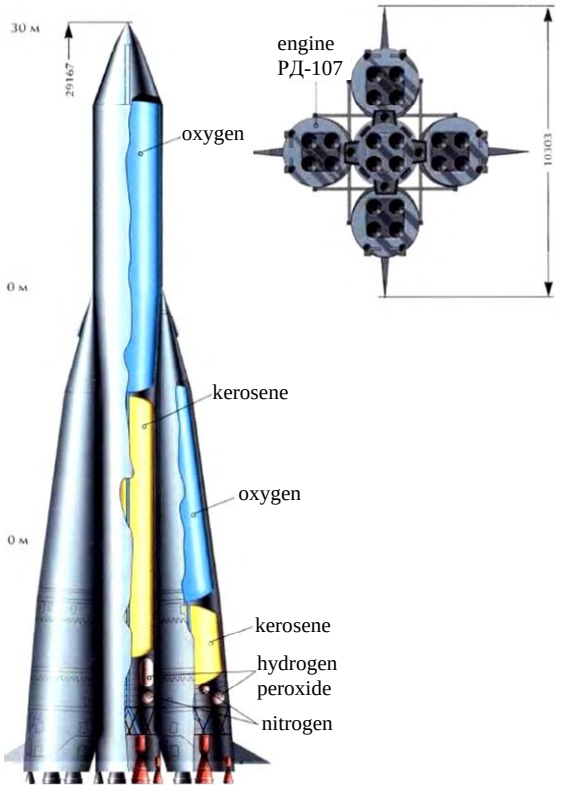

Fig. 4. Soviet ICBM P-7 and its main elements [22]

Figures 5, 6 show the general views of liquid propellant rocket engines of the types РД-107 and РД 108, respectively (Chief Designer – Academician of the Academy of Sciences of the USSR V.P. Glushko [23]), installed in an amount of 4 at the first stage (side blocks, see Fig. 4) and in the amount of 1 (in the center of ICBM) at the second stage of the Soviet P-7 ICBM (with index 8K71) [20, 22].

Note that the P-7 rocket was made with parallel division of stages. It consisted of one central and four side rocket blocks. At its start, propulsion systems – LREs of all five rocket blocks were launched simultaneously. Such a scheme was characteristic of the first ICBMs of the USSR. To control the movement of the P-7 ICBM (launch weight 280 tons), its design used for the first time not gas rudders, but rudder rocket engines (RREs). On each of the four lateral blocks of P-7, two single-chamber RREs were installed, and on a single central block – four similar RREs (see Fig. 5, 6) [20, 22].

In 1955, long before the development and flight tests of the ICBM P-7, Corresponding Member of the Academy of Sciences of the USSR (since 1953) S.P. Korolev, Academician of the Academy of Sciences of the USSR M.V. Keldysh and Doctor of Technical Sciences M.K. Tikhonravov «came out» with an offer to the Council of Ministers of the USSR about the launch into space using ICBM of the Soviet artificial Earth satellite (AES) [20].

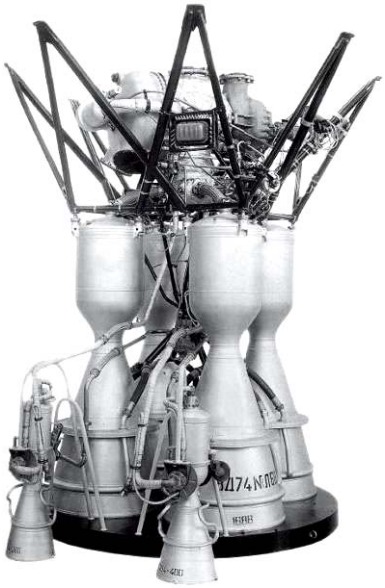

Fig. 5. Four-chamber LRE of РД-107 type used at the first stage of the Soviet P-7 (8K71) ICBM [22]

Fig. 6. Four-chamber LRE of РД-108 type used at the second stage of the Soviet P-7 (8K71) ICBM [22]

The Soviet Government, headed by N.S. Khrushchev, supported this proposal, which promised the USSR, if successful, large political dividends. After the creation in 1956 of a reliable nuclear missile «shield» in the USSR (a thermonuclear bomb of the РДС-6с type [24] and a means of delivering it anywhere in the world in the form of P-7 ICBM), capable of teaching wise American wisdom «hawks», it was possible to do space for a demonstration of Soviet missile power. To implement these important peaceful plans, at the SDB-1 in the period 1957-1966 under the leadership of the Chief Designer S.P. Korolev a whole family of new missile carriers based on the P-7 ICBMs was developed (Fig. 7) [22].

On October 4, 1957, the USSR, using a modified P-7 ICBM with an index of 8K71PS (see Fig. 7), launched from the Baikonur Cosmodrome, launched the first in the world AES with a mass of 83.6 kg to the near-Earth orbit [20, 25]. The first Soviet AES, flying over the

planet Earth, continuously emitted electromagnetic signals into the surrounding space, received by radio amateurs of all countries of the world. Figure 8 shows a general view of the Soviet P-7 (8K71PS) ICBM, which launched the world's first AES in space during its prelaunch training at the Baikonur Cosmodrome [22].

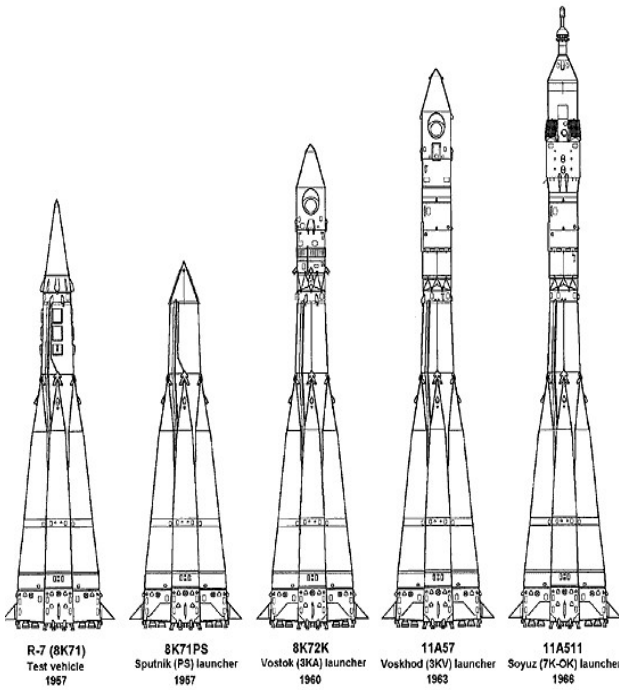

Fig. 7. The family of launch vehicles created at SDB-1 under the leadership of S.P. Korolev based on the ICBM P-7 (8K71) [22]

Fig. 8. The Soviet ICBM P-7 (8K71PS), which launched the world's first AES to the Earth's orbit in 1957, on the launch pad of the Baikonur Cosmodrome during its preparation for launch (Chief Designer – S.P. Korolev, 1957) [22]

The launch and flight of the first Soviet AES have a stunning success in the world. American rocket experts and the US leadership were in real shock. The whole world community was delighted with this breakthrough of the USSR into space. Later, S.P. Korolev, who directed all the work in the USSR to launch this satellite, said [1]: «*...It was small, this the very first artificial satellite of our old planet, but its sonorous callsigns spread across all continents and among all peoples as the embodiment of the bold dream of mankind*». In SDB-1 under the leadership of S.P. Korolev in parallel with the preparation of rocket technology for manned spaceflight, work on satellites of scientific, economic and defense purposes was actively continued during this period. In 1958, Soviet geophysical satellites were designed and launched into space intended to study the Earth's radiation belts.

In 1959, in the USSR under the leadership of S.P. Korolev three automatic stations (AS) are created and launched to the Moon. Here [1]: AS Luna-1 flew near the surface of the Moon; AS Luna-2 symbolically delivered the pennant of the USSR to the Earth's satellite, turning into a plasma upon impact on its surface; AS Luna-3 was the first in the world to photograph the back (invisible from the Earth) side of the Moon. Since 1960, the Soviet SDB-1 began to develop a new spacecraft designed for soft landing on the lunar surface and transmitting the lunar panorama to Earth using it.

On April 12, 1961 S.P. Korolev and the large team of Soviet rocket designers headed by him again amazes the world community [1]: in the USSR, using the first manned spacecraft Vostok-1 and the P-7 (8K72K) launch vehicle (see Fig. 7), the world's first flight of man in outer space around the Earth is carried out (the Vostok-1 ship completed in 108 minutes one revolution around our planet and returned to Earth). This legendary man-cosmonaut was a citizen of the USSR Yuriy Alekseevich Gagarin (Fig. 9).

Fig. 9. Chief Designer of SDB-1 Academician of the Academy of Sciences of the USSR S.P Korolev and the world's first cosmonaut Yu.A. Gagarin [4]

In 1962, S.P. Korolev completed training and conducted a group flight around the Earth of the manned spacecrafts Vostok-3 and Vostok-4. In the same year, he and his SDB-1 participated in the launch of the Mars-1 interplanetary station [2]. In 1963, a design of the P-7

(11A57) type rocket carrier (see Fig. 7) for the Voskhod manned spacecraft was developed at SDB-1. In 1965, he directed the space flight of the Voskhod-2 spacecraft, during which the Soviet cosmonaut A.A. Leonov for the first time in the history of world cosmonautics went into open space (for about 12 minutes) [2]. He participated with his team of scientists and specialists in the rocket launches of the Soviet ASs Luna-5, Luna-6, Luna-7, Luna-8, Venus-2, Venus-3, and the spacecraft «Probe-3» as well as the communications satellite «Lightning-1» [2]. In 1966, at the SDB-1 under the leadership of S.P. Korolev a project of the P-7 (11A511) type rocket carrier was developed (see Fig. 7) for the Soyuz new-generation manned spacecraft [2]. Academician of the Academy of Sciences of the USSR S.P. Korolev took a direct part not only in the design developments of Soviet rocket and space technology. He was the author and co-author of more than 250 scientific papers and inventions [4]. S.P. Korolev was married twice. The first time he married in 1931, his wife was his classmate Ksenia Vincentini. In 1935, his only daughter Natalia was born in this marriage, who later became a medical doctor, MD and Professor. In 1948, the S.P. Korolev's family broke up [5]. His second wife (since 1949) was Nina Ivanovna Kotenkova (1920 – 1999), she worked as a translator in the indicated above secret RSI-88 [5].

Designer S.P. Korolev since the 1950s «nurtured» the idea of launching man on the Moon. The corresponding space program of the USSR was developed with the support of the Head of the Soviet Government N.S. Khrushchev [1]. Initially, the USSR's program for the development of the Moon was carried out using unmanned spacecrafts. The first attempts of S.P. Korolev to create of a new powerful rocket carrier (the H-1 rocket project) for delivering a manned spacecraft to the Moon proved unsuccessful [17, 20]. Premature death of the Chief Designer of the SDB-1 S.P. Korolev interrupted the creative flight of his thoughts in the implementation of the Soviet Lunar Program. His successor V.P. Mishin in a short time to create a lunar space complex also failed. In this regard, the Government of the USSR decided to close this program. As we know, the United States achieved success in landing on the Moon in 1969 thanks to the creation of the powerful Saturn-5 rocket carrier under the leadership of the prominent German-American designer of rocketry Wernher von Braun [10].

Famous scientist-mathematician and mechanic, President and Academician of the Academy of Sciences of the USSR M.V. Keldysh characterizes the «father» of domestic rocket science and practical cosmonautics, Academician of the Academy of Sciences of the USSR S.P. Korolev as follows [5]: «*... Dedication, unusual talent of a scientist and designer, ardent faith in his ideas, vigorous energy and outstanding organizational skills. He possessed a tremendous gift and courage of scientific and technical foresight, and this contributed to the implementation of the most complicated scientific and technical ideas*». On January 14, 1966 S.P. Korolev died during a complicated surgical operation on the intestine (rectal sarcoma was found during the operation). The urn with its ashes is located in the Kremlin wall on the Red Square of Moscow (Russia) [4]. After his death, the pace of development of space programs in the USSR decreased [5]. And to this day, neither in Russia nor in the USA, as the most developed «space» countries of the world, the equal S.P. Korolev has appeared, on the scale of personality and talent, a person capable of breakthrough success in space exploration.

5. Awards, distinctions and recognition of merits of S.P. Korolev. This great designer in the field of rocket science of the USSR and a practical scientist was awarded the following Soviet state awards and such honorary titles [1]:

- two gold medals of the Hero of Labor «Hammer and Sickle» (1956, 1961);
- three orders of Lenin and the Order of the Badge of Honor (1956, 1961, 1965, 1945);
- Laureate of the Lenin Prize (1957);
- Academician of the Academy of Sciences of the USSR (1958);
- K.E. Tsiolkovsky gold medal of the Academy of Sciences of the USSR (1958);
- medals «For Labor Valor» and «Valiant Labor in the Great Patriotic War of 1941-1945» (1945);
- Honorary Citizen of city of Korolev (city of Kaliningrad near Moscow renamed in 1996 at the initiative of the Russian public) and city of Kaluga.

In 1966, the Academy of Sciences of the USSR instituted S.P. Korolev gold medal «For outstanding services in the field of rocket and space technology». Monuments were erected for him in Zhitomir and Moscow, and memorial plaques-reliefs (Fig. 10) on the building of JSC KMPO (former Aircraft Plant No. 16 and SDB-16) at the Baikonur Cosmodrome and in Kazan.

Fig. 10. A memorial plaque in honor of the outstanding Soviet designer of rocket and space technology S.P. Korolev installed on SDB-16 building of the former Kazan Aircraft Plant No. 16 at which he was in the period 1942-1945 worked on improving the aircrafts (Kazan, Russia) [11]

His name is «carried» by Samara Aerospace University (formerly Kuybyshev Aviation Institute), the research ship of Russia, the Russian rocket and space corporation Energia (successor to the legendary SDB-1), streets of the cities of the former USSR, including the

cities of Ukraine: Odessa, Kyiv, Dnipro, Cherkasy, Uzhgorod [20]. His name is given to the high mountain peak in the Pamirs («Roof of the World») and the mountain pass on the transcendent Tien Shan.

Conclusions. The name of the outstanding designer of space and rocket technology S.P. Korolev is connected with the creation in the USSR in the late 1950s of strategic missile weapons, which became the basis of the Soviet nuclear missile «shield», the launch of the world's first artificial Earth satellite and the launch of the first human cosmonaut to Earth orbit. He was a pioneer in the USSR in the field of many areas of the creation and development of domestic nuclear missile weapons and rocket and space technology for the peaceful exploration of outer space. He, as the Chairman of the Council of Chief Designers of the USSR (1950-1966), coordinated all the most important Soviet work in the field of development and creation of military and civil missile equipment. He was inherent in the design talent and the talent of the organizer of scientific and technical works of large scale.

REFERENCES

1. Available at: http://odesskiy.com/k/korolyov-sergej-pavlovich.html (accessed 07 May 2018). (Rus).

2. Available at: https://kpi.ua/ru/node/11087 (accessed 22 July 2018). (Rus).

3. Baranov M.I. An anthology of the distinguished achievements in science and technique. Part 48: Aircraft designer Andrey Tupolev and his accomplishments in airplane design. *Electrical engineering & electromechanics*, 2019, no.2, pp. 3-8. **doi: 10.20998/2074-272X.2019.2.01.**

4. Available at: http://ptiburdukov.ru/Справочник/Биографии/Королев_Сергей_Павлович (accessed 11 October 2018). (Rus).

5. Available at: https://24smi.org/celebrity/3744-sergei-korolev.html (accessed 26 August 2018). (Rus).

6. Available at: http://stuki-druki.com/authors/Korolev.php (accessed 04 May 2018). (Rus).

7. Available at: https://ru.wikipedia.org/wiki/Костиков,_Андрей_Григорьевич (accessed 20 June 2018). (Rus).

8. Golovanov Ya.K. Korolev: *Fakty i mify* [Korolev: Facts and myths]. Moscow, Nauka Publ., 1994. 800 p. (Rus).

9. Available at: http://epizodsspace.airbase.ru/bibl/ogonek/1988/ljeotets.html (accessed 14 December 2018). (Rus).

10. Baranov M.I. An anthology of the distinguished achievements in science and technique. Part 50: Rocket-space technology designer Wernher von Braun and his accomplishments in missile design. *Electrical engineering & electromechanics*, 2019, no.4, pp. 3-11. **doi: 10.20998/2074-272X.2019.4.01.**

11. Available at: https://histrf.ru/lichnosti/biografii/p/koroliev-sierghiei-pavlovich (accessed 20 November 2018). (Rus).

12. Available at: https://pravo.ru/process/view/12232 (accessed 06 March 2018). (Rus).

13. Available at: https://zn.ua/SOCIETY/samaya_bolshaya_tayna_sovetskoy_raketnoy_tehniki.html (accessed 16 April 2018). (Rus).

14. Chertok B.E. *Rakety i liudi. V 4-kh tomakh. Tom 1* [Rockets and people. In 4-th volumes. Vol. 1]. Moscow, Mashinostroenie Publ., 1999. 416 p. (Rus).

15. Chertok B.E. *Rakety i liudi. Fili–Podlipki–Tiuratam. V 4-kh tomakh. Tom 2* [Rockets and people. Fili–Podlipki–Tyuratam. In 4-th volumes. Vol. 2]. Moscow, Mashinostroenie Publ., 1999. 448 p. (Rus).

16. Chertok B.E. *Rakety i liudi. Goriachie dni kholodnoi voiny. V 4-kh tomakh. Tom 3* [Rockets and people. Hot days of cold war. In 4-th volumes. Vol. 3]. Moscow, Mashinostroenie Publ., 1999. 448 p. (Rus).

17. Chertok B.E. *Rakety i liudi. Lunnaia gonka. V 4-kh tomakh. Tom 4* [Rockets and people. Lunar race. In 4-th volumes. Vol. 4]. Moscow, Mashinostroenie Publ., 1999. 538 p. (Rus).

18. Available at: https://history.wikireading.ru/81266 (accessed 21 November 2018). (Rus).

19. Available at: http://www.astronaut.ru/bookcase/books/chert1/text/20.htm?reload_coolmenus (accessed 01 May 2018). (Rus).

20. Available at: http://space.hobby.ru/korolev.html (accessed 11 April 2018). (Rus).

21. Available at: http://www.makeyev.ru/about/history/makeev (accessed 19 February 2018). (Rus).

22. Available at: http://oruzhie.info/raketi/335-r-7 (accessed 08 March 2018). (Rus).

23. Available at: http://space.hobby.ru/glushko.html (accessed 18 June 2018). (Rus).

24. Baranov M.I. An anthology of outstanding achievements in science and technology. Part 7: Nuclear and thermonuclear weapon creation. *Electrical engineering & electromechanics*, 2012, no.2, pp. 3-15. **doi: 10.20998/2074-272X.2012.2.01.**

25. Baranov M.I. *Antologiia vydaiushchikhsia dostizhenii v nauke i tekhnike: Monografiia v 2-kh tomakh. Tom 2.* [An anthology of outstanding achievements in science and technology: Monographs in 2 vols. Vol.2]. Kharkov, NTMT Publ., 2013. 333 p. (Rus).

Received 23.04.2019

M.I. Baranov, Doctor of Technical Science, Professor,
Scientific-&-Research Planning-&-Design Institute «Molniya»,
National Technical University «Kharkiv Polytechnic Institute»,
47, Shevchenko Str., Kharkiv, 61013, Ukraine,
phone +380 57 7076841,
e-mail: baranovmi@kpi.kharkov.ua

How to cite this article:
Baranov M.I. An anthology of the distinguished achievements in science and technique. Part 51: Rocket-space technology designer Sergey Korolev and his accomplishments in missile design. *Electrical engineering & electromechanics*, 2019, no.5, pp. 3-11. **doi: 10.20998/2074-272X.2019.5.01.**

UDC 621.316+621.316.53 **doi: 10.20998/2074-272X.2019.5.02**

Ye.I. Baida, M. Clemens, B.V. Klymenko, O.G. Korol, M.G. Pantelyat, P.Ye. Pustovoitov

PECULIARITIES OF CALCULATING STATIONARY HEATING OF WINDINGS OPERATING IN COMPLEX FORCED CONTROL SYSTEMS

Загальний опис теми дослідження. ***Розглядаються запропоновані авторами методика і алгоритм розрахунку теплового поля електромагнітів, що працюють в складних форсованих системах. Широке застосування в електромеханічних комутаційних апаратах подібних пристроїв дозволяє не тільки підвищити їх швидкодію, але також істотно зменшити розміри, масу і втрати енергії, що свідчить про*** **актуальність даної теми.** ***Запропонована авторами математична модель нагріву обмоток форсованих електромагнітів являє собою систему одновимірних диференціальних рівнянь стаціонарної теплопровідності в циліндричній системі координат, доповнену рівняннями електричного та магнітного кіл. Ця модель дозволяє врахувати пульсації струмів в обмотках, а також втрати в магнітопроводі, обумовлені цими пульсаціями, містить певні ознаки*** **наукової новизни** ***і є*** **метою статті.** ***Розроблений авторами алгоритм розрахунку теплового поля електромагнітів, що працюють в системах форсованого керування, являє собою складний ітераційний цикл, програмування якого істотно спрощується за рахунок застосування математичного пакету Maple, що дозволяє здійснювати складні і громіздкі математичні перетворення, автоматизувати процес розрахункових досліджень, отримувати результати комп'ютерного моделювання в зручній табличній та / або графічній формі, що свідчить про*** **практичну значимість** ***даної роботи. Наведені в статті результати зіставлення розрахунків з експериментальними даними, свідчать про*** **адекватність** ***запропонованих моделі та алгоритму.*** Бібл. 17, табл. 1, рис. 7.

Ключові слова: **електромагніти, теплове поле, форсоване керування, комутаційні апарати, математичний пакет Maple, комп'ютерне моделювання.**

Общее описание темы исследования. ***Рассматриваются предложенные авторами методика и алгоритм расчета теплового поля электромагнитов, работающих в сложных форсированных системах. Широкое применение в электромеханических коммутационных аппаратах подобных устройств позволяет не только повысить их быстродействие, но также существенно уменьшить размеры, массу и потери энергии, что свидетельствует об*** **актуальности** ***данной темы. Предложенная авторами математическая модель нагрева обмоток форсированных электромагнитов представляет собой систему одномерных дифференциальных уравнений стационарной теплопроводности в цилиндрической системе координат, дополненную уравнениями электрической и магнитной цепей. Эта модель позволяет учесть пульсации токов в обмотках и потери в магнитопроводе, обусловленные этими пульсациями, содержит определенные признаки*** **научной новизны и является целью статьи.** ***Разработанный авторами алгоритм расчета теплового поля электромагнитов, работающих в системах форсированного управления, представляет собой сложный итерационный цикл, программирование которого существенно упрощается за счет применения математического пакета Maple, позволяющего осуществлять сложные и громоздкие математические преобразования, автоматизировать процесс расчетных исследований, получать результаты компьютерного моделирования в удобной табличной и/или графической форме, что свидетельствует о*** **практической значимости** ***данной работы. Приведенные в статье результаты сопоставления расчетов с экспериментальными данными, свидетельствуют об*** **адекватности** ***предложенных модели и алгоритма.*** Библ. 17, табл. 1, рис. 7.

Ключевые слова: **электромагниты, тепловое поле, форсированное управление, коммутационные аппараты, математический пакет Maple, компьютерное моделирование.**

Introduction.

International Standards suggest that electromechanical switching devices can operate in such rated duties: eight-hour duty, uninterrupted duty, intermittent duty, temporary duty, and periodic duty. For the coils of such apparatus, the most hard mode in terms of heating their windings (the coil may contain one or more windings) is uninterrupted duty. Therefore, the basic Standard IEC 60947-1:1999, Low-voltage switchgear and controlgear – Part 1: General rules indicates that «coils and electromagnets shall be tested ... for a sufficient time for the temperature-rise to reach a steady-state value» (IEC 60947-1, 8.3.3.3.6). At the same time, that Standard makes a reservation that «coils and electromagnets of equipment intended for intermittent duty shall be tested as prescribed in the relevant product standard». Manufacturers rarely use this feature, because if the device is designed to operate in intermittent duty, but operates, for example, in eight-hour duty or in uninterrupted duty, then its coil will necessarily overheat and will be damaged. In this case, it will be difficult for the manufacturer to prove that the damage is due to improper operation, and not to structural defects. Therefore, the vast majority of electromechanical switching devices are oriented to operate in continuous modes (eight-hour or uninterrupted duty), which means to ensure operability in these modes, including in steady state, when the temperature of the windings reaches its maximum value.

The use of forced electromagnetic systems (FEMS) in electromechanical switching devices [1] not only allows to increase their speed, but also to significantly reduce the size, mass and energy losses in an electromagnet.

When designing a switching devices with FEMS, it is necessary to take into account the specific features of heat release in the windings and, possibly, in the magnetic core of the drive electromagnet associated with the pulsations of currents in the windings, as well as the features of heat exchange between the windings and the features of heat transfer from the windings to the magnetic core and to the environment.

Although there are a large number of publications devoted to methods for calculating the heating of electromagnets, some of which are given in References

[1–9]. In the authors' opinion, insufficient attention has been paid to the processes of heating the windings while taking into account the above features, taking into account the wide variety of existing FEMS and some peculiarities of the operation of forced electromagnets in switching devices. At first glance, the task of calculating the stationary heating of the electromagnet windings may seem quite simple, however, for forced systems, especially in cases where the control device is supplied from an AC voltage source through a rectifier, this task is greatly complicated, taking into account the complex harmonic composition of currents in windings and magnetic core.

The goal of this work is the description of a mathematical model of the process of stationary heating of the windings of electromagnets operating in the FEMS. This model has to take into account the features of heat exchange between the windings, heat transfer from the windings to the magnetic core and the environment, taking into account the ripple currents, and other features of the operation of electro-magnets in FEMC. The algorithm for calculating the temperature distribution in the windings of these electromagnets is focused on using the Maple computing environment, which greatly simplifies the programming process.

The geometric model.

The coils of forced electromagnets, in most cases, are located on cores having a cylindrical shape and are axi-symmetrical, even when the electromagnet itself does not have axial symmetry. Thus, the thermal calculation can be performed in a cylindrical coordinate system. A sketch of a coil and a fragment of a magnetic core of a forced electromagnet is shown in Fig. 1. The coil of such an electromagnet can have one or two windings: booster and holding ones, and, most often, the booster winding is wound first, and the holding one is wound on top of it. The axial size l_w of the coil winding space, as a rule, far exceeds its radial size. Therefore, with a high degree of adequacy, the temperature field in it can be considered as 1D one, which is greatly facilitated by the insulating cheeks of the coil frame.

Heat transfer from the external surface of the second (holding) winding into the environment (air) is carried out through the thickness of the shell from its external surface (Fig. 2), whose area is S_e:

$$S_e = 2 \cdot \pi \cdot r_e \cdot l_w, \quad (1)$$

where r_e is the radius of the external surface of the shell of the coil.

The heat flux P_e dissipated into the surrounding air from the external surface of the coil is equal to:

$$P_e = k_e \cdot S_e \cdot \theta_e, \quad (2)$$

where k_e is the coefficient of heat transfer to the ambient air from the external surface of the shell of the coil; θ_e is the temperature rise of the external surface of the shell of the coil:

$$\theta_e = \vartheta_e - \vartheta_a, \quad (3)$$

ϑ_e is the temperature of the external surface of the shell of the coil, °C; ϑ_a is the ambient air temperature.

Expression (2) can be considered as the heat equivalent of Ohm law, in which the role of the electric current is played by the heat flux (power), and the role of voltage is played by the temperature rise. Then the product $k_e \cdot S_e$ is the thermal conductivity $G_{\theta e}$, i.e., the reciprocal of the thermal resistance $R_{\theta e}$:

$$R_{\theta e} = 1 / G_{\theta e} = 1 / (k_e \cdot S_e). \quad (4)$$

Thus, expression (2) can be represented as follows:

$$P_e = \theta_e / R_{\theta e}. \quad (5)$$

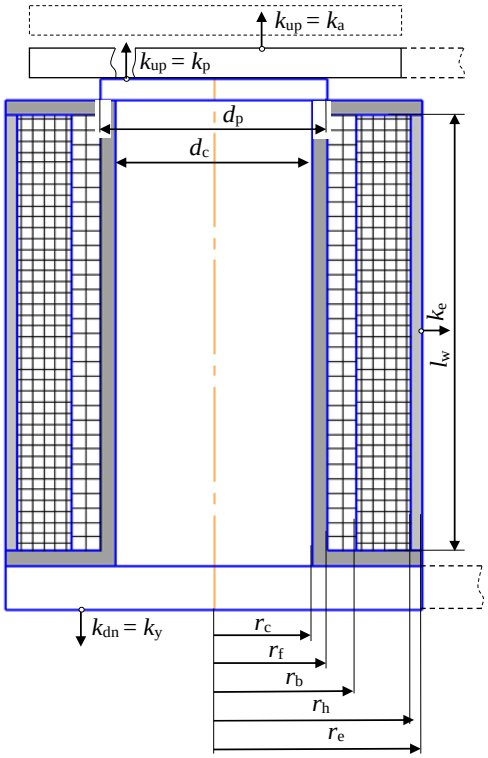

Fig. 1. Sketch of a coil and a fragment of a magnetic core of a forced electromagnet

Heat transfer from the internal surface of the first (booster) winding to the environment is carried out through the thickness of the tubular part of the insulating frame to the core, from it to other parts of the magnetic core, from the external parts of which to the surrounding air.

The heat flux dissipated into the environment from the **d**ow**n** part of the magnetic core P_{dn} is:

$$P_{dn} = k_{dn} \cdot S_{dn} \cdot \theta_c = \theta_c / R_{\theta dn}. \quad (6)$$

where k_{dn} is the coefficient of heat transfer to the surrounding air from the down part of the magnetic core. S_{dn} is the cooling surface area from the down part of the magnetic core; θ_c is the temperature rise of the core and adjacent parts of the magnetic core – the **y**oke, the **p**ole piece and the **a**rmature above the temperature ϑ_a of the ambient air; $R_{\theta dn}$ is the thermal resistance to cooling from the down part of the magnetic core.

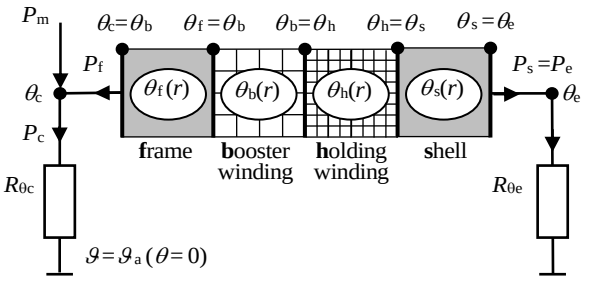

Fig. 2. Equivalent circuit showing the process of heat transfer from the windings of a forced electromagnet to the environment

In particular, for double-rod electromagnets, as the area of the cooling surface from the bottom part of the magnetic core, with a certain margin in the direction of heating of the windings, we can take:

$$S_{dn} = b_y \cdot l_{yp} / 2, \quad (7)$$

where b_y, l_{yp} are the **b**readth and the **l**ength of the **y**oke (**p**iece), respectively.

The heat flux dissipated into the environment from the **up**per part of the magnetic core P_{up} is:

$$P_{up} = k_{up} \cdot S_{up} \cdot \theta_c = \theta_c / R_{\theta up}, \quad (8)$$

where k_{up} is the coefficient of heat transfer to the surrounding air from the upper part of the magnetic core; S_{up} is the cooling surface area from the upper part of the magnetic core; $R_{\theta up}$ is the thermal resistance to cooling from the upper part of the magnetic core.

If the electromagnet operated and its armature is pulled to the fixed part of the magnetic core, then as S_{up} for two-rod electromagnets, we can take:

$$S_{up} = b_a \cdot l_{ap} / 2, \quad (9)$$

where b_a , l_{ap} are the breadth and the length of the **a**rmature (**p**iece), respectively.

If the electromagnet did not operate and its armature is in the released position, then the area of the pole tip S_p can be taken as S_{up}:

$$S_p = \pi \cdot d_p^{\,2} / 4, \quad (10)$$

where d_p is the diameter of the pole tip.

The heat flux P_c dissipated into the environment from the entire cooling surface of the magnetic circuit is equal to the sum of P_{dn} and P_{up}:

$$P_c = \theta_c / R_{\theta dn} + \theta_c / R_{\theta up} = \theta_c \cdot (R_{\theta dn} + R_{\theta up}) / (R_{\theta dn} \cdot R_{\theta up}) = \\ = \theta_c / R_{\theta c} = \theta_c \cdot k_c \cdot S, \quad (11)$$

where $R_{\theta c}$ is the resulting thermal resistance to cooling from the surface of the magnetic core; S is the area of an arbitrary surface; k_c is the equivalent heat transfer coefficient from the surface of the magnetic core reduced to surface S:

$$k_c = ((R_{\theta dn} + R_{\theta up}) / (R_{\theta dn} \cdot R_{\theta up})) / S = (k_{dn} \cdot S_{dn} + k_{up} \cdot S_{up}) / S. \quad (12)$$

Heat transfer coefficients.

The heat transfer coefficients k from the solid's surface are usually represented as a sum of the **c**onvective (k_c) and **r**adiant (k_r) heat transfer coefficients. A technique of the determination of these coefficients used at this problem solution is considered below.

The radiant heat transfer coefficient may be in principle determined from the Stefan-Boltzmann law for each point of the radiating surface if the temperature ϑ of this point, the temperature ϑ_a of the region to which the energy is radiated, and the emissivity ε of the radiating surface are known:

$$k_r = \frac{k_1 \cdot \varepsilon}{\theta} \left[\left(\frac{\theta + \vartheta_a + 273}{100} \right)^4 - \left(\frac{\vartheta_a + 273}{100} \right)^4 \right], \quad (13)$$

where $k_1 = k_B \cdot 10^8 = 5.67$ W·m^{-2}·K^{-4} is the coefficient of radiation of the absolutely black body, k_B is the Stefan-Boltzmann constant – $k_B = 5.67 \cdot 10^{-8}$ W·m^{-2}·K^{-4}, ε is the emissivity (in the calculations we took $\varepsilon = 0.5$) θ is the temperature rise ($\theta = \vartheta - \vartheta_a$).

Convective heat transfer coefficient depends on many factors, but its value adapted to the operating conditions of electrical apparatus can be determined by the formula [2]:

$$k_c = k \cdot (\theta / l)^{0,25}, \quad (14)$$

where k is the empirical coefficient equal to 1.33 for vertical surfaces, with $1.33 \cdot 1.3 = 1.73$ for a flat surface that radiates heat upward, and $1.33 \cdot 0.7 = 0.93$ for a flat surface that radiates heat down; l is the determining size, for which the vertical size is taken for vertical surfaces, therefore, for the external surface of the shell $l = l_w$; for horizontal rectangular surfaces, l is taken to be smaller, and for round surfaces the diameter is taken, therefore, to calculate the convective heat transfer coefficient from the yoke surface $l = b_y$, from the armature surface $l = b_a$ (if the electromagnet operated) otherwise $l = d_p$.

Thus, the heat transfer coefficients can be calculated by the formulas:

$$k_e = \frac{5{,}67 \cdot \varepsilon}{\theta_e} \cdot \left[\left(\frac{\theta_e + \vartheta_a + 273}{100} \right)^4 - \left(\frac{\vartheta_a + 273}{100} \right)^4 \right] + 1{,}33 \cdot (\theta_e / l_w)^{0,25}, \quad (15)$$

$$k_{dn} = \frac{5{,}67 \cdot \varepsilon}{\theta_c} \cdot \left[\left(\frac{\theta_c + \vartheta_a + 273}{100} \right)^4 - \left(\frac{\vartheta_a + 273}{100} \right)^4 \right] + 1{,}73 \cdot (\theta_c / b_y)^{0,25}, \quad (16)$$

$$k_{up} = \frac{5{,}67 \cdot \varepsilon}{\theta_c} \cdot \left[\left(\frac{\theta_c + \vartheta_a + 273}{100} \right)^4 - \left(\frac{\vartheta_a + 273}{100} \right)^4 \right] + 0{,}93 \cdot (\theta_c / l)^{0,25}. \quad (17)$$

In expression (17), the value of l is taken equal to b_a if the electromagnet operated, otherwise $l = d_p$.

Thermal conductivity.

Methods for calculating the equivalent thermal conductivity λ_w of **w**indings were considered in the works of a number of authors in the 30s - 60s of the last century [10-12]. In those works, empirical formulas are presented that were obtained by processing experimental data for impregnated windings. Among them there is a formula used in our calculations:

$$\lambda = \lambda_i \cdot 0{,}5 \cdot \left[1{,}45 \cdot (d / \Delta)^{0,75} + (d / \Delta)^{0,67} \right], \quad (18)$$

where d is the diameter of the winding wire, Δ is the thickness of the insulation of the wire. λ_i is the thermal conductivity of internal **i**nsulation, depending on the **av**erage temperature:

$$\lambda_i = \lambda_{i0} \cdot (1 + \alpha_{\lambda 0} \cdot \vartheta_{av}) = \lambda_{ia} \cdot (1 + \alpha_{\lambda a} \cdot \theta_{av}), \quad (19)$$

where λ_{i0} , λ_{ia} are the thermal conductivities of the internal insulation, respectively, at temperature of **0**°C and at **a**mbient temperature ϑ_{av}; $\alpha_{\lambda 0}$, $\alpha_{\lambda a}$ is the temperature coefficient of thermal conductivity of the internal insulation, assigned respectively to temperature 0°C and to ambient temperature:

$$\lambda_{ia} = \lambda_{i0} \cdot (1 + \alpha_{\lambda 0} \cdot \vartheta_{av}); \quad \alpha_{\lambda a} = \alpha_{\lambda 0} / (1 + \alpha_{\lambda 0} \cdot \vartheta_{av}). \quad (19)$$

In this work, when calculating the equivalent thermal conductivities of the booster and holding windings, the same insulation characteristics were taken: $\lambda_{i0} = 0.32$ W/(m·K), $\alpha_{\lambda 0} = 0.0018$ 1/K (at temperature $\vartheta_{av} = 35$°C we have $\lambda_{ia} = 0{,}33$, $\alpha_{\lambda a} = 0.0017$). However, since wires of different diameters are used in these windings ($d_b = 0.28$ mm, $\Delta_b = 0.025$ mm, $d_h = 0.18$ mm, $\Delta_h = 0.015$ mm) and, in addition, they differ from each other by average temperatures, the equivalent heat conductivities of these windings will also differ from each other, for the calculation of which the following formulas are used:

$$\lambda_b = 2{,}35 \cdot (1 + 0{,}0017 \cdot \theta_{bav}), \quad (20)$$

$$\lambda_h = 1{,}98 \cdot (1 + 0{,}0017 \cdot \theta_{hav}). \quad (21)$$

Differential equations and density of heat sources.

The system of differential equations, which is used to solve the problem of calculating the stationary temperature field ϑ in an electromagnet, consists of n (in the number of subdomains) Poisson (for subdomains with internal heat sources) and Laplace (for subdomains without internal sources) differential heat transfer equations. This system looks like this [2, 14, 15]:

$$-\mathrm{div}(\lambda_{wk} \cdot \mathrm{grad}\,\vartheta) = q \qquad (22)$$

for subdomains with internal heat sources (windings) with number k and thermal conductivity λ_{wk}, and

$$\mathrm{div}(\lambda_k \cdot \mathrm{grad}\,\vartheta) = 0 \qquad (23)$$

for subdomains without internal heat sources, where q is the volumetric density of internal heat sources; λ_k is the thermal conductivity of the material of the subdomain with number k.

In our problem, four subdomains are considered – the frame and the shell (without internal heat sources) and two windings – the booster and holding (both with internal heat sources). In the iterative process of calculating the stationary thermal field, at each iteration the rms currents I_1, I_2 which pass sequentially through all the turns of the corresponding windings are determined. It should be borne in mind that although the current density in all turns is the same the turns will be heated differently, since the specific resistance of the conductor material depends on temperature (in the temperature range from 0°C to 200°C this dependence has an almost linear character), in coils with higher temperature more energy will be released than in coils with lower temperature.

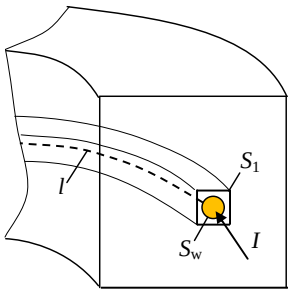

Fig. 3. To the determination of volumetric density of heat sources

In the general case, the density of sources is defined as the derivative in volume of the power loss. This derivative can be replaced by the ratio of small quantities – the power losses in the turn ΔP and the volume occupied by the turn, taking into account the insulation of the conductor and the internal insulation of the winding ΔV:

$$q = \frac{\mathrm{d}P}{\mathrm{d}V} \approx \frac{\Delta P}{\Delta V}. \qquad (24)$$

Since shunt windings contain a large number of turns, the volume occupied by one turn and the power dissipated in one turn can be considered with a high degree of certainty as small quantities:

$$\Delta P = I^2 \cdot \rho_0 \cdot (1 + \alpha_0 \cdot \vartheta) \cdot l / S_w, \qquad (25)$$

$$\Delta V = l \cdot S_1 = l \cdot S_w / k_f, \qquad (26)$$

where I is the rms current in the winding (and in the turn); ρ_0 is the specific resistance of the material of the winding wire at 0°C (for copper ρ_0 = 1.586 · 10^{-8} Ω·m); α_0 is the temperature coefficient of resistivity, referred to the temperature of 0°C (for copper α_0 = 0.00423 1/K); l is the length of the turn; S_w is the cross-sectional area of the winding wire; S_1 is the cross-sectional area occupied by the cross-section of the turn, taking into account the insulation of the conductor and the internal insulation of the winding; k_f is the fill factor of the winding space with copper.

Substituting (14) and (15) into (13), we obtain:

$$q = J^2 \cdot k_f \cdot \rho_0 \cdot (1 + \alpha_0 \cdot \vartheta) = q_0 \cdot (1 + \alpha_0 \cdot \vartheta), \qquad (27)$$

where J is the rms current density in the conductor:

$$J = I / S_w, \qquad (28)$$

$$q_0 = J^2 \cdot k_f \cdot \rho_0, \qquad (29)$$

The density of the heat sources can be expressed not through the temperature ϑ, but through the temperature rise θ over the ambient temperature ϑ_a:

$$q = q_a \cdot (1 + \alpha_a \cdot \theta), \qquad (30)$$

where

$$q_a = q_0 \cdot (1 + \alpha_0 \cdot \vartheta_a), \qquad (31)$$

$$\alpha_a = \alpha_0 / (1 + \alpha_0 \cdot \vartheta_a). \qquad (32)$$

The system of equations in 1D formulation of the problem of calculating the temperature field.

As noted above, in this problem, four adjacent subdomains are considered, the axial section of each of which has a rectangular shape: the **f**rame, the **b**ooster winding, the **h**olding winding as well as the **s**hell of the coil. The letters in bold are used hereinafter as markers denoting the belonging of a particular physical quantity to the corresponding subdomain. The axial dimensions of the cross-sections of these domains far exceed their radial dimensions, which gives reason to solve this problem in 1D formulation. The corresponding differential equations describing the distribution of temperature rise in these subdomains in a cylindrical coordinate system take the following form:

$$\frac{\mathrm{d}^2\theta_f}{\mathrm{d}r^2} + \frac{1}{r} \cdot \frac{\mathrm{d}\theta_f}{\mathrm{d}r} = 0; \qquad (33)$$

$$\frac{\mathrm{d}^2\theta_b}{\mathrm{d}r^2} + \frac{1}{r} \cdot \frac{\mathrm{d}\theta_b}{\mathrm{d}r} = -\frac{q_{ab}}{\lambda_b} \cdot (1 + \alpha_a \cdot \theta_b); \qquad (34)$$

$$\frac{\mathrm{d}^2\theta_h}{\mathrm{d}r^2} + \frac{1}{r} \cdot \frac{\mathrm{d}\theta_h}{\mathrm{d}r} = -\frac{q_{ah}}{\lambda_h} \cdot (1 + \alpha_a \cdot \theta_h); \qquad (35)$$

$$\frac{\mathrm{d}^2\theta_s}{\mathrm{d}r^2} + \frac{1}{r} \cdot \frac{\mathrm{d}\theta_s}{\mathrm{d}r} = 0. \qquad (36)$$

The general solutions of these equations have the following form:

$$\theta_f = C_1 + C_2 \cdot \ln(r); \qquad (37)$$

$$\theta_b = C_3 \cdot \mathrm{J}_0\left(\sqrt{\frac{q_{ab} \cdot \alpha_a}{\lambda_b}} \cdot r\right) + C_4 \cdot \mathrm{Y}_0\left(\sqrt{\frac{q_{ab} \cdot \alpha_a}{\lambda_b}} \cdot r\right) - \frac{1}{\alpha_a}; \qquad (38)$$

$$\theta_h = C_5 \cdot \mathrm{J}_0\left(\sqrt{\frac{q_{ah} \cdot \alpha_a}{\lambda_h}} \cdot r\right) + C_6 \cdot \mathrm{Y}_0\left(\sqrt{\frac{q_{ah} \cdot \alpha_a}{\lambda_h}} \cdot r\right) - \frac{1}{\alpha_a}; \qquad (39)$$

$$\theta_s = C_7 + C_8 \cdot \ln(r), \qquad (40)$$

where J_0, Y_0 are the zero-order Bessel functions of the first and second kind.

Calculation of the distribution of temperature rises, based on the conditions of uniqueness of the solution.

Equations (33) – (36) are second-order equations, the general solution of each of them (38) – (40) includes two arbitrary constants – a total of eight constants. To determine

them under specific heat transfer conditions, it is necessary to compose eight equations that determine the uniqueness of the solution. The joint solution of these equations will make it possible to determine the values of the indicated arbitrary constants and to obtain particular solutions, that is, to find the temperature distribution in the subdomains that correspond to the formulated uniqueness conditions.

Six of the eight conditions mentioned are the conditions of continuity – at the points of conjugation of the subdomains the values of the temperature rises and heat fluxes should be continuous (should not change stepwise):

$$\theta_{\rm f}(r_{\rm f}) = \theta_{\rm b}(r_{\rm f}); \tag{41}$$

$$\theta_{\rm b}(r_{\rm b}) = \theta_{\rm h}(r_{\rm b}); \tag{42}$$

$$\theta_{\rm h}(r_{\rm h}) = \theta_{\rm s}(r_{\rm h}); \tag{43}$$

$$\left[\lambda_{\rm f}\cdot\frac{{\rm d}\theta_{\rm f}}{{\rm d}r} = \lambda_{\rm b}\cdot\frac{{\rm d}\theta_{\rm b}}{{\rm d}r}\right]_{r=r_{\rm f}}; \tag{44}$$

$$\left[\lambda_{\rm b}\cdot\frac{{\rm d}\theta_{\rm b}}{{\rm d}r} = \lambda_{\rm h}\cdot\frac{{\rm d}\theta_{\rm h}}{{\rm d}r}\right]_{r=r_{\rm b}}; \tag{45}$$

$$\left[\lambda_{\rm h}\cdot\frac{{\rm d}\theta_{\rm h}}{{\rm d}r} = \lambda_{\rm s}\cdot\frac{{\rm d}\theta_{\rm s}}{{\rm d}r}\right]_{r=r_{\rm h}}. \tag{46}$$

The remaining two conditions are determined from the boundary conditions – on the external surface of the shell of the coil and on the internal surface of the tubular part of the frame. The boundary condition on the external surface of the shell of the coil is obtained on the basis of the equality of the heat flux approaching the external surface of the shell from its thickness and the heat flux passing into the surrounding air. The first of them is determined based on the Fourier law:

$$P_{\rm e} = -\lambda_{\rm s}\cdot({\rm grad}_{\rm n}\theta_{\rm s})\Big|_{r=r_{\rm e}}\cdot S_{\rm e} = -\lambda_{\rm s}\cdot\frac{{\rm d}\theta_{\rm s}}{{\rm d}r}\Big|_{r=r_{\rm e}}\cdot S_{\rm e}, \tag{47}$$

where $S_{\rm e}$ is calculated by (1).

Heat flow to ambient air is determined based on Newton formula:

$$P_{\rm e} = k_{\rm e}\cdot\theta_{\rm e}\cdot S_{\rm e} = k_{\rm e}\cdot\theta_{\rm s}(r_{\rm e})\cdot S_{\rm e}. \tag{48}$$

Equating the right sides of (47) and (48), we obtain the boundary condition on the external surface of the coil shell:

$$\left[-\lambda_{\rm s}\cdot\frac{{\rm d}\theta_{\rm s}}{{\rm d}r} = k_{\rm e}\cdot\theta_{\rm s}\right]_{r=r_{\rm e}}. \tag{49}$$

The boundary condition on the internal surface of the tubular part of the frame is determined based on the balance of heat fluxes on this surface (Fig. 2):

$$P_{\rm m} + P_{\rm f} = P_{\rm c}. \tag{50}$$

Heat flux approaching the internal surface of the frame from its thickness is determined based on the Fourier law:

$$P_{\rm f} = -\lambda_{\rm f}\cdot({\rm grad}_{\rm n}\theta_{\rm f})\Big|_{r=r_{\rm s}}\cdot S_{\rm f} = \lambda_{\rm f}\cdot\frac{{\rm d}\theta_{\rm f}}{{\rm d}r}\Big|_{r=r_{\rm e}}\cdot S_{\rm f}, \tag{51}$$

where $S_{\rm f}$ is the area of the internal surface of the tubular part of the frame:

$$S_{\rm f} = 2\cdot\pi\cdot r_{\rm c}\cdot l_{\rm w}, \tag{52}$$

In expression (51), in contrast to (47), the "–" sign is missing after the second equal sign, since the direction of the external normal to the surface $S_{\rm f}$ is opposite to the direction of the r axis.

The heat flux $P_{\rm c}$ dissipated into the environment from the entire cooling surface of the magnetic circuit can be calculated based on (11), in which the surface $S_{\rm f}$ is taken as an arbitrary surface S:

$$P_{\rm c} = \theta_{\rm c}\cdot k_{\rm c}\cdot S_{\rm f} = \theta_{\rm f}(r_{\rm c})\cdot k_{\rm c}\cdot S_{\rm f}. \tag{53}$$

In this case, the equivalent heat transfer coefficient from the surface of the magnetic core reduced to the surface $S_{\rm f}$ is equal to:

$$k_{\rm c} = (k_{\rm dn}\cdot S_{\rm dn} + k_{\rm up}\cdot S_{\rm up})/S_{\rm f}. \tag{54}$$

Substituting (53) and (51) into (50), we obtain the boundary condition on the internal surface of the tubular part of the frame:

$$\left[\lambda_{\rm f}\cdot\frac{{\rm d}\theta_{\rm f}}{{\rm d}r} = k_{\rm c}\cdot\theta_{\rm f} - P_{\rm m}/S_{\rm f}\right]_{r=r_{\rm c}}. \tag{55}$$

RMS currents in the windings. Power losses in the magnetic core.

The procedure for calculating the currents in the windings and the losses in the magnetic core is determined by the connection circuit of the windings to the power source and its type (DC voltage source or AC voltage source with a rectifier). In this paper, as an example, we consider the control device that is most often used in contactors (Fig. 4). The calculation circuit differs from the circuit diagram by the presence of scattering inductances $L_{\sigma{\rm B}}$ and $L_{\sigma{\rm H}}$ due to fluxes not passing through the sections of the magnetic core.

In previous works [16, 17], the features of the operation of this device were analyzed in detail, and a methodology for calculating the dynamic characteristics of an electromagnet, including the currents in its booster and holding windings, was considered. This technique is based on the joint solution of the equations of the electric circuit (Fig. 4*b*) and the magnetic circuit (Fig. 5*b*).

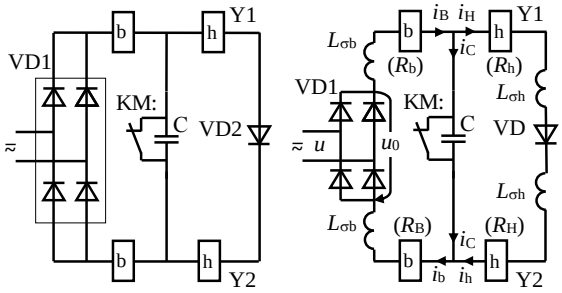

Fig. 4. Circuit diagram (a) and calculation circuit (b) of the forced control system, which is used in low and medium voltage vacuum contactors and in some SF6 medium voltage contactors [16]; u is the instantaneous value of the nominative voltage of the control circuit; u_0 is the voltage at the output of the diode bridge

This electrical circuit is too complicated for programming. Its description will be much simpler if the parallel connection of the capacitor C with the auxiliary control contact KM:, which is closed when the coordinate s of the armature stroke does not exceed the value of the opening stroke of this contact $s_{\rm a}$, is replaced by ***one*** capacitor, whose capacitance is assumed to be very large – $C_{\rm M}$ for $s \le s_{\rm a}$, and for $s > s_{\rm a}$ the capacitance of this capacitor becomes equal to its nominal value C_0:

$$C = \begin{cases} C_{\rm M} & \text{at } s \le s_{\rm a}; \\ C_0 & \text{at } s > s_{\rm a}. \end{cases} \tag{56}$$

In this case, we obtain the following differential equations:

$$u_0 = 2 \cdot R_b \cdot i_b + 2 \cdot L_{\sigma b} \cdot \frac{di_b}{dt} + 2 \cdot N_b \cdot \frac{d\Phi_0}{dt} + u_C; \quad (57)$$

$$u_C = 2 \cdot R_h \cdot i_h + 2 \cdot L_{\sigma h} \cdot \frac{di_h}{dt} + 2 \cdot N_h \cdot \frac{d\Phi_0}{dt} + u_d(i_h); \quad (58)$$

$$C \cdot \frac{du_C}{dt} = i_b - i_h, \quad (59)$$

where N_b, N_h are the number of turns of the booster (b) and holding (h) windings, respectively.

In [16] various variants of magnetic circuit equivalent circuits were considered, including a relatively simple two-contour circuit with a concentrated scattering flux (Fig. 5*b*).

The equations compiled for two contours with magnetic fluxes Φ_0 and Φ_1 have the following form:

$$-G_a \cdot \frac{d\Phi_0}{dt} = H(\Phi_0 / S_a) \cdot l_a + \frac{2 \cdot \Phi_0}{\Lambda_\delta} - (\Phi_1 - \Phi_0) / \Lambda_{ofe}; \quad (60)$$

$$2 \cdot i_b \cdot N_b + 2 \cdot i_h \cdot N_H - (2 \cdot G_c + G_y) \cdot \frac{d\Phi_1}{dt} = \\ = H(\Phi_1 / S_y) \cdot l_y + 2 \cdot H(\Phi_1 / S_c) \cdot l_c + (\Phi_1 - \Phi_0) / \Lambda_{ofe} \quad . \quad (61)$$

The designations of the quantities in (57)–(61) correspond to the designations given in Fig. 4*b*, 5. Here, the MMF F_m is the sum of the MMFs of the booster and the holding windings:

$$F_m = i_b \cdot N_b + i_h \cdot N_h \, . \quad (62)$$

In addition, in (60), (61) it is indicated: G_c, G_a, G_y are the electrical conductivities in the path of eddy currents in the core, armature, and yoke. The values of these quantities can be determined by the following formulas [1]:

$$G_c = l_c / (8 \cdot \pi \cdot \rho_{st}) \, ; \quad (63)$$

$$G_{a,y} = l_{a,y} / (16 \cdot \rho_{st} \cdot (h_{a,y} / b_{a,y} + b_{a,y}) / h_{a,y})) \, , \quad (64)$$

where l_c is the length of the core; ρ_{st} is the specific resistance of the material of the magnetic core (steel); h_a is the height of the armature part; h_y is the height of the yoke part.

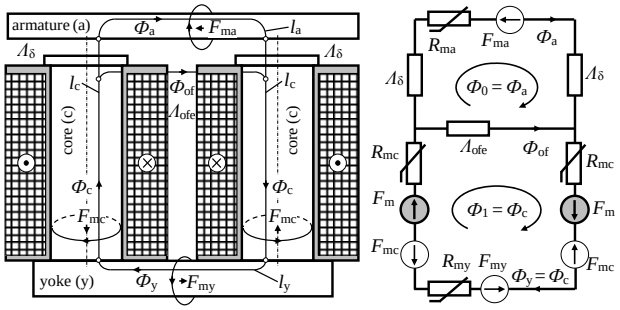

Fig. 5. Sketch of the double-rod electromagnet magnetic circuit and its simplified equivalent circuit used in calculations of transients

If this device is powered from a source with DC voltage value U, then the calculation of currents in the windings in stationary mode does not cause difficulties. For the circuit shown in Fig. 4*a*, the corresponding formulas look like this. If the electromagnet operated, then all the windings turn on in series and there are also three diodes in this circuit – two diodes of the rectifier bridge VD1 and a «locking» diode VD2, therefore:

$$I_b = I_h = (U - 3 \cdot U_d) / (2 \cdot (R_b + R_h)). \quad (65)$$

If the electromagnet did not operate and the contact KM: did not open, then the holding windings remain shorted by the contact KM: and the current does not flow in them. The booster windings remain connected in series and there are two diodes of the rectifier bridge VD1 in their circuit, therefore:

$$I_b = (U - 2 \cdot U_d) / (2 \cdot R_b); \; I_h = 0. \quad (66)$$

The voltage drop on the diode is small – about 1 V, but when powered by an ultra-low voltage source, three diodes give a significant decrease in current in the windings.

Since there are no current pulsations in the windings when powered from a DC voltage source in the stationary mode, there are no pulsations of the magnetic flux in the magnetic core, and therefore losses in it:

$$P_m = 0. \quad (67)$$

If this device is powered by an AC voltage source, for example, with frequency of 50 Hz, then a two-half-period rectified voltage is formed at the output of the diode bridge – a periodic curve with frequency of the fundamental harmonic of the variable component equal to 100 Hz. The presence of nonlinear elements in the electric and magnetic circuits leads to the appearance of higher harmonics, which greatly complicates the calculation of such circuits.

In [16] an algorithm focused on the use of the Maple computing environment was considered, developed to calculate the dynamics of electromagnets operating in complex forced control systems, for example, in the forced control device circuit shown in Fig. 4*a*. Comparison of the calculation results by this algorithm with experimental data [16] showed that even a simplified representation of the magnetic circuit in the form of a two-contour equivalent circuit provides good agreement between the results of mathematical and field experiments. This holds, even when the control device is powered from an AC voltage source, when complex shapes of current curves in windings are observed.

Calculations and experiments also show that the stable shape of currents curves in the booster and holding windings occurs almost immediately after the completion of the movement of the armature. For an electromagnet, the dimensions of which are given in [16], the response time ranges from 50 ms (with supply voltage equal to the rated voltage of the control circuit 220 V) to 80 ms (with a supply voltage equal to 180 V). At low voltage (150 V or less), the electromagnet did not operate, but the shape of the current curves stabilized no later than after 100 ms. Figure 6 shows the curves of changes in currents in the windings during two periods – from 150 ms to 170 ms after the beginning of the transient.

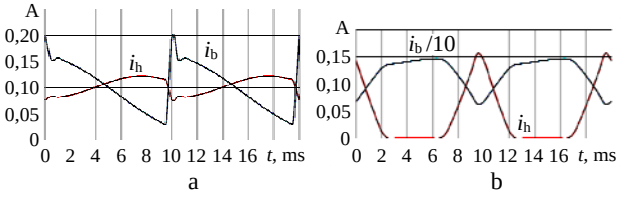

Fig. 6. Curves of current changes in the forced electromagnet windings: a – at supply voltage in the control circuit of 220 V (the electromagnet operated); b – at supply voltage of 150 V (the electromagnet did not operate)

Apparently, in both modes (the electromagnet operated / did not operate), the transient almost ends quickly enough – in 150 ms, that is, after seven to eight periods T of voltage change in the grid of 50 Hz). Consequently, there is no need to build a special iterative technique for calculation of currents in stationary mode. It is enough to use a well-tested methodology for calculating dynamics, setting a knowingly large finite value of time t_k, to record in the computer memory the instantaneous values i_b and i_h of currents in the windings during the last period T and using one of the known numerical integration methods calculate the rms currents I_b and I_h:

$$I_{b,h} = \left[\frac{1}{T} \cdot \int_{t_k - T}^{t_k} \left[i_{b,h}(t) \right]^2 \cdot dt \right]^{0,5} . \quad (68)$$

As a result of the joint solution of the equations of the electric and magnetic circuits, it is possible to calculate the magnetic fluxes in the armature, core and yoke, as well as their time derivatives. These derivatives can be considered as EMF in single-turn contours equivalent in losses in the armature, core and yoke and calculate the instantaneous values of currents i_a, i_c and i_y in these circuits in transient mode. Having fixed these instantaneous values during the last period of the calculation of the transient in the computer memory, using one of the known numerical integration methods using a formula similar to (68), it is possible to calculate the rms currents I_a , I_c, I_y and losses in the magnetic core:

$$P_m = I_a^2 / G_a + I_c^2 / G_c + I_y^2 / G_y. \quad (69)$$

An iterative algorithm for calculating the temperature distribution in the windings of forced electromagnets using the Maple computing environment.

In order to calculate the rms currents in the windings, it is necessary to know their resistances, which depend on the average temperature values of the corresponding windings. In order to calculate the temperatures of the windings, it is necessary to know the rms currents in the windings. This problem can be solved using the iteration method:

0) to set arbitrary average values of the temperature rises of the windings $\theta_{bavi} = \theta_{bav0}$ and $\theta_{havi} = \theta_{hav0}$;

1) to calculate the winding resistances:

$$R_{bi} = R_{ba} \cdot (1 + \alpha_a \cdot \theta_{bavi}) \text{ and } R_{hi} = R_{ha} \cdot (1 + \alpha_a \cdot \theta_{havi}); \quad (70)$$

2) to calculate the rms currents in the windings and the power losses in the magnetic core according to the technique described in the corresponding section of this paper;

3) to calculate the distribution of temperature rises in the booster and holding windings $\theta_b(r)$ and $\theta_h(r)$ according to the procedure described in the corresponding section of this paper;

4) to calculate the volumetric average temperature rises in the booster and holding windings:

$$\theta_{bav} = \left[\frac{2}{r_b^2 - r_f^2} \cdot \int_{r_f}^{r_b} \theta_b(r) \cdot r \cdot dr \right], \quad (71)$$

$$\theta_{hav} = \left[\frac{2}{r_h^2 - r_b^2} \cdot \int_{r_b}^{r_h} \theta_h(r) \cdot r \cdot dr \right]. \quad (72)$$

4) if the obtained values of temperature rises significantly differ from the values of θ_{bavi} and θ_{havi}, that is, the following conditions are not satisfied:

$$|(\theta_{bavi} - \theta_{bav}) / \theta_{bavi}| < \varepsilon \text{ and } |(\theta_{havi} - \theta_{hav}) / \theta_{havi}| < \varepsilon, \quad (73)$$

where ε is a small predetermined positive number, then θ_{bavi} and θ_{havi} are assigned the values of θ_{bav} and θ_{hav}, respectively, and the calculations are repeated starting from step 1) for new values of θ_{bavi} and θ_{havi}.

The described calculation cycle is repeated until condition (73) is satisfied.

The experience of calculations shows that this iteration process converges quite quickly (the number of iterations n usually does not exceed 12), and the use of the Maple computing environment significantly simplifies the programming of this very cumbersome task.

Calculation results and comparison with experimental data.

In order to verify the operability of the above technique and algorithm for calculating, the thermal field of electromagnets operating in complex forced control systems, the authors performed test calculations of heating of the electromagnet windings of the serial vacuum contactor КВТн-250/1,14 [16], in which the forced control system the circuit of which is shown in Fig. 4 is used, intended for operation in control networks with a nominal voltage of 220 V. The calculations are performed in accordance with the initial data indicated in [16], with the additions given below (if the corresponding data are not given in the text of this paper): r_c = 13 mm; r_f = 15 mm; r_b = 19 mm; r_h = 27.5 mm; r_e = 29.5 mm; l_{ap} = 75 mm; l_{yp} = 75 mm; l_w = 64 mm; b_a = 50 mm; b_y = 70 mm. The designations of the initial data correspond to the designations that are used in the text of this paper. The calculation results are presented in Table 1, which also shows the experimental data indicated to the right of the slashes. As it can be seen, the calculation results are slightly different from the experimental data: the difference does not exceed 10%, which can be considered acceptable for thermal calculations. (69)

Table 1

Results of calculations and experimental data

U, V	220DC	220AC	80DC	80AC
θ_b, K	62,8/61,7	55,5/57,9	121,9/126	114,1/122,5
θ_h, K	63,9/66,9	56,4/59,6	117,8/112,7	110,6/105,9
θ_c, K	54,6/57,3	48,6/47,0	111,5/112,3	104,6/103,4
θ_{max}, K	64,2 (h)	56,6 (h)	122 (b)	114,0 (b)
R_b, Ω	79/82	77/81	91/99	90/98
R_h, Ω	1115/1047	1090/1023	1295/1193	1271/1171
I_b, A	0,092/0,093	0,097/0,098	0,49/0,50	0,463/0,475
I_h, A	0,092/0,093	0,086/0,088	0/0	0,025/0,025
P_c, W	0	0,10	0	0,15
I_c, A	0	24,2	0	16,3
n	6	8	12	12

Notes:

1. At U = 220 V (AC and DC), the electromagnet clearly operated, and at U = 80 V (AC and DC) the electromagnet did not operate.

2. The experimental determination of temperature rise was carried out using the resistance method (IEC 60947-1, 8.3.3.3.2)

Calculations show that despite significant current ripples in the booster winding (Fig. 7), the eddy currents in the magnetic core do not reach such values at which the magnetic core would be a heat source: as can be seen from Table 1, the power of losses in it is at the level of 1 – 2 W.

This means that the magnetic core of the electromagnet in such forced control systems can be considered as a kind of radiator contributing to a decrease in the heating of the windings or, while maintaining the temperature of their heating, to a decrease in the consumption of the winding wire. Such an effect can be achieved with certain structural and technological solutions: the coil frame should be made of insulating material with large thermal conductivity, and its tubular part should be as small as possible in thickness and it should be tightly pressed on to the core.

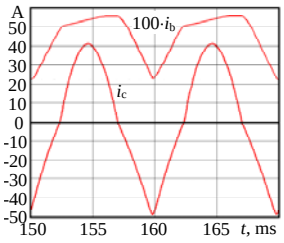

Fig. 7. Currents in the booster winding i_b and in the magnetic core i_c at U = 80 V AC

Conclusions.

1. The multiphysics model of stationary heating of the windings presented in the paper allows to take into account the peculiarities of the operation of electromagnets in complex forced control systems, in particular, ripple currents in the windings and losses in the magnetic core when powered by a rectified voltage source.

2. The algorithm developed by the authors for calculating the thermal field of electromagnets operating in forced control systems is a complex iterative cycle. Its implementation is significantly simplified by using the Maple computing environment, which allows to speed up the modeling process, perform cumbersome transformations, and obtain computer simulation results in a convenient tabular and/or graphical form.

3. The adequacy of the developed mathematical model and algorithm for complex shapes of current curves in windings is confirmed by experimental data.

4. The magnetic core of an electromagnet in such forced control systems, not only when powered from DC voltage sources, but when powered from AC voltage sources through a rectifier, can be considered as a kind of radiator that reduces the heating temperature of the windings or, while maintaining their heating temperature, allowing to reduce the consumption of winding wire.

REFERENCES

1. Klymenko B.V. *Forced electromagnetic systems*. Moscow, Enegroatomizdat Publ., 1989. 160 p. (Rus).

2. Zalessky A.M., Kukekov G.A. *Thermal calculations of electrical apparatus*. Leningrad, Energy Publ., 1967. 378 p. (Rus).

3. Loginov V.S. *Approximate methods for thermal calculation of the active elements of electrophysical installations*. Moscow, Physmatlit Publ., 2009. 272 p. (Rus).

4. Chunihin A.A. *Electrical apparatus. General course*. Moscow, Energoatomizdat Publ., 1988. 720 p. (Rus).

5. Akimov E.G., Belkin G.S., Godzhello A.G. *Fundamentals of the theory of electrical apparatus. Textbook. Ed. P.A. Kurbatov. 5th Edition*. St. Petersburg, Lan Publ., 2015. 588 p. (Rus).

6. Kuznetsov R.S. *Apparatus for the distribution of electrical energy for voltages up to 1000 V*. Moscow, Energy Publ., 1970. 544 p. (Rus).

7. Taev I.S. *Electrical control apparatus*. Moscow, High school Publ., 1969. 444 p. (Rus).

8. Alexandrov G.N., Borisov V.V., Kaplan G.S. *Theory of electrical apparatus: Textbook for Universities. Ed. Prof. G.N. Alexandrov. 2nd Edition*. St. Petersburg, Publishing House of SPbTU, 2000. 540 p. (Rus).

9. Pekker I.I., Nikitenko A.G. *Calculation of electromagnetic mechanisms on computers*. Moscow, Energy Publ., 1967. 168 p. (Rus).

10. Petrov G.N. On the heating of current-flowing coils. *Bulletin of Electrical Engineering Industry*, 1930, no.2 (Rus).

11. Jakob M. Influence of non-uniform development of heat upon the temperature distribution in electrical coils and similar heat sources of simple form. *Trans. ASME*, 1943, vol.65, pp. 593-605.

12. Liubchik M.A. *Calculation and design of DC and AC electromagnets of direct and alternating current*. Moscow, GEI Publ., 1959. 227 p. (Rus).

13. Mikheev M.A., Mikheeva I.M. *Heat transfer basics. 2nd Edition*. Moscow, Energy Publ., 1977. 344 p. (Rus).

14. Holman J.P. *Heat Transfer*. McGraw-Hill, NY, 2002. 665 p.

15. Lykov A.V. *Heat conductivity theory*. Moscow, High school Publ., 1967. 600 p. (Rus).

16. Baida Ye.I., Clemens M., Klymenko B.V., Korol O.G., Pustovoitov P.Ye., Application of the computing environment maple to the calculation of the dynamics of the electromagnets in the complicated systems of forced control. *Electrical Engineering & Electromechanics*, 2019, no.3, pp. 18-23. **doi: 10.20998/2074-272X.2019.3.03**.

17. Korol O.G., Klymenko B.V., Eresko O.V. Investigations of transients in the forced control device of the vacuum contactor monostable electromagnet. *Bulletin of NTU «KhPI». Series: Problems of Electrical Machines and Apparatus Perfection. The Theory and Practice*, 2018, no.32(1308), pp. 34-40 (Ukr). **doi: 10.20998/2079-3944.2018.32.06.**

Received 18.07.2019

Ye.I. Baida[1], *M. Clemens*[2], *B.V. Klymenko*[1], *O.G. Korol*[1], *M.G. Pantelyat*[1] *P.Ye. Pustovoitov*[1]

[1] National Technical University «Kharkiv Polytechnic Institute», 2, Kyrpychova Str., Kharkiv, 61002, Ukraine, phone +380 57 7076281, e-mail: b.v.klymenko@gmail.com

[2] University of Wuppertal, Rainer-Gruenter-Straße 21, 42119 Wuppertal, Germany, phone +49 202 439-1924, e-mail: clemens@uni-wuppertal.de

Peculiarities of calculating stationary heating of windings operating in complex forced control systems.

General description of the research topic. *A technique and an algorithm for calculating the thermal field of electromagnets operating in complex forced systems proposed by authors are considered. The widespread use of such devices in electromechanical switching devices allows not only to increase their speed but also significantly reduce the size, mass and energy losses, which indicates the relevance of this topic. The mathematical model of heating the windings of forced electromagnets proposed by the authors is a system of 1D differential equations of stationary heat transfer in a cylindrical coordinate system, supplemented by equations of electrical and magnetic circuits. This model allows to take into account the ripple of the currents in the windings and the losses in the magnetic core due to these ripples, contains certain signs of* ***scientific novelty*** *and represents the* ***goal of the paper****. The algorithm developed by the authors for calculating the thermal field of electromagnets operating in forced control systems is a complex iterative cycle. Its implementation is greatly simplified by using the Maple computing environment which allows to realize complicated and cumbersome mathematical transformations, automates the process of computations, and obtain results of numerical simulation in a convenient tabular and/or graphic form, which indicates the* ***practical significance*** *of this works. The results of comparison of computation results with experimental data presented in the paper indicate the adequacy of the model and algorithm proposed.* References 17, tables 1, figures 7.

Key words: **electromagnets, thermal field, forced control, switching devices, Maple computing environment, computer simulation.**

How to cite this article:

Baida Ye.I., Clemens M., Klymenko B.V., Korol O.G., Pantelyat M.G., Pustovoitov P.Ye. Peculiarities of calculating stationary heating of windings operating in complex forced control systems. *Electrical engineering & electromechanics*, 2019, no.5, pp. 12-19. **doi: 10.20998/2074-272X.2019.5.02.**

UDC 621.313.333 **doi: 10.20998/2074-272X.2019.5.03**

V.V. Rymsha, I.N. Radimov, M.V. Gulyy, I.V. Merkulov

MOTORSOLVE SOFTWARE PACKAGE: VERIFICATION OF PARAMETERS AND CHARACTERISTICS OF THE BRUSHLESS PERMANENT MAGNET MOTOR

Purpose. ***The purpose of this paper is to include comparison of results of the modeling and calculation in the Mentor Siemens software MotorSolve and experiment of the brushless permanent magnet motor.*** ***Methodology.*** ***Numerical investigation using licensed software MotorSolve is performed. Calculations of motor parameters and characteristics are made using Finite Element Method. The experimental investigations were made on the hysteresis dynamometer AHD-603.*** ***Results.*** ***The results of the investigations show that the calculations of the parameters and characteristics of the motor in MotorSolve software almost match with the results of the experiments.*** ***Practical value.*** ***The high efficiency of the MotorSolve software for the modeling, calculation and research of the brushless permanent magnet motors are confirmed.*** References 4, tables 2, figures 10.
Key words: **brushless permanent magnet motor, stator winding data, experimental investigations.**

Розглянуто деякі можливості програмного комплексу MotorSolve для моделювання і аналізу вентильних двигунів з постійними магнітами. ***Наведено результати розрахунку параметрів і характеристик вентильного двигуна з відомими геометричними розмірами і даними обмотки статора.*** ***Результати розрахунку зіставлені з результатами експериментальних досліджень.*** Бібл. 4, табл. 2, рис. 10.
Ключові слова: **вентильний двигун з постійними магнітами, обмоткові дані статора, експериментальні дослідження.**

Рассмотрены некоторые возможности программного комплекса MotorSolve для моделирования и анализа вентильных двигателей с постоянными магнитами. ***Представлены результаты расчета параметров и характеристик вентильного двигателя с известными геометрическими размерами и обмоточными данными статора.*** ***Результаты расчета сопоставлены с результатами экспериментальных исследований.*** Библ. 4, табл. 2, рис. 10.
Ключевые слова: **вентильный двигатель с постоянными магнитами, обмоточные данные статора, экспериментальные исследования.**

Introduction. One of the advanced computer systems for the design and analysis of electric machines is the Mentor Siemens MotorSolve system, which is a software package that allows to simulate and calculate the parameters and characteristics of various types of electric machines [1]. The use of the MotorSolve system significantly speeds up the design process due to the availability of ready-made templates of designs for stators and rotors of induction machines, DC collector machines, and brushless permanent magnet machines, as well as an extensive library of materials used in electric machines.

Modeling an electric machine in the MotorSolve code, as well as determining its parameters and characteristics, is based on a circuit-field model. Magnetic field of the machine is calculated by the Finite Element Method, as well as in the well-known FEMM code. However, the FEMM code is not suitable for the direct calculation of the parameters and characteristics of the designed electrical machines without additional calculations outside the software.

Currently, brushless permanent magnet motors (BPMM) are a popular type of electric machine for special applications. There are a number of publications devoted to theoretical studies of BPMM in the MotorSolve software package, for example [2, 3]. However, there are very few publications devoted to verifying the calculation results of such machines in MotorSolve with the experimental results, and these are mainly scattered materials on the Internet. Verification is also of interest because the models and algorithms embedded in the MotorSolve code are closed to the user, which makes it impossible to assess the accuracy of the results obtained in the calculation.

In this regard, **the goal of the paper** is to compare the calculation results in the licensed software package MotorSolve of a BPMM which has known geometric dimensions and winding data with the experimental results.

Object of study. The object of the study is the BPMM, which was designed at «Electrical Engineering – New Technology» Ltd (Odessa) and is currently mass-produced (Fig. 1).

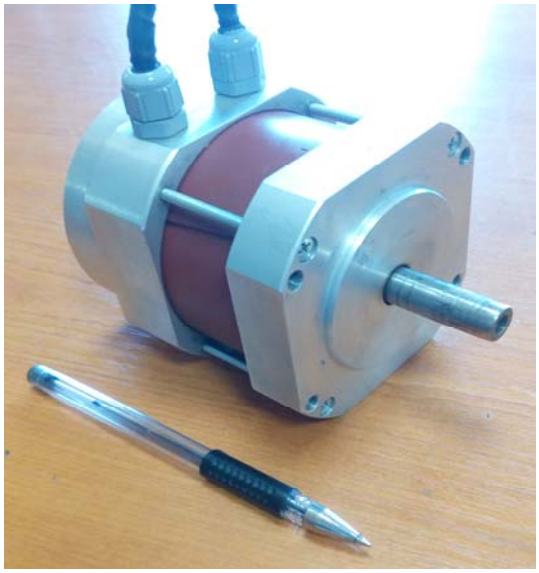

Fig. 1. External view of BPMM

For operation from a single-phase AC network 220 V 50 Hz, BPMM is equipped with a rotor position sensor and an electronic converter, which is a controllable

electronic switch and a rectifier device. The electronic switch according to the signals of the rotor position sensor provides BPMM operation in the mode of a brushless DC motor with 120-degree phase switching.

The geometric dimensions of the active part of the studied BPMM and its winding data are given in Table 1.

Table 1

BPMM geometric dimensions and winding data

Name	Value
Outer stator diameter, mm	82
Inner stator diameter, mm	50
Number of phases *m*	3
Number of stator slots *Z*	12
Number of rotor poles 2*P*	10
Gap between stator and rotor, mm	0,25
Stator package length, mm	42
Magnet height, mm	2,5
Magnet width, mm	12
Brand of magnet	N38SH
Winding connection circuit	Y
Number of turns in the coil	80
Wire diameter, mm	0,5

Creating a model of BPMM in the MotorSolve software package. Figure 2 shows the cross section of the active part of the studied BPMM obtained in the MotorSolve software package.

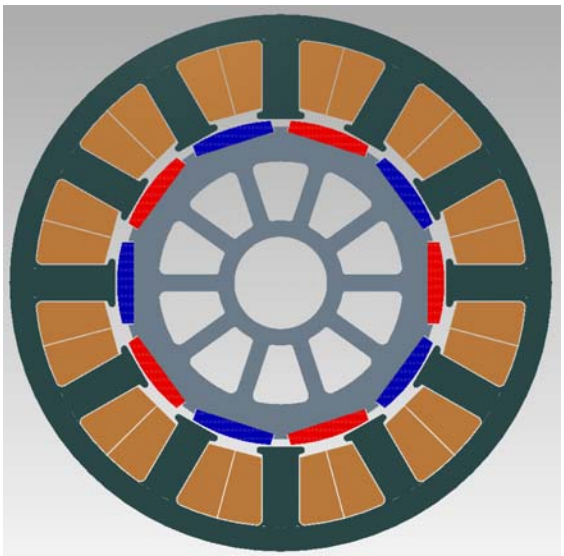

Fig. 2. Cross section of the BPMM active part

To reduce the mass and moment of inertia, the BPMM rotor is made in the form of a wheel with spokes and a low yoke height. The BPMM stator has open slots and a winding with a fractional number of slots per pole and phase: $q = \frac{Z}{2p \cdot m} = \frac{12}{10 \cdot 3} = \frac{2}{5}$. Pole division: $\tau = m \cdot q = 3 \cdot \frac{2}{5} = 1\frac{1}{5}$. Then the step of the winding is 1 and each of the coils covers one tooth. In this case, the stator coil winding has short frontal parts, which improves the temperature regime of the winding and, in addition, reduces the possibility of its breakdown due to the lack of phase overlap in the area of the frontal parts. The stator winding diagram is shown in Fig. 3.

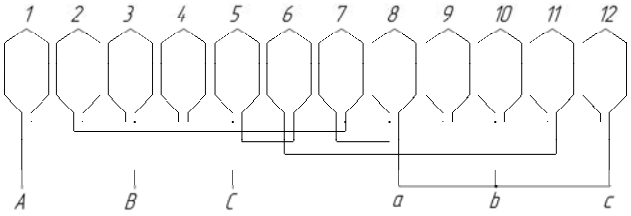

Fig. 3. BPMM stator winding diagram

The initial data for the procedure for forming a winding in the MotorSolve code are its type and connection circuit, wire diameter, number of parallel branches and the number of turns in the coil of the winding.

After setting the geometric dimensions, selecting active and structural materials, as well as forming the winding, the code allows to visualize the magnetic field in the form of lines of force for the selected position of the motor's rotor (Fig. 4).

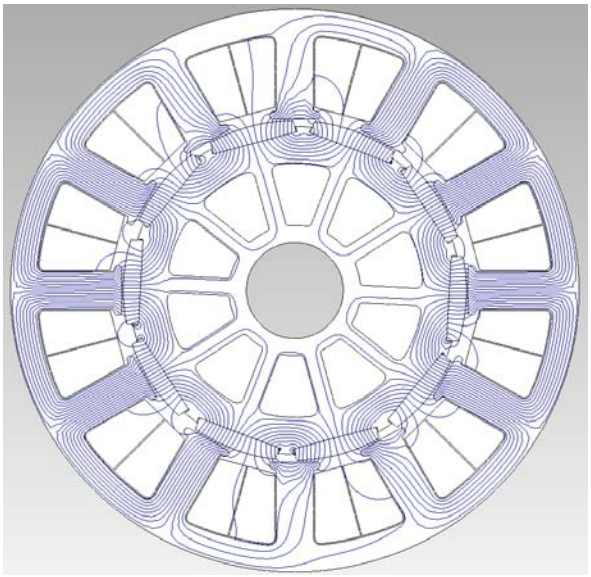

Fig. 4. BPMM magnetic field lines

Analysis of the distribution of the magnetic field of the motor allows to check the model of BPMM for the absence of errors in its formation. Figure 4 shows that the distribution of the magnetic field corresponds to the physics of the process occurring in electric machines.

After creating the BPMM model, the MotorSolve code calculates the masses of active materials and the total mass of the motor, the resistance of its winding, the moment of inertia of the rotor, as well as a number of other quantities.

Among the calculation results there is a recommendation on the advisability of skewing the stator magnetic core to eliminate cogging torque. For the considered BPMM, a skew of the stator magnetic core is recommended at an angle of 0.2 tooth divisions or at 6 mechanical degrees (30 electrical degrees). It should be noted here that the same skew value was determined on the basis of field calculations in the FEMM code when designing a serial BPMM and was incorporated into the

design documentation for the electric motor. As practice has shown, in serially produced electric motors, the cogging torque is practically absent.

Verification of parameters, design constants and characteristics of BPMM. The results of calculating the parameters and constants of the studied BPMM in the MotorSolve code are presented in Fig. 5.

	Prototype Design
Ke (peak line-line Back-EMF over speed) (V/krpm)	116
Kt (derived from Ke) (N·m/A)	1.36
Ld (d-axis inductance) (mH)	6.55
Lq (q-axis inductance) (mH)	8.76
Lllmin (minimum line-line inductance) (mH)	13.1
Lllmax (maximum line-line inductance) (mH)	17.5
Rs (stator phase resistance) (Ω)	3.27
Rll (stator line-line resistance) (Ω)	6.54
Phi_m (magnet d-axis flux linkage) (Wb)	0.123

Fig. 5. MotorSolve code output after BPMM parameters calculation

It is advisable to begin verifying the BPMM parameters with inductances, the values of which are necessary in the calculations of transients, the electromagnetic time constant, and the reactive component of the electromagnetic torque.

In Fig. 5: $Lll_{\min}$ (minimum line-line inductance) is the stator winding inductance along the longitudinal (d) axis, and $Lll_{\max}$ (maximum line-line inductance) is the stator winding inductance along the transverse (q) axis. The values of these inductances are twice as large as the values of the inductances of the stator winding phase, indicated in Fig. 5 as L_d and L_q respectively ($Lll_{\min} = 2 \cdot L_d$, $Lll_{\max} = 2 \cdot L_{dq}$).

Let us compare the calculation results with experimental data. The inductances of the serial BPMM were measured using the DCR-9935 LCR-meter and a mechanical device that allows the motor shaft to be rotated by a predetermined angle. The results of comparing inductances are summarized in Table 2.

Table 2

BPMM inductances

Value	Calculation	Experiment
$Lll_{\min}$, mH	13,1	13,8
$Lll_{\max}$, mH	17,5	18,1

Table 2 shows that the results of calculation and experiment have good convergence. In addition, as is known, a feature of BPMM (unlike synchronous motors with electromagnetic excitation) is that the stator winding inductance along the d axis is smaller than the stator winding inductance along the q axis, which is confirmed by the data in Fig. 5 and Table 2.

Consider the correspondence between the calculated and experimental data of the flux linkage of the stator winding of the motor, the value of which is included in the equation for calculating the active (main) component of the electromagnetic torque of BPMM [4]. As a result of calculation in MotorSolve, the value of the flux linkage of the phase of the winding is obtained at its orientation along the d axis (*Phi_m* in Fig. 5) $\Psi_f = 0.123$ Wb. In this case, there is a maximum linkage of the winding phase with the flux created by the permanent magnets of the rotor. When the winding is connected according to the «Y» circuit, two winding phases connected in series are shifted in the magnetic field of the permanent magnets by an angle of 60 electrical degrees. In this case, the value of the flux linkage of the winding is greater than the flux linkage of the phase at $\sqrt{3}$ time, i.e. $\Psi_{MS} = \sqrt{3}\Psi_f =$ = 0.213 Wb.

To experimentally determine the flux linkage of the stator winding, the rotor of the serial BPMM is rotated at a constant speed from the racing electric motor (generator mode without connecting the load). Using the ADDS1062CM digital oscilloscope, an oscillogram of the change in the linear EMF of the BPMM stator winding in time $e = f(t)$ is recorded (Fig. 6).

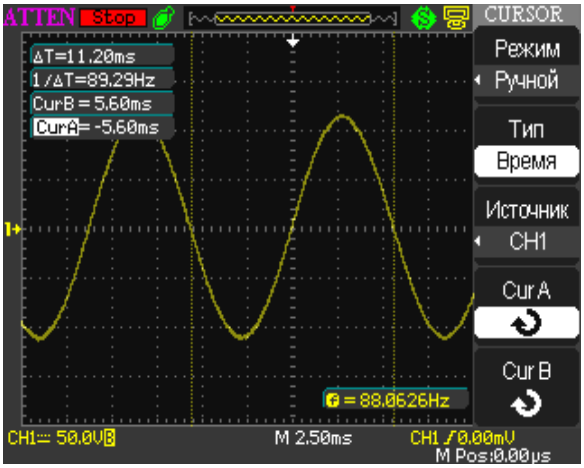

Fig. 6. Experimental oscillogram $e = f(t)$

Scale on the oscillogram: vertical – 50 V/div., horizontal – 2.5 ms/div.

As can be seen from Fig. 6, the linear EMF has a shape close to sinusoidal. Based on the presented experimental oscillogram, we calculate the flux linkage of the BPMM stator winding:

$$\Psi_{\text{E}} = \frac{E_{\max} \cdot \Delta T}{2\pi} = \frac{118{,}5 \cdot 10^{-3}}{2\pi} = 0{,}211 \text{ Wb}, \qquad (1)$$

where $E_{\max}$ is the amplitude EMF value; ΔT is the EMF change period.

Thus, a practical coincidence with the result of calculating the stator winding flux linkage obtained in the MotorSolve software package Ψ_{MS} = 0.213 Wb is confirmed.

Knowing the flux linkage, it is possible to determine the constant of EMF of the electric motor K_e and the constant of the torque of the electric motor K_t. These constants characterize the electromechanical conversion of energy in electrical machines. They are numerically equal to each other when applying a single system of units.

The constant of EMF K_e is equal to the product of the number of pole pairs p and flux linkage of the stator winding. According to the experiment, the constant K_e when calculating through flux linkage:

$$K_e = p \cdot \Psi_{\text{E}} = 5 \cdot 0{,}211 = 1{,}055 \text{ V·s}, \qquad (2)$$

and obtained in the MotorSolve code:

$$K_e = p \cdot \Psi_{MS} = 5 \cdot 0{,}213 = 1{,}065 \text{ V·s}. \quad (3)$$

On the other hand, according to Fig. 5, the constant K_e = 116 V/1000 min^{-1}, or $K_e = 116 \cdot \frac{9{,}55}{1000} = 1{,}107$ V·s.

Thus, the discrepancy between the constant of EMF K_e obtained in two ways based on the calculated data of MotorSolve shown in Fig. 5 is 3.9 %. This difference is most likely due to the calculation error in the MotorSolve of EMF obtained by differentiating the stator winding flux linkage. Unfortunately, the MotorSolve code does not have the ability to evaluate the degree to which the stator winding flux linkage matches the sine waveform.

The torque constant K_t, numerically equal to the constant of EMF K_e, which is calculated through the flux linkage of the winding from the MotorSolve code, is K_t = 1.065 N·m/A.

As for the torque constant K_t = 1.36 N·m/A shown in Fig. 5, it is determined artificially from the constant of EMF K_e by dividing by K_e, and therefore is not a parameter of BPMM. At the same time, the above other parameters obtained by calculation in the MotorSolve program have good agreement with the experiment.

It is of interest to compare the calculated and experimental mechanical characteristics of the studied BPMM, as well as the change in the motor current in time at a given load on the shaft. The mechanical characteristics were experimentally determined on a bench with the AHD-603 hysteresis dynamometer, with which the BPMM was loaded (Fig. 7).

The calculations and experimental determination of the characteristics were carried out at a constant («smooth») voltage in the DC link of the 270 V electronic switch to exclude the influence of the rectification circuit on the characteristics of BPMM. Figure 8 shows the calculated (in MotorSolve) and experimental «natural» mechanical characteristics of the studied BPMM obtained when the motor was running without speed control (filling the PWM signal is 1).

The presented mechanical characteristics show acceptable convergence of the calculation with the experiment. The idle rotation speed of the calculated characteristic is less than the experimental idle rotation speed by 3.3 %. At the same time, the stiffness of the calculated mechanical characteristic is slightly greater than the rigidity of the experimental mechanical characteristic.

Figures 9, 10 show the calculated and experimental oscillograms of the phase current of BPMM during its operation with the opposing load torque on the shaft of 1 N·m.

The calculated characteristic was determined at a rotational speed of 2270 rpm. The average current value was 1.04 A.

Comparison of the oscillograms in Fig. 9, 10 allows to conclude that the calculated and experimental values of the currents correspond to physical representations of transients during switching of the phases of the stator winding, are correlated in shape and amplitude, and also once again confirm the adequacy of the calculation of the BPMM parameters in the MotorSolve software package.

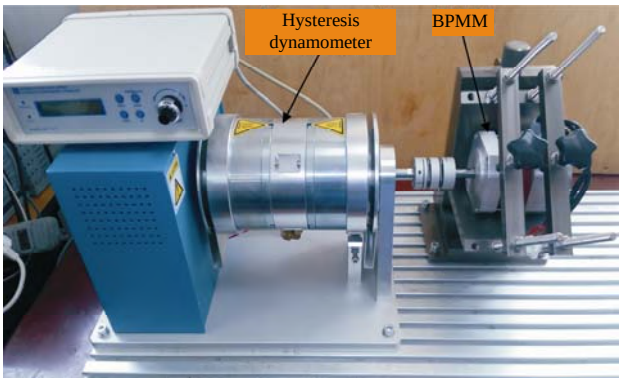

Fig. 7. General view of the experimental bench

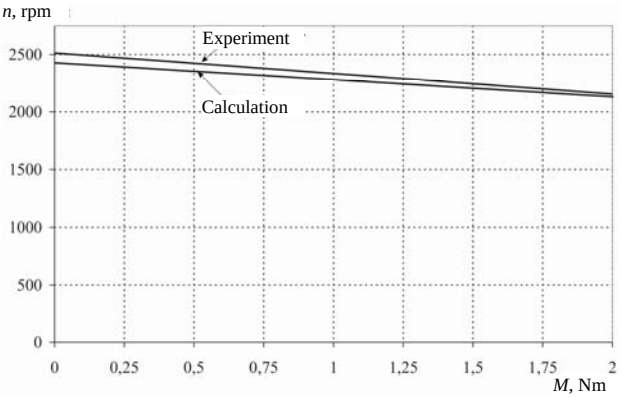

Fig. 8. BPMM «natural» mechanical characteristics

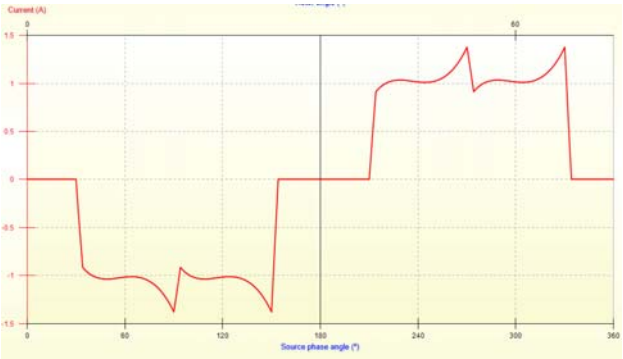

Fig. 9. Calculated oscillogram of the BPMM phase current at BPMM operation with load of 1 N·m

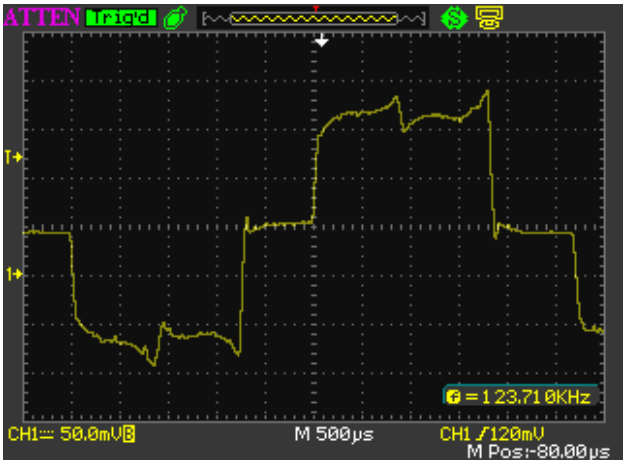

Fig. 10. Experimental oscillogram of the phase current at BPMM operation with load of 1 N·m

Experimental oscillogram of the phase current was obtained using an ADS1062CM digital oscilloscope using a current sensor on a resistor with a resistance of 0.1 Ω. Scale on the experimental oscillogram: vertical – 0.5 A/div., horizontal – 0.5 ms/div. In the experiment, the BPMM rotation frequency was 2330 rpm, and the average current value was 1.1 A.

Conclusions.

1. Using the MotorSolve software package, the parameters and characteristics of the mass-produced BPMM were calculated. The calculation results have a slight difference from the data obtained experimentally, which confirms the high efficiency of the MotorSolve software package.

2. Unlike well-known codes for calculating the magnetic field, such as FEMM, the MotorSolve software package fully provides the calculation of parameters, transients and characteristics of the electric machine without the use of additional software.

REFERENCES

1. Available at: https://www.mentor.com/products/mechanical/motorsolve/ (accessed 10 April 2019).

2. Grebenikov V.V. Comparison of characteristics of electric motors with permanent magnets with external and internal rotors. *Hydropower Ukraine*, 2018, no.3-4, pp. 46-50. (Rus).

3. Grebenikov V.V., Pryimak M.V. Comparative analysis of magnetic electric motors with permanent magnets for electric buses. *Bulletin of NTU «KhPI». Series: «Electric machines and electromechanical energy conversion»*, 2016, no.11(1183). – pp. 42-48. (Rus).

4. Hendershot J.R., Miller T.J.E. *Design of brushless permanent-magnet motors*. Magna Physics Publishing and Clarendon Press, Oxford, 1994. 579 p.

Received 12.04.2019

V.V. Rymsha[1], *Doctor of Technical Science, Professor,*
I.N. Radimov[2], *Candidate of Technical Science, Associate Professor,*
M.V. Gulyy[2], *Candidate of Technical Science,*
I.V. Merkulov[1], *Senior Instructor,*
[1] Odessa National Polytechnic University,
1, Shevchenko Avenue, Odessa, 65044, Ukraine,
phone +380 48 7385855,
e-mail: rimsha61@gmail.com, miv080452@gmail.com
[2] Ltd. «Electrical Engineering – NewTechnology»,
26/2, Melnitskaya Str., Odessa, 65005, Ukraine,
e-mail: igor.radimov@gmail.com, mv.skbss@gmail.com

How to cite this article:
Rymsha V.V., Radimov I.N., Gulyy M.V., Merkulov I.V. MotorSolve software package: verification of parameters and characteristics of the brushless permanent magnet motor. *Electrical engineering & electromechanics*, 2019, no.5, pp. 20-24. **doi: 10.20998/2074-272X.2019.5.03.**

UDC 621.314 **doi: 10.20998/2074-272X.2019.5.04**

G.G. Zhemerov, D.S. Krylov, A.V. Mashura

ENERGY EFFICIENCY OF THE SUBWAY ELECTRICAL SUPPLY SYSTEM WITH ELECTRICAL ENERGY RECOVERY AT BRAKING

Purpose. ***The purpose of the paper is to assess the efficiency of the subway power supply system, which uses a four-quadrant DC drive with energy recovery in the supply network in the braking mode.*** ***Methodology.*** ***We have applied the theory of electrical circuits and mathematical simulation in Matlab package.*** ***Results.*** ***The theoretical dependence of the efficiency of the electrical supply system with a bidirectional flow of energy on the coefficient of resistive short circuit at the load terminals has been obtained. The theoretical result is verified by modeling.*** ***Originality.*** ***The equivalent circuit of the subway power supply system with a four-quadrant DC drive and the possibility of energy recovery to the supply network in braking mode is developed, its parameters are determined, and the schedule of the electric train movement was set.*** ***Practical value.*** ***The use of the obtained dependencies and simulation results will allow to determine the direction of the future development of the subway power supply system and optimize its energy efficiency.*** References 8, tables 1, figures 5.

Key words: **power supply system, energy, energy return coefficient, efficiency, energy recovery.**

Мета. ***Метою статті є оцінка ККД системи електропостачання метрополітену, в якій використовується чотирьохквадрантний привід постійного струму з рекуперацією енергії в мережу живлення в режимі гальмування.*** ***Методика.*** ***Для проведення досліджень використовувалася теорія електричних кіл, математичне моделювання в пакеті Matlab.*** ***Результати.*** ***Отримана теоретична залежність ККД СЕ з двонаправленим потоком енергії від коефіцієнта резистивного короткого замикання на клемах навантаження. Теоретичний результат перевірений моделюванням.*** ***Наукова новизна.*** ***Розроблена еквівалентна схема системи електропостачання метрополітену з чотирьохквадрантним приводом постійного струму і можливістю рекуперації енергії в мережу живлення в режимі гальмування, визначені її параметри, заданий графік руху електропоїзда.*** ***Практичне значення.*** ***Використання отриманих залежностей і результатів моделювання дозволить визначити напрямок перспективного розвитку системи електропостачання метрополітену, оптимізувати її енергоефективність.*** Бібл. 8, табл. 1, рис. 5.

Ключові слова: **система електропостачання, енергія, коефіцієнт повернення енергії, коефіцієнт корисної дії, рекуперація енергії.**

Цель. ***Целью статьи является оценка КПД системы электроснабжения метрополитена, в которой используется четырёхквадрантный привод постоянного тока с рекуперацией энергии в питающую сеть в режиме торможения.*** ***Методика.*** ***Для проведения исследований использовалась теория электрических цепей, математическое моделирование в пакете Matlab.*** ***Результаты.*** ***Получена теоретическая зависимость КПД СЭ с двунаправленным потоком энергии от коэффициента резистивного короткого замыкания на клеммах нагрузки. Теоретический результат проверен моделированием.*** ***Научная новизна.*** ***Разработана эквивалентная схема системы электроснабжения метрополитена с четырёхквадрантным приводом постоянного тока и возможностью рекуперации энергии в питающую сеть в режиме торможения, определены её параметры, задан график движения электропоезда.*** ***Практическое значение.*** ***Использование полученных зависимостей и результатов моделирования позволит определить направление перспективного развития системы электроснабжения метрополитена, оптимизировать её энергоэффективность.*** Библ. 8, табл. 1, рис. 5.

Ключевые слова: **система электроснабжения, энергия, коэффициент возврата энергии, коэффициент полезного действия, рекуперация энергии.**

Introduction. The functioning of the transport system of a modern large city is impossible without the use of the subway, which provides a significant part of passenger traffic. Its high reliability is combined with not the highest energy efficiency, which is due to the use of a DC collector electric drive of sequential excitation without the possibility of returning energy to the supply network. Many scientific works have been devoted to improving the efficiency of the subway power supply system [1-3]. One of the solutions to the problem of energy conservation is the use of a four-quadrant DC electric drive, which makes it possible to organize a bi-directional flow of electrical energy between the source and the load. This will allow the energy stored in the moving train to be return to the industrial network of three-phase alternating current, which, in turn, should increase the efficiency of the entire supply power supply system. However, as shown in [3], the effect of energy saving from the use of regenerative braking is not always obvious. It depends on the configuration of the used power supply system and the operating modes of the electric drive. Under certain conditions, the effect of reducing the total efficiency of the system due to the occurrence of additional losses during the return of energy to the network is possible.

The goal of the work is the assessment of the efficiency of the subway power supply system, which uses a four-quadrant DC drive with energy recovery to the supply network in the braking mode.

Traction substation structure. A traditional traction substation uses uncontrolled diode rectifiers to convert AC voltage to DC, which does not allow the return of energy to the supply network. To implement a possible increase in the efficiency of the circuit, instead of diode bridges, it is necessary to use a four-quadrant thyristor rectifier, shown in Fig. 1.

The network 6(10) *kV* is represented by a three-phase symmetric system of sinusoidal voltages u_{SA}, u_{SB}, u_{SC}. The network parameters are taken into account by the

active resistance R_0. The parameters of the line connecting the traction substation and the three-phase converter transformer 6(10) *kV* / 0.71 *kV* are determined by the active resistance R_1. The network windings of the transformer T_1 are connected to the network 6(10) *kV*, and the valve windings are connected to the six-pulse four-quadrant bridge rectifier *VS*1 – *VS*12. Losses in the thyristor bridge are represented by an equivalent source of counter-EMF of level of 1 *V* in the forward and reverse directions and transferred to the DC circuit. Line parameters from transformer T_1 to rectifier bridges correspond to the active resistance R_2. The load is represented by a DC motor with independent excitation. The line parameters from the controlled rectifier (CR) to the DC motor are taken into account by the resistance of the contact rail R_{KR}. The inductances in the power line, which are present there in fact, do not participate in the formation of losses during energy transfer, therefore they are transferred to the load and they are not shown in the equivalent circuit.

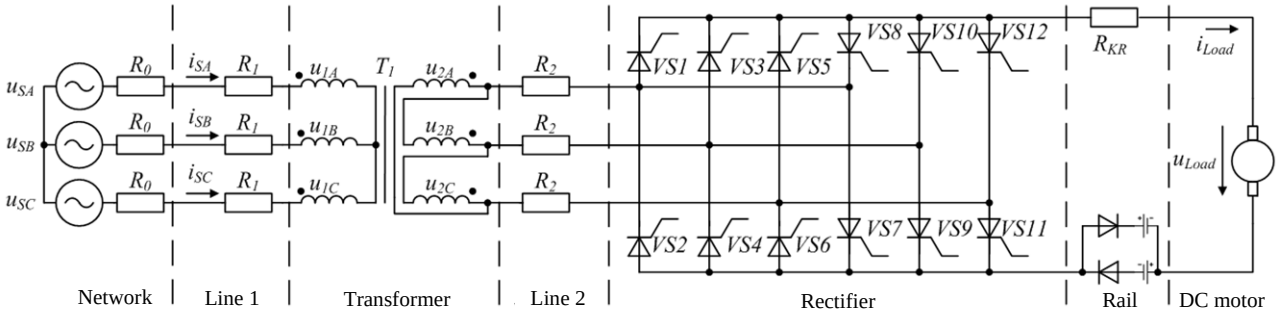

Fig. 1. Equivalent circuit of SPSS with four-quadrant CR

To adequately assess the energy efficiency of the subway power supply system (SPSS), it is necessary to know the train schedule, which, according to [1-3], contains the following intervals: the acceleration interval from zero to nominal speed (time t_{ac}) averages 20-30 *s*; braking time from nominal to zero speed (t_{br}) is on average 40-50 *s*; the train stop interval (time t_{st}) is usually 25 *s*; the interval of movement with nominal speed (t_{mov}) is 110-130 *s*. Taking into account that the time of movement of rolling stock between two stations is on average three minutes [1], in accordance with [3] we accept the following values of traffic intervals: t_{ac} = 25 *s*, t_{mov} = 115 *s*, t_{br} =45 *s*, t_{st} = 25 *s*.

The graph of changes in current, voltage, and load power for the indicated intervals of movement of the train in the considered SPSS can be of the form shown in Fig. 2.

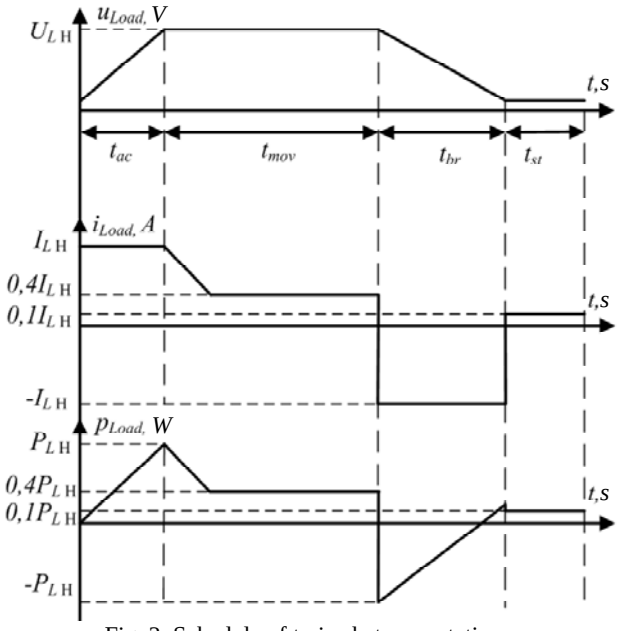

Fig. 2. Schedule of trains between stations

In the interval of the train acceleration t_{ac}, the automatic control system linearly changes the speed of the train from zero to nominal, which, with independent excitation of the DC machine, corresponds to a linear increase in the load voltage from zero to nominal. The load current is limited at the nominal level. The power developed at this stage also linearly rises to the nominal value. In the interval of movement t_{mov} at nominal speed, the nominal voltage will be applied to the load, and the train will overcome the drag and friction, developing up to 30-50 % of the nominal power. The current consumed by the load will be at the same level. In braking mode, the automatic control system provides a smooth linear decrease in speed to zero level during t_{br}. The load voltage will also decrease linearly to zero. In order to ensure the return of kinetic energy stored by the train to the supply network, it is necessary to change the polarity of the load current with its limitation at a level not exceeding the nominal value. With the beginning of recovery, the load current passes to the reversible valve group and is maintained negative until the energies returned and consumed by the train are equal at the braking stage. After that, the linearly changing load power becomes positive again, and the load current transfers to the positive valve group as a result of switching the rectifier bridges. In the stop interval t_{st} the electric drive of the train does not consume energy. At all stages of movement, the train consumes energy of its own needs, which is spent on heating, lighting and ventilation of cars, its value can reach 10 % of the nominal one. This is taken into account in the graphs presented in Fig. 2.

The power developed at the stages of movement depends on the physical parameters of the train, on its speed and mass. The mass of rolling stock is determined by the number of cars and the number of passengers in each car. According to [4], the train consists of five cars with a mass of 33 *t* each. The car accommodates from 200 to 300 passengers with an average weight of 60-70 *kg*.

Thus, we can assume that the mass of the train is 200-250 *t*. The nominal speed is 25 *m/s* or 90 *km/h*. According to [4], trains operating on the subway lines are equipped with an electric drive with nominal power of up to 2 *MW*. In an equivalent circuit for further calculations and modeling, an *NP800KS* motor with a nominal power of 2.013 *MW* and a nominal current of 3053 *A* was chosen. Moments of resistance and inertia of the train are reduced to its rotor.

To calculate the energy of losses in a bidirectional flow, it is necessary to set the parameters of the SPSS circuit shown in Fig. 1. The characteristics of the supply network are determined by the parameters of the three-phase transformer of the supply substation type TMH 4000/35/6 [1], for which the phase resistance R_0 = 0.1 Ω [1]. The parameters of line 1 (see Fig. 1) are determined by the distance between the traction substation and the converter transformer, which, on average, is from 1 to 3 *km* [1]. The aluminum three-wire cable used in line 1 has a phase resistance value R_1 of 0.3 Ω/*km*, and its cross section is selected according to the current that the considered drive can consume, and is equal to 95 mm^2 [1]. The ТСЗП-2500/10У3 6(10)/0.71 *kV* series converter transformer has a nominal power of 2.509 *MW* and short circuit losses of 20 *kW*. The total equivalent resistance of his phase R_{TV} will be 2 *m*Ω. The parameters of line 2 are determined by the distance between the converter transformer T_1 and the rectifier, which is assumed to be 50 *m*. In this case, the cross section of the copper cable will be equal to 1000 mm^2, the value of the phase resistance R_2 is 0.9 *m*Ω. The R_{KR} steel contact rail has a standard cross-section of 6600 mm^2 and a resistance of 9 *m*Ω/*km*. Its length can vary from 1 to 3 *km*, depending on the location of the train on the run between stations. The active resistance of the previously selected DC machine is 8 *m*Ω.

Efficiency of SPSS with bidirectional energy flow. Let us evaluate the efficiency of the power supply system shown in Fig. 1. According to [3], the maximum possible efficiency of SPSS with a bi-directional energy flow is determined by the formula:

$$\eta_{\max\leftrightarrow} = \frac{\eta_{\max\rightarrow}(2-\eta_{\max\leftarrow}^{-1})-k_E}{1-k_E}, \qquad (1)$$

where $\eta_{\max\rightarrow}$ and $\eta_{\max\leftarrow}$ are the maximum possible values of the efficiency of three-phase SPSS in the forward and reverse energy flows, respectively; k_E is the coefficient of energy return from the load to the source, determined by the expression from [3]:

$$0 \le k_E = \frac{P_{S\leftarrow}}{P_{S\rightarrow}} \le 1, \qquad (2)$$

where $P_{S\leftarrow}$ and $P_{S\rightarrow}$ are the source powers in forward and reverse energy flows, respectively.

The value of the maximum possible efficiency of the SPSS in a direct energy flow $\eta_{\max\rightarrow}$ is determined by the expression [3]:

$$\eta_{\max\rightarrow} = \frac{1}{2} + \sqrt{\frac{1}{4} - \frac{1}{k_{SC}}}, \qquad (3)$$

where k_{SC} is the short circuit coefficient, determined by the ratio of the short circuit power at the load terminals to the net active load power:

$$k_{SC} = \frac{P_{SC}}{P_{usf}}, \qquad (4)$$

where P_{SC} is the power of the resistive short circuit of SPSS with the load off; P_{usf} is the average value of the effective active load power in the repeatability interval of the train schedule according to Fig. 2.

The values of P_{usf} and k_E depend on the train schedule, task intervals, acceleration and braking speeds of the train. The power of the resistive short circuit P_{SC} depends on the configuration of SPSS and can be determined from the relation:

$$P_{SC} = \frac{3U_{sm}^2}{2R_\Sigma}, \qquad (5)$$

where U_{sm} is the amplitude of the sinusoidal phase voltage of the power source; R_Σ is the equivalent active resistance of SPSS shown in Fig. 1.

The value of the active equivalent resistance of the power supply system, according to Fig. 1 includes the following components:

$$R_\Sigma = R_0^{'} + R_1^{'} + R_{TV} + R_2 + R_{RF} + R_{KR} + R_J, \qquad (6)$$

where $R_0^{'}$ is the phase resistance of the AC voltage source 6(10) *kV*, reduced to the secondary winding of the converter transformer (CT); $R_1^{'}$ is the resistance of the section phase of line 1, reduced to the secondary winding of the CT; R_{TV} is the total resistance of the CT phase; R_2 is the resistance of the section phase of line 2 from the transformer to the rectifier; R_{RF} is the resistance of the controlled rectifier; R_{KR} is the resistance of the contact rail; R_J is the resistance of the armature circuit of the DC motor.

The value of the maximum possible efficiency of the SPSS in the reverse energy flow $\eta_{\max\leftarrow}$ can be determined by the following expression [3]:

$$\eta_{\max\leftarrow} = \frac{1}{1+k_E^2 k_{SC}^{-1}}. \qquad (7)$$

We find the value of the maximum possible efficiency of SPSS with a bi-directional energy flow and determine the possible range of its changes using the above expressions.

To determine the coefficient of energy return from the load to the source k_E, according to (2), it is necessary to know $P_{S\leftarrow}$ and $P_{S\rightarrow}$. Their values can be determined from the train schedule shown in Fig. 2. Having calculated the area under the curve of the graph of power changes for the forward and reverse energy flows, we obtain the values $P_{S\rightarrow}$ = 50.3 *MW*, $P_{S\leftarrow}$ = 108.7 *MW* and, in accordance with (2), k_E = 0.5.

We find the average value of the effective load active power by integrating the instantaneous power graph in the interval of train repeatability. The value P_{usf} = 1.44 *MW* was obtained.

To find the power of the resistive short circuit P_{SC}, we determine the components of the equivalent active

resistance of the power supply system R_Σ and the possible range of their changes.

According to the above data, the reduced phase resistance of the source phase $R_0^{'}$ can be calculated by the expression:

$$R_0^{'} = kR_0, \quad (8)$$

where $k = 1/k_{tr}^2$ is the coefficient of reduction of the parameters of the elements of the primary winding of the converter transformer to the secondary, equal to 0.014. The resistance $R_0^{'}$ value is 1.4 *m*Ω.

Similarly, the reduced phase resistance of line 1 $R_1^{'}$ is calculated:

$$R_1^{'} = kR_1. \quad (9)$$

The remaining components of expression (6) and the possible range of their changes were determined above, the parameter values are summarized in Table 1, according to which the resistance $R_1^{'}$ lies in the range from 4.2 *m*Ω to 12.6 *m*Ω. Active equivalent resistance of SPSS R_Σ, shown in Fig. 1 will have values ranging from 27 *m*Ω to 44 *m*Ω.

Table 1

Resistances of the SPSS circuit and the range of their changes

Parameter		Value
$R_0^{'}$, *m*Ω		1.4
$R_1^{'}$, *m*Ω	1000 *m*	4.2
	2000 *m*	8.4
	3000 *m*	12.6
R_{TV}, *m*Ω		3
R_2, *m*Ω		1
R_{RF}, *m*Ω		1
R_{KR}, *m*Ω	1000 *m*	9
	2000 *m*	13.5
	3000 *m*	18
R_J, *m*Ω		8

The short-circuit power P_{SC} calculated according to (5), depending on the circuit parameters, has a value from 34 to 56 *MW*. The short circuit coefficient calculated according to (4), depending on the active equivalent resistance, lies in the range from 25 to 40.

In a real power supply system, additional losses of electricity may be present, which can be taken into account in theoretical calculations by introducing the coefficient of additional losses k_{add}. In this case, the efficiency of the SPSS can be calculated from [3] by the expression:

$$\eta_{real\leftrightarrow} = \frac{\dfrac{1-k_E^2 k_{SC}^{-1} k_{add\leftarrow}}{1+\left(\left(0.5+\sqrt{0.25-k_{SC}^{-1}}\right)^{-1}-1\right)k_{add\rightarrow}} - k_E}{1-k_E}. \quad (10)$$

A graph of the real efficiency of SPSS with a bi-directional energy flow on the short-circuit coefficient at the load terminals k_{sc} is shown in Fig. 3 by dashed line.

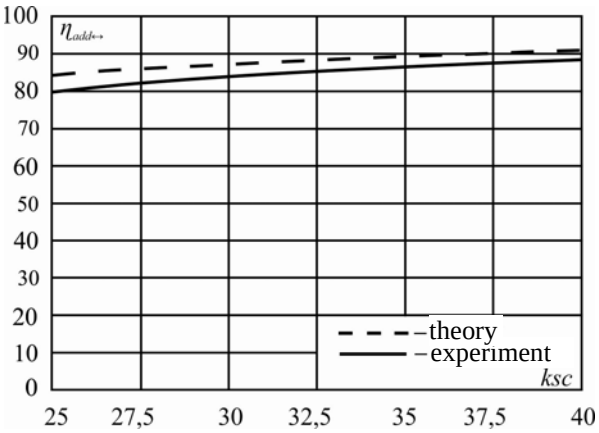

Fig. 3. Efficiency of SPSS

Modeling of SPSS with bidirectional energy flow. For experimental verification of theoretical results, the *MatLab* model of SPSS with a four-quadrant controlled rectifier, simulating the circuit shown in Fig. 1 was developed. *MatLab* model is shown in Fig. 4. It consists of the following blocks:

- power circuit – blocks 1, 3, 4, 5, 7, 8, 10;
- thyristor CR control system – block 6;
- torque, current and speed controllers – blocks 9, 13;
- current and voltage sensor – block 2;
- calculator – block 11;
- multipath oscilloscope – block 12.

Purpose of power circuit blocks: 1 – industrial network; 3 – cables connecting the traction substation and the three-phase conversion transformer 6(10) *kV* / 0.71 *kV*, which is indicated by block 4; 5 – cables coming from the transformer 4 to the rectifier bridges 7; 8 – steel contact rail connecting the CR with a DC motor 10.

The parameters of the power circuit elements in the model were set in strict accordance with SPSS data given above. Data of the DC motor model correspond to those for a *NP800KS* type machine. The mechanical part of the electric drive was reduced to the rotor of a DC machine, and the kinetic energy stored by the train during movement was reduced to the energy of an equivalent flywheel. The DC machine load specified in block 9 takes into account both the losses of own needs and the friction and drag of the air to the moving train.

The rectifier control system is built on a vertical principle and has an arccosinusoidal characteristic of a phase-shifting device. The bridge switching logic monitors the reference signal from the controller output and the instantaneous value of the load current, making a decision to transfer pulses depending on their superposition.

The autoregulation system is made in a closed manner using a dual-circuit slave current-speed controller tuned to a technical optimum. This ensured the qualitative maintenance of the set speed in accordance with the train schedule.

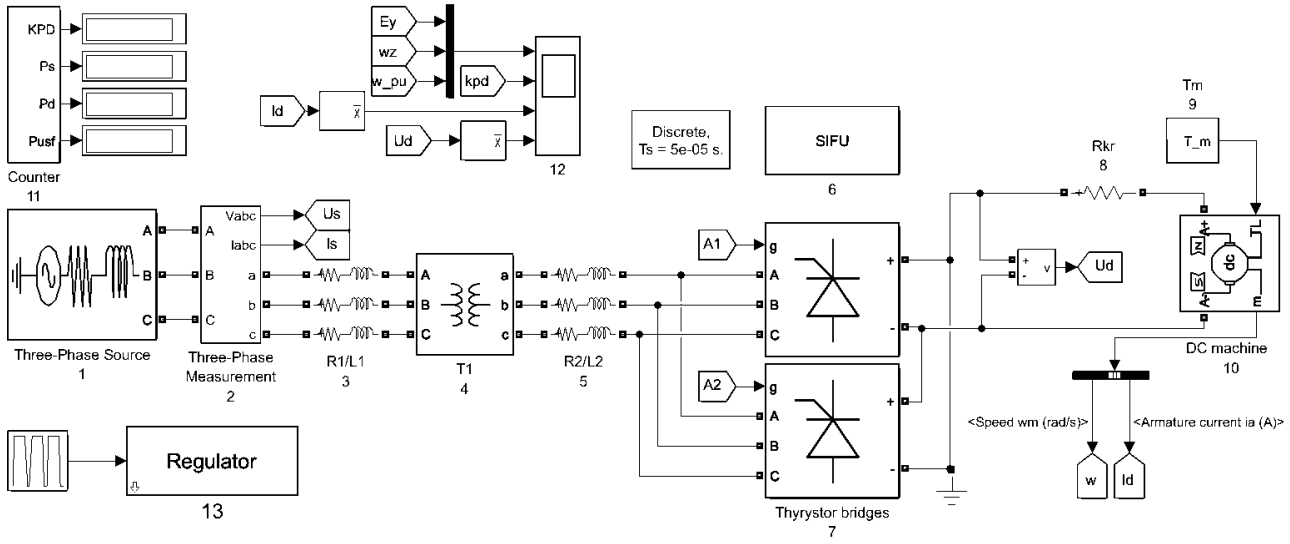

Fig. 4. MatLab model of SPSS

As a result of the simulation, the following were obtained: oscillograms of changes in current, voltage, and energy flow rate for the train motion intervals in the considered SPSS, shown in Fig. 5. A graph of the real efficiency of SPSS with a bi-directional energy flow versus short-circuit coefficient at the load terminals is built, which, for clarity, is shown in Fig. 3, together with a theoretical graph.

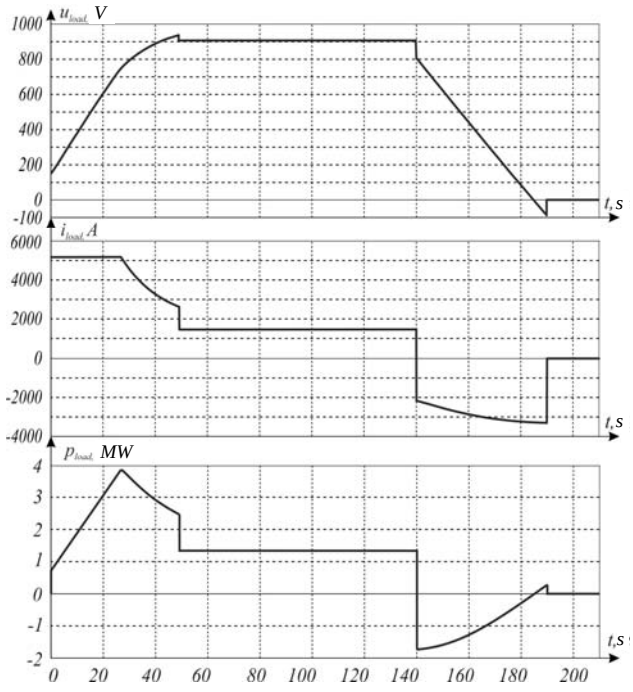

Fig. 5. Oscillograms of the circuit operation

Conclusions.

1. An equivalent circuit of the subway power supply system with a four-quadrant DC drive and the ability to recover energy to the supply network in the braking mode is developed, its parameters are determined, and the train schedule is set.

2. Using well-known formulas for the developed power supply system, a theoretical dependence of the efficiency of SPSS with a bi-directional energy flow on the coefficient of resistive short circuit at the load terminals is obtained.

3. A *MatLab* model of SPSS with a four-quadrant DC electric drive based on the base of a six-pulse controlled bridge rectifier with the possibility of realizing a bi-directional flow of electrical energy between the source and load is built.

4. Using the *MatLab* model, the real dependence of the efficiency of SPSS with a bi-directional energy flow on the short-circuit coefficient at the load terminals, which repeats the dynamics of the theoretical curve, is taken. Some discrepancy between the theoretical curve and the data of the obtained model can be explained by taking into account additional energy losses in the model, such as friction, air resistance, switching losses, etc.

REFERENCES

1. Zhemerov G.G., Ilyina N.A., Tugay D.V., Kholod O.I. Subway power systems with modern semiconductor converters and energy storage devices. *Electrical engineering & electromechanics*, 2013, no.1, pp. 41-49. (Rus) **doi: 10.20998/2074-272X.2013.1.10.**

2. Zhemerov G.G., Tugay D.V., Kholod O.I. Energy efficiency of power supple systems for a subway. *Technical electrodynamics*, 2014, no.1, pp. 67-74. (Rus).

3. Zhemerov G.G., Ilina N.A., Mashura A.V., Tugay D.V. Efficiency of regenerative braking in energy supply systems with electric regulated drives. *Technical electrodynamics*, 2018, no.8, pp. 73-76. (Ukr). **doi: 10.15407/techned2018.06.073.**

4. *Electric carriage types 81-718/719, 81-718.0/719.0 and 81-718.2/719.2*. Available at: http://vagon.metro.ru/passenger/81-718.html (Accessed 12 May 2016). (Rus).

5. Kostin N.A., Nikitenko A.V. Autonomy of recuperative braking – the basis of reliable energy-efficient recovery on the electromotive force constant current. *Railway Transport of Ukraine*, 2014, no.3, pp. 15-23. (Rus).

6. Shcherbak Ya.V., Nerubatsky V.P. Analysis of the use of recuperative inhibition on the railways of Ukraine. *Railway Transport of Ukraine*, 2011, no.2, pp. 30-34. (Ukr).
7. Sablin O.I. Analysis of the quality of the recovered electricity in the electric transport system. *Bulletin of NTU «KhPI»*, 2013, no.38, pp. 187-190. (Rus).
8. Posokhov I.M. Research of the car-building market of Ukraine and competitiveness of the industrial enterprises of railway transport in the world market and CIS markets. *Bulletin of NTU «KhPI»*, 2015, no.60, pp. 115-118. (Ukr).

Received 05.06.2019

G.G. Zhemerov[1], *Doctor of Technical Science, Professor,*
D.S. Krylov[1], *Candidate of Technical Science, Associate Professor,*
A.V. Mashura[1], *Postgraduate Student,*
[1] National Technical University «Kharkiv Polytechnic Institute», 2, Kyrpychova Str., Kharkiv, 61002, Ukraine,
phone +380 577076312,
e-mail: zhemerov@gmail.com

How to cite this article:
Zhemerov G.G., Krylov D.S., Mashura A.V. Energy efficiency of the subway electrical supply system with electrical energy recovery at braking. *Electrical engineering & electromechanics*, 2019, no.5, pp. 25-30. **doi: 10.20998/2074-272X.2019.5.04**.

UDC 621.315 **doi: 10.20998/2074-272X.2019.5.05**

M.M. Rezinkina

CALCULATION OF ELECTROMAGNETIC FIELDS IN INHOMOGENEOUS MEDIA FOR SELECTION OF PROTECTIVE COATINGS

The aim of the work is to develop a method for high-frequency EMFs calculation in terms of the modified vector potential and to use it for choice of the parameters of the layered absorbing coatings that provide effective absorption of radio wave radiation. Methodology. A method for calculation of electromagnetic fields in inhomogeneous media is described. It is performed in terms of the modified magnetic potential at presented a plane electromagnetic wave as an incident and reflected one. To reduce the computational domain size, additional uniaxially perfectly matched layers ensuring fast and non-reflective attenuation of electromagnetic field (EMF) strengths are used at its boundaries. It is supposed that electrical parameters of such layers have not only resistive, but also magnetic losses. Results. Modification of the known methods for dividing the wave into the incident and reflected, as well as introducing uniaxially perfectly matched layers at the domain boundaries and formulation of the problem in terms of the modified vector potential, provide a possibility to solve the problem of the electromagnetic wave incidence onto heterogeneous media at reduced memory and counting time compared to the formulation tasks through the EMF strengths. Practical value. The described method was used to select parameters of radio-absorbing coatings, application of which on conductive bodies reduces the reflections from them of the incident electromagnetic waves. This provides a possibility to choose the electrical parameters of layered coatings with active losses, as well as magnetic losses, which provide a decrease of the reflected waves amplitude by an order of magnitude or more. Originality. For the first time, the problem of calculating the incidence of an electromagnetic wave on an inhomogeneous medium with active electrical and magnetic losses was formulated in terms of the modified vector potential. The parameters of a multilayer lossy coating, which ensures decrease of the reflected EMF wave strengths by an order of magnitude or more are determined. References 11, figures 3.

Key words: **electromagnetic field, inhomogeneous media, modified vector magnetic potential, finite integration method, uniaxially perfectly matched layers.**

Описаний метод розрахунку електромагнітних полів в неоднорідних середовищах, виконаний в термінах модифікованого магнітного потенціалу при поділі плоскої електромагнітної хвилі на падаючу і відбиту. Для зменшення габаритів розрахункової області на її границях введені додаткові одновісне ідеально поглинаючі шари, що забезпечують швидке і безвідбивне загасання напруженостей електромагнітних полів (ЕМП). Особливістю таких шарів є вибір їх електричних параметрів такими, щоб забезпечити наявність в них не тільки резистивних, але і магнітних втрат. Математичне моделювання процесів при падінні ЕМП на провідне середовище, перед яким поміщені покриття з подібними властивостями показало можливість ефективного загасання в них ЕМП радіочастотного діапазону. В результаті проведених досліджень обрані параметри покриттів, що забезпечують мінімальне відбиття падаючих електромагнітних хвиль. Бібл. 11, рис. 3.

Ключові слова: ***електромагнітне поле, неоднорідні середовища, модифікований векторний магнітний потенціал, метод кінцевого інтегрування, ідеально узгоджені поглинаючі граничні шари.***

Описан метод расчета электромагнитных полей в неоднородных средах, выполненный в терминах модифицированного магнитного потенциала при разделении плоской электромагнитной волны на падающую и отраженную. Для уменьшения габаритов расчетной области на ее границах введены дополнительные одноосно идеально поглощающие слои, обеспечивающие быстрое и безотражательное затухание напряженностей электромагнитных полей (ЭМП). Особенностью таких слоев является то, что их электрические параметры выбраны такими, чтобы обеспечить наличие в них не только резистивных, но и магнитных потерь. Математическое моделирование процессов при падении ЭМП на проводящую среду, перед которой помещены покрытия с подобными свойствами, показало возможность эффективного затухания в них ЭМП радиочастотного диапазона. В результате проведенных исследований выбраны параметры покрытий, обеспечивающих минимальное отражение падающих электромагнитных волн. Библ. 11, рис. 3.

Ключевые слова: **электромагнитное поле, неоднородные среды, модифицированный векторный магнитный потенциал, метод конечного интегрирования, идеально согласованные поглощающие граничные слои.**

Introduction. When solving a number of problems of theoretical electrical engineering and electrophysics, the problems of calculating electromagnetic fields (EMF) arise, including when a wave is incident on inhomogeneous media with flat interfaces. Such problems have to be solved, for example, when choosing the parameters of protective radar absorbing coatings of extended conductive objects from high-frequency radiation. Since in this case the application of analytical methods [1] is impossible, the development of numerical methods is necessary. Taking into account the flat geometry of the systems under consideration, the use of finite-difference methods seems most effective (see, for example, [2, 3]). To reduce the order of the system of equations being solved, the problem formulation in terms of the modified vector magnetic potential can be used [4]. In contrast to the traditional formulation of electromagnetic fields through EMF strengths, this approach allows to reduce the required computer resources due to the fact that in the calculation 3 components of the modified vector magnetic potential are unknown, rather than 3 components of the electric field strength and 3 components of the magnetic field strength [4].

If there are several media interfaces with flat interfaces, it seems efficient to use the numerical finite integration method (FIM) [5]. The essence of this method is to impose a rectangular computational mesh on the considered region and integrate Maxwell equations over the volumes or faces of its cells. Thus, equations to be solved are obtained using conservation laws. Moreover, the formulation of the calculation problem using the finite integration method in terms of a modified vector magnetic potential with a special choice of the computational mesh ensures the automatic fulfillment of conditions at the media interfaces for the vectors of strengths and the flux density of the EMF [6, 7].

To limit the calculation region when determining the EMF in open areas when formulating the problem using EMF strengths, the so-called *UPML* (uniaxially perfectly

matched layers) are used [8]. To solve the problems associated with the propagation of high-frequency oscillations in inhomogeneous media with losses, it seems important to develop *UPML* in relation to the formulation of problems in terms of a modified vector magnetic potential.

The goal of the work is to develop a method for calculating high-frequency EMFs in lossy media using modified vector potential and *UPML*.

Definition of the problem of calculating the process of incidence of a plane electromagnetic wave on layered media. In order to reduce the number of equations in solving the problem of calculating EMF, we use the so-called modified vector magnetic potential $\boldsymbol{A}$ [4].

In the absence of external sources of electric charge, an additional condition when using the scalar electric (φ) and the vector magnetic ($\boldsymbol{A}$) potentials, instead of electric ($\boldsymbol{E}$) and magnetic ($\boldsymbol{H}$) field strengths, the gauging condition $\varphi = 0$ can be chosen (see, for example, [1]). Then vectors of the magnetic flux density $\boldsymbol{B}$ and the electric field strength $\boldsymbol{E}$ are expressed through $\boldsymbol{A}$ in the form:

$$\boldsymbol{B} = \mathrm{rot}\,\boldsymbol{A} = \mu\mu_0\boldsymbol{H}\ ; \tag{1}$$

$$\boldsymbol{E} = -\frac{\partial \boldsymbol{A}}{\partial t}\ . \tag{2}$$

In order for the reflectionless EMF attenuation to occur upon falling onto the radar absorbing coating, it is necessary to ensure the presence of losses not only related to the active conductivity of the medium, but also magnetic losses.

The second Maxwell equation, taking into account magnetic losses, has the form [9, p. 69]:

$$\mathrm{rot}\boldsymbol{E} = -\left(\frac{\partial \boldsymbol{B}}{\partial t} + \gamma_\mu \boldsymbol{H}\right), \tag{3}$$

where γ_μ are the equivalent magnetic losses [Ω/m].

Taking into account (1), rewrite the right-hand side of (3) in the form:

$$\frac{\partial \boldsymbol{B}}{\partial t} + \gamma_\mu \boldsymbol{H} = \mathrm{rot}\frac{\partial \boldsymbol{A}}{\partial t} + \frac{\gamma_\mu}{\mu\mu_0}\mathrm{rot}\boldsymbol{A}\ .$$

Then write (3) as

$$\mathrm{rot}\boldsymbol{E} = -\mathrm{rot}\frac{\partial \boldsymbol{A}}{\partial t} - \frac{\gamma_\mu}{\mu\mu_0}\mathrm{rot}\boldsymbol{A}\,,$$

whence, for piecewise homogeneous media, $\boldsymbol{E}$ can be expressed in terms of $\boldsymbol{A}$ as follows:

$$\boldsymbol{E} = -\frac{\partial \boldsymbol{A}}{\partial t} - \frac{\gamma_\mu}{\mu\mu_0}\boldsymbol{A}\,. \tag{4}$$

Here, the first Maxwell equation

$$\mathrm{rot}\,\boldsymbol{H} = \gamma\boldsymbol{E} + \frac{\partial \boldsymbol{D}}{\partial t},$$

where $\boldsymbol{D}$ is the electric field induction; γ is the electrical conductance takes the form:

$$\mathrm{rot}\frac{\mathrm{rot}\boldsymbol{A}}{\mu\mu_0} = -\gamma\frac{\partial \boldsymbol{A}}{\partial t} - \varepsilon_0\varepsilon\frac{\partial^2 \boldsymbol{A}}{\partial t^2} - \frac{\gamma\gamma_\mu}{\mu\mu_0}\boldsymbol{A} - \frac{\gamma_\mu\varepsilon_0\varepsilon}{\mu\mu_0}\frac{\partial \boldsymbol{A}}{\partial t}\,. \tag{5}$$

To obtain a numerical solution for the vector potential, the considered region was divided into parallelepiped cells (Fig. 1) so that the nodes of the computational mesh (i, j, k) lay at the interfaces of the media. It was assumed that the electrical properties of the medium within each of the cells are homogeneous.

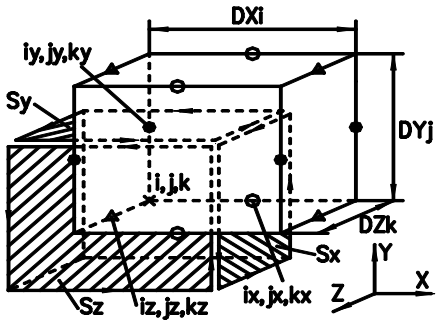

Fig. 1. Cell of the calculation scheme

The equation to be solved was obtained by integrating (5) over sections perpendicular to the coordinate axes. Then the equations for the components of the vector $\boldsymbol{A}$ can be written as a result of integration of (5) over the sections S_x, S_y, S_z (see Fig. 1) and using the Stokes theorem. So for A_y – the y-th component of the vector $\boldsymbol{A}$ – we obtain:

$$\oint_{l_y}\frac{\mathrm{rot}\boldsymbol{A}}{\mu\mu_0}d\boldsymbol{l} = \int_{S_y}(-\gamma\frac{\partial A_y}{\partial t} - \varepsilon_0\varepsilon\frac{\partial^2 A_y}{\partial t^2} - \\ -\frac{\gamma\gamma_\mu}{\mu\mu_0}A_y - \frac{\gamma_\mu\varepsilon_0\varepsilon}{\mu\mu_0}\frac{\partial A_y}{\partial t})dS, \tag{6}$$

where l_y is the contour covering the area S_y.

As a result of integration of (5) over the corresponding areas: S_x for A_x and S_z for A_z (see Fig. 1), similar expressions are written for the remaining components of the vector potential. Passing to the difference form of writing, we obtain a system of equations to be solved.

Features of the numerical calculation of EMF using a modified vector magnetic potential. When calculating electromagnetic processes when a plane electromagnetic wave having a finite length and harmonic filling is incident on objects, the problem arises of setting conditions for the strengths and potential of the EMP at the boundaries of the computational domain. To limit the computational domain when applying finite-difference methods of numerical computation, the introduction of so-called uniaxial perfectly matched layers (*UPML*) at the external boundaries of the computational domain is usually used, which ensure fast and reflectionless attenuation of the EMF. However, in this case, for the problem formulation under consideration, it is impossible to specify zero boundary conditions for the EMF potentials and strengths at the external *UPML* boundaries. The fact is that in addition to the reflected wave, which can really be assumed to be equal to zero at a sufficient distance from the object causing it, there is also an incident wave, which over time can be non-equal to zero and at a sufficient distance from the object. To solve this problem, a representation of the electromagnetic wave in the form of the sum of the incident and reflected waves is used. The propagation of both of these waves is described by the same Maxwell equations. In this case, the computational domain is also divided into two zones: the first (I), the inner, in which the studied object is located, and the second (II), the outer, located between the boundaries of the 1st region and the *UPML* inner borders. Here, in zone I, the propagation of the total wave is calculated, which contains both the incident and reflected waves. In zone II, only the propagation of the reflected wave is calculated. At the boundaries of zones I and II, the transition from calculating

only the reflected and total waves is taken into account. At the outer boundaries of *UPML*, zero conditions can be used for the potentials and strengths of the EMF, since they relate only to the reflected wave.

In [9], the solution of the problem of propagation and reflection of electromagnetic waves is presented using the described approach when using the Yee algorithm to calculate the components of the electric and magnetic field strengths. This approach was applied to solve the problem formulated in terms of a modified vector potential using the finite integration method. In this case, terms appearing in difference schemes containing the known values of the vector potential corresponding to the incident wave. The addition or subtraction of these terms when writing the equations to be solved for the nodes adjacent to the interface of subregions I and II allowed to implement the approach described above. Since the values of the incident wave at each moment of time and for each node of the calculation scheme are known, they are transferred to the right side of the equations. Such terms are added to the right sides of the difference equations written for nodes lying on the boundaries of subregions I and II, and are subtracted from the right sides of difference equations written for nodes located in II in planes in front of the boundaries of subregions I and II.

The introduction of *UPML* in calculating the propagation of an electromagnetic wave in terms of a modified vector magnetic potential requires a different approach than when solving through electric and magnetic field strengths. This is due to the fact that the parameter s_μ

$$s_\mu = 1 + \frac{\gamma_\mu}{j\omega\mu\mu_0}, \qquad (7)$$

which is chosen equal to s_ε

$$s_\varepsilon = 1 + \frac{\gamma}{j\omega\varepsilon\varepsilon_0}, \qquad (8)$$

when formulating the problem through $\underline{\boldsymbol{A}}$ appears in the denominator of the equation to be solved. Therefore, its conversion during the transition from the frequency domain to the time domain is impossible. To use *UPML* in such a formulation, it is proposed to use a medium in which $\varepsilon\cdot\omega$ and $\mu\cdot\omega$ are much smaller than γ and γ_μ, respectively, as absorbing layers. To ensure the constancy of the propagation speed of electromagnetic waves and the absence of reflections when the EMF falls on the *UPML* layers, it is necessary $s_\mu = s_\varepsilon$. At $\mu\cdot\omega << \gamma_\mu$ and $\varepsilon\cdot\omega << \gamma$:

$$s_\varepsilon \approx \frac{\gamma}{j\omega\varepsilon\varepsilon_0}, \qquad (9)$$

$$s_\mu \approx \frac{\gamma_\mu}{j\omega\mu\mu_0}. \qquad (10)$$

Then from (9, 10) we obtain:

$$\frac{\gamma_\mu}{\mu\mu_0} = \frac{\gamma}{\varepsilon\varepsilon_0}.$$

Hence the relation between γ and γ_μ:

$$\gamma_\mu = \gamma\frac{\mu\mu_0}{\varepsilon\varepsilon_0} \approx 0.142\cdot 10^6 \gamma\frac{\mu}{\varepsilon}\ [\Omega/\mathrm{m}]. \qquad (11)$$

We obtain expressions for EMF in *UPML* layers by writing (6) through complexes (indicated by an underscore of the corresponding value) and taking into account (7), (8):

$$\oint_{l_y}\frac{\mathrm{rot}\,\underline{\boldsymbol{A}}}{\mu_0\mu}d\boldsymbol{l} = \int_{S_y}(-j\omega\gamma\underline{A}_y - (j\omega)^2\varepsilon_0\varepsilon\underline{A}_y -$$

$$-\frac{\gamma\gamma_\mu}{\mu_0\mu}\underline{A}_y - j\omega\frac{\varepsilon_0\varepsilon}{\mu_0\mu}\gamma_\mu\underline{A}_y)dS =$$

$$= \int_{S_y}[-(j\omega)^2\varepsilon_0\varepsilon\underline{A}_y(1+\frac{\gamma}{j\omega\varepsilon_0\varepsilon}) -$$

$$- j\omega\frac{\varepsilon_0\varepsilon}{\mu_0\mu}\gamma_\mu\underline{A}_y(1+\frac{\gamma}{j\omega\varepsilon_0\varepsilon})]dS =$$

$$= -\int_{S_y}(j\omega)^2\varepsilon_0\varepsilon\underline{A}_y s_\varepsilon s_\mu dS.$$

Dividing both parts of the resulting expression into $\hat{s}_\mu$, we write:

$$\oint_{l_y}\frac{\mathrm{rot}\,\underline{\boldsymbol{A}}}{\mu_0\mu s_\mu}d\boldsymbol{l} = -\int_{S_y}(j\omega)^2\varepsilon_0\varepsilon\underline{A}_y s_\varepsilon dS.$$

In view of (9), (10), we transform the last expression to the form:

$$\oint_{l_y}\frac{j\omega\cdot\mathrm{rot}\,\underline{\boldsymbol{A}}}{\gamma_\mu}d\boldsymbol{l} = -\int_{S_y}j\omega\gamma\underline{A}_y dS$$

Then, in the last expression, we move from the complex form of writing to the functions of time:

$$\oint_{l_y}\frac{\mathrm{rot}[\partial\boldsymbol{A}/\partial t]}{\hat{\gamma}_\mu}d\boldsymbol{l} = -\int_{S_y}\hat{\gamma}\cdot\frac{\partial A_y}{\partial t}ds. \qquad (12)$$

A numerical solution was obtained by writing equations of the form (6), (12) for nodes of the computational mesh and replacing the differential operators in them by difference analogues. To solve the obtained system of equations, the sweep method was used (for more details see [6, 7]).

To evaluate the effectiveness of the proposed method of introducing *UPML*, numerical experiments were carried out to calculate electromagnetic processes in the case of a plane electromagnetic wave incident on a perfectly conducting sheet. It was assumed that the EMF with $|\boldsymbol{E}|$=1 V/m from time $t = 0$ falls in the direction of the *Oz* axis onto a conductive sheet whose thickness is $d = 3\cdot\Delta$ (where Δ is the spatial step). It is believed that this sheet is located in the z = const plane and has dimensions in the x and y coordinates many orders of magnitude greater than the wavelength of the incident EMF. When calculating at the boundaries of the computational domain in the directions of the *Ox*, *Oy*, and *Oz* axes zero conditions were used for the vector potential of the reflected waves. The frequency of the incident EMF was assumed to be 10 GHz. In the calculations, the time step was set equal to $\Delta_t = T/200$, $\Delta = c\cdot T/200$ ($c = 3\cdot 10^8$ m/s). The *UPML* parameters were as follows: the number of layers $N = 10$, γ varied according to the exponential law with an exponent of 3 [8] from 35 S/m at the inner *UPML* boundary, γ_μ varied depending on γ in accordance with (11). The dimensions of the computational domain in the direction of the *Oz* axis are $Z_{\max} = 0.5\cdot\lambda$ (where λ is the wavelength), and the number of steps in reflection zone II is 10.

Figure 2 shows the calculated time sweeps of the reflected (scattered) electric field strength $|\boldsymbol{E}_{\mathrm{scat}}|$ when a plane electromagnetic wave falls on a conductive sheet.

As can be seen from the Figure, due to the fact that *UPML* layers with the parameters described above are located at the boundaries of the computational domain, the relative error in calculating the strength $|\boldsymbol{E}_{scat}|$ does not exceed 3%, despite a significant truncation of the length of the computational domain.

Thus, a technique for calculating the propagation of an electromagnetic wave in media with magnetic losses in terms of a modified vector magnetic potential is described. This ensures the introduction of *UPML* at the boundaries of the computational domain, which was previously possible only when formulating the problem through EMF strengths.

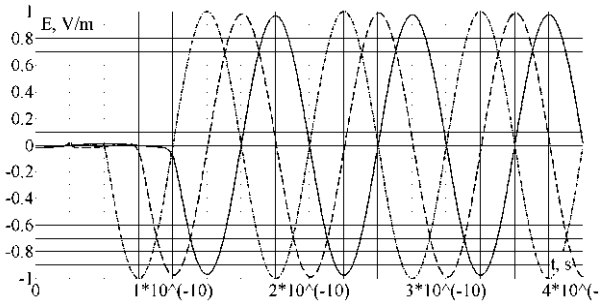

Fig. 2. Calculated dependencies $|\boldsymbol{E}_{scat}|(t)$ for nodes located at different distances (z) from the conducting sheet: $z = \lambda$ (——), $-z = 0.5 \cdot \lambda$ (– – –), $-z = 0$ (– · – · –)

Mathematical modelling of EMF fall on layered coatings with dielectric and magnetic losses. In some cases, various dielectrics with low values of the reflection coefficient and high values of the absorption coefficient of radio waves are used as protective coatings from high-frequency radiation. Scopes of radar absorbing coatings are various. So, they are used to create screens for radio receivers, to protect biological objects from electromagnetic radiation, to equip special research chambers, etc. A large number of works have been devoted to this issue (see, for example, [10, 11]), but the problem of choosing coating parameters remains relevant, since the question of a significant decrease in the amplitude of waves reflected from conductive objects has not been completely resolved.

Figure 3 shows the calculated time sweeps of the electric field strength when a plane electromagnetic wave falls on a conductive sheet, before which a radar absorbing coating is placed with the following parameters: the 1st layer (closest to the conductive sheet) – $\varepsilon = \mu = 300$, $\gamma = 315$ S/m, the next layer – $\varepsilon = \mu = 100$, $\gamma = 275$ S/m, the last layer – $\varepsilon = \mu = 60$, $\gamma = 17.5$ S/m (γ_μ changed depending on γ in accordance with (11)). As can be seen from the Figure, due to the attenuation of the electromagnetic wave in the coating layers, the reflection from the conducting sheet in the steady state does not exceed 10% of the initial reflection level.

Conclusions.

1. A method for calculating the propagation of an electromagnetic wave in lossy media located in open areas at formulating the problem in terms of a modified vector magnetic potential and using *UPML* the implementation of which allows to reduce the memory and calculation time compared to formulation of the problem through EMF strengths is proposed and tested by comparison with an analytical solution.

2. The proposed calculation method is the theoretical basis for developing a method for selecting parameters of radar absorbing coatings with electric and magnetic losses, the application of which to conductive objects provides a significant reduction in the amplitude of the reflected radio waves.

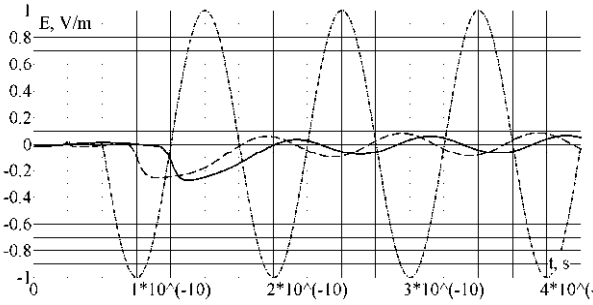

Fig. 3. Calculated dependencies $|\boldsymbol{E}_{scat}|(t)$ in the presence in front of the conductive sheet of the radar absorbing coating for nodes located at different distances (z) from the conductive sheet: $z = \lambda$ (——), $-z = 0.5 \cdot \lambda$ (– – –), $-z = 0$ (– · – · –)

REFERENCES

1. Stratton J.A. *Electromagnetic theory*. NJ, IEEE Press, 2007. 614 p.

2. Yee K.S., Chen Jei Shuan, Chang A.H. Conformal finite-different time-domain (FDTD) with overlapping grids. *IEEE Transactions on Antennas and Propagation*, 1992, vol.40, no.9, pp. 1068-1075. **doi: 10.1109/8.166532**.

3. Werner D.H., Mittra R. *Frontiers in electromagnetics*. New York, IEEE Press, 1999. 876 p.

4. Biro O., Preis K. On the use of the magnetic vector potential in the finite-element analysis of three-dimensional eddy currents. *IEEE Transactions on Magnetics*, 1989, vol.25, no.4, pp. 3145-3159. **doi: 10.1109/20.34388**.

5. Clemens M., Weiland T. Discrete electromagnetism with the finite integration technique. *Progress in Electromagnetics Research*, 2001, vol.32, pp. 65-87. **doi: 10.2528/PIER00080103.**

6. Rezinkina M.M., Rezinkin O.L. Modeling of the electromagnetic wavefront sharpening in a nonlinear dielectric. *Technical Physics*, 2011, vol.56, iss.3, pp. 406-412. **doi: 10.1134/S1063784211030169.**

7. Rezinkina M.M. Modeling of the dendrite shape variation with applied electric field strength in poly(ethylene). *Technical Physics Letters*, 2000, vol.26, iss.3, pp. 196-198. **doi: 10.1134/1.1262789.**

8. Berenger J.-P. A perfectly matched layer for the absorption of electromagnetic waves. *Journal of Computational Physics*, 1994, vol.114, no.2, pp. 185-200. **doi: 10.1006/jcph.1994.1159**.

9. Taflove A., Hagness S.C. *Computational Electrodynamics: the Finite-Difference Time-Domain Method*. Boston – London, Artech House, 2000. 852 p.

10. Zhou Z., Chen K., Zhu B., Zhao J., Feng Y., Li Y. Ultra-Wideband Microwave Absorption by Design and Optimization of Metasurface Salisbury Screen. *IEEE Access*, 2018, vol.6, pp. 26843-26853. **doi: 10.1109/access.2018.2835815**.

11. Bottauscio O., Chiampi M., Manzin A. Numerical analysis of magnetic shielding efficiency of multilayered screens. *IEEE Transactions on Magnetics*, 2004, vol.40, iss.2, pp. 726-729. **doi: 10.1109/tmag.2004.825171.**

Received 12.04.2019

M.M. Rezinkina, Doctor of Technical Science, Professor,
[1] National Technical University «Kharkiv Polytechnic Institute», 2, Kyrpychova Str., Kharkiv, 61002, Ukraine,
e-mail: maryna.rezynkina@gmail.com

How to cite this article:
Rezinkina M.M. Calculation of electromagnetic fields in inhomogeneous media for selection of protective coatings. *Electrical engineering & electromechanics*, 2019, no.5, pp. 31-34. **doi: 10.20998/2074-272X.2019.5.05.**

UDC 621.3.022: 621.315.3: 537.311.8 **doi: 10.20998/2074-272X.2019.5.06**

M.I. Baranov

A CHOICE OF CRITICAL SECTIONS OF ELECTRIC WIRES AND CABLES IN POWER CIRCUITS OF ELECTRICAL EQUIPMENT OF POWER INDUSTRY

Purpose. *Implementation of close calculation determination of critical sections of S_{Ci} and critical amplitudes of density of alternating current δ_{Ci} of frequency 50 Hz in wires and cables of power circuits of electrical equipment of power industry, characterized flowing in it at malfunctions of operation current $i_k(t)$ of short circuit (SC) with set amplitude-temporal parameters (ATP).* ***Methodology.*** *Scientific and technical bases of power engineering, electrophysics bases of technique of high-voltage and large pulsed currents, theoretical bases of the electrical engineering.* ***Results.*** *The results of the developed electrical engineering approach are resulted in a calculation choice on the condition of electric explosion (EE) of current-carrying parts of cable and conductor products (CCP) of critical sections of S_{Ci} for the copper (aluminum) cores of the uninsulated wires, and also for the insulated wires and cables with a polyvinilkhloride (PVC), rubber (R) and polyethylene (PET) insulation with copper (aluminum) cores (shells) on which in the power circuits of electrical equipment of the general industrial equipment in malfunction the current of SC $i_k(t)$ flows with set ATP. On the basis of determination of sizes of the real critical sections S_{Ci} for the indicated wires and cables the calculation numeral estimation of critical amplitudes of density δ_{Ci} of SC current $i_k(t)$ is executed with set ATP in current-carrying parts of investigated CCP of power circuits of the examined electrical equipment. It is determined that in the power circuits of electric equipment of the general industrial installations (for permanent time of slump of T_a=50 ms of aperiodic to the constituent of current of SC) critical amplitudes of density δ_{Ci} of SC current $i_k(t)$ at time of his disconnecting t_k=100 ms in copper (aluminum) cores for the uninsulated wires and insulated wires (cables) with copper (aluminum) cores (shells), PVH, R and PET it is numeral made an insulation according to approximately 1,57 (1,18) kA/mm^2. At time of disconnecting t_k=160 ms of SC current $i_k(t)$ in the power circuits of the examined electrical equipment (T_a=50 ms) critical amplitudes of density δ_{Ci} of SC current $i_k(t)$ for the copper (aluminum) cores (shells) of indicated CCP become accordingly numeral equal approximately 1,33 (0,99) kA/mm^2.* ***Originality.*** *First by a calculation way taking into account information for ATP of SC current $i_k(t)$ and quantitative values of time of his disconnecting t_k in the power circuits of electrical equipment of the general industrial installations the numerical values of critical sections S_{Ci} and critical amplitudes of density δ_{Ci} of AC SC current $i_k(t)$ are certain for the uninsulated wires, and also insulated wires and cables with copper (aluminum) cores (shells), PVH, R and PET insulation.* ***Practical value.*** *Obtained results for the critical sections S_{Ci} and amplitudes of density δ_{Ci} of AC SC current $i_k(t)$ of frequency 50 Hz (at the period of oscillations of T_p=20 ms for of periodic constituent of emergency current of SC) can be utilized in power industry in practice at a choice thermally by a bar to the action of large SC currents $i_k(t)$ of CCP with copper (aluminum) bars (shells), intended for reliable operation in the power circuits of electrical equipment of industrial power industry.* References 8, tables 5.

Key words: **power industrial, electrical equipment, electric wires and cables of circuits of electrical equipment, calculation choice of critical sections of wires and cables in the circuits of electrical equipment.**

Надані результати *розробленого електротехнічного підходу до розрахункового вибору по умові електричного вибуху (ЕВ) струмопровідних частин кабельно-провідникової продукції критичних перерізів S_{Ci} неізольованих дротів, а також ізольованих дротів і кабелів з полівінілхлоридною (ПВХ), гумовою (Г) і поліетиленовою (ПЕТ) ізоляцією з мідними (алюмінієвими) жилами (оболонками), по яких в силових колах електрообладнання загальнопромислового призначення в аварійному режимі протікає струм $i_k(t)$ короткого замикання (КЗ) із заданими амплітудно-часовими параметрами (АЧП).* ***На підставі*** *даного підходу здійснений реальний вибір критичних перерізів S_{Ci} для вказаних дротів (кабелів) силових кіл електрообладнання, що розглядається.* ***Виконана*** *розрахункова чисельна оцінка критичних амплітуд щільностей δ_{Ci} струму $i_k(t)$ КЗ із заданими АЧП в дротах і кабелях силових кіл вказаного електрообладнання.* ***Отримані*** *дані сприятимуть забезпеченню термічної стійкості електричних неізольованих дротів, а також дротів і кабелів з ПВХ, Г і ПЕТ ізоляцією, які широко застосовуються в силових колах електрообладнання загальнопромислового призначення.* Бібл. 8, табл. 5.

Ключові слова: **промислова електроенергетика, електрообладнання, електричні дроти і кабелі кіл електрообладнання, розрахунковий вибір критичних перерізів дротів і кабелів в колах електрообладнання.**

Приведены результаты *разработанного электротехнического подхода к расчетному выбору по условию электрического взрыва (ЭВ) токонесущих частей кабельно-проводниковой продукции критических сечений S_{Ci} неизолированных проводов, а также изолированных проводов и кабелей с поливинилхлоридной (ПВХ), резиновой (Р) и полиэтиленовой (ПЭТ) изоляцией с медными (алюминиевыми) жилами (оболочками), по которым в силовых цепях электрооборудования общепромышленного назначения в аварийном режиме протекает ток $i_k(t)$ короткого замыкания (КЗ) с заданными амплитудно-временными параметрами (АВП).* ***На основании*** *данного подхода осуществлен реальный выбор критических сечений S_{Ci} для указанных проводов (кабелей) силовых цепей рассматриваемого электрооборудования.* ***Выполнена*** *расчетная численная оценка критических амплитуд плотностей δ_{Ci} тока $i_k(t)$ КЗ с заданными АВП в проводах и кабелях силовых цепей указанного электрооборудования.* ***Полученные*** *данные будут способствовать обеспечению термической стойкости электрических неизолированных проводов, а также проводов и кабелей с ПВХ, Р и ПЭТ изоляцией, широко применяемых в силовых цепях электрооборудования общепромышленного назначения.* Библ. 8, табл. 5.

Ключевые слова: **промышленная электроэнергетика, электрооборудование, электрические провода и кабели цепей электрооборудования, расчетный выбор критических сечений проводов и кабелей в цепях электрооборудования.**

Introduction. In [1] the results of a calculation and experimental determination of critical sections S_{Ci} and critical amplitudes of current densities δ_{Ci} for non- and insulated electric wires (cables) containing metal cores (i=1) and shells (i=2) and used in discharge circuits of high-voltage high-current pulse technology are presented. The basis for this choice of S_{Ci} cross-sectional values of

conductive wires (shells) and current density amplitudes δ_{Ci} for cable-conductor products (CCP) with pulsed axial current varying in the nano-, micro-, and millisecond time ranges was known in electrophysics the electric explosion (EE) condition [2, 3] of metal cores (shells) of the indicated wires and cables, leading to the sublimation of their current-carrying parts and the CCP failure. In the field of power industry in emergency operation of the power circuits of its electrical equipment, accompanied by the flow of short-circuit (SC) current $i_k(t)$ through the current-carrying parts of the CCP with frequency f = 50 Hz and amplitude of up to (40-125) kA [4], at unreasonable use in the power circuits of the electric equipment of the CCP, cases of the occurrence of the EE phenomenon of copper (aluminum) cores and shells (reverse conductors) of their wires and cables are also possible. Insufficient attention was paid by electrical engineers and power engineers to such emergency conditions in power circuits of electrical equipment of general industrial use with similar dire consequences for their CCP. In this regard, the calculation determination of the critical cross-sections S_{Ci} of electric wires (cables) used in power circuits of electrical equipment of general industrial use is an urgent applied problem in the field of power engineering.

The goal of the paper is to perform an approximate calculation determination of critical sections S_{Ci} and critical amplitudes of densities δ_{Ci} of AC current with frequency f = 50 Hz in the wires and cables of power circuits of electrical equipment of power industry, characterized by flowing in them in emergency modes of SC current $i_k(t)$ with specified amplitude-temporal parameters (ATPs).

1. Problem definition. Let us consider widely used in power circuits of electrical equipment of general industrial use uninsulated copper and aluminum wires, as well as insulated wires and cables with copper (aluminum) inner cores and outer shells-current conductors with the initial specific conductivity γ_{0i} of their non-magnetic material, having polyvinyl chloride (PVC), rubber (R) and polyethylene (PET) belt insulation [4, 5]. We assume that along round continuous or split copper (aluminum) cores (shells) of the indicated wires and cables of power electric circuits of the considered electrical equipment in emergency mode in their longitudinal direction current $i_k(t)$ of the three-phase SC with specified ATPs flows. We indicate that this particular type of SC current is the calculated emergency current for the electrical equipment under study [4]. We believe that the wires and cables under consideration are located in an ambient air environment, the temperature of which corresponds to room temperature and is equal to θ_0=20 °C [2, 4]. The above value of the specific conductivity γ_{0i} of the core (shell) material of the CCP corresponds to this temperature. We believe that the wires (cables) under consideration, before exposure to their current-carrying parts of the SC current $i_k(t)$ with specified ATPs, can be both de-energized and under nominal current load. In this regard, the initial temperature θ_{0i} of the material of the current-carrying parts of the CCP, depending on the current mode of operation of the power circuits of the electrical equipment, can correspond to θ_0=20 °C or the value of the long-term allowable heating temperature θ_{li} of their material. It is known that for non- and insulated wires and cables with PVC, R and PET insulation, the temperature θ_{li} does not numerically exceed the levels of 70 and 65 °C regulated by current requirements, respectively [4, 6]. We use the assumption that the axial SC current $i_k(t)$ is almost uniformly distributed over the cross-section S_i of the core (shell) of the wire (cable) of the electrical equipment considered. The justification for this assumption is that the minimum penetration depth Δ_i of the magnetic field (skin layer thickness) from the SC current $_k(t)$ in the quasi-stationary approximation into the considered non-magnetic conductive materials, determined from the calculated relation of the form $\Delta_i \approx [1/(\pi f \mu_0 \gamma_{0i})]^{1/2}$ [2], where γ_{0i} is the electrical conductance of the core (shell) material of the CCP at θ_0=20 °C, and $\mu_0=4\pi\cdot10^{-7}$ H/m is the magnetic constant, numerically for copper is approximately 9.3 mm, and for aluminum is 11.8 mm. It can be seen that the presented numerical values of Δ_i are comparable with the real radii (thicknesses) of the current-carrying conductors (shells) of wires and cables used in electrical equipment circuits of general industrial use. We use the condition of the adiabatic nature of the occurring at times of action of the SC current $i_k(t)$ in the power circuits of the specified electrical equipment of no more than 1000 ms in the materials of the conductors (shells) of the investigated CCP of the electrothermal processes under which heat transfer from surfaces of current-carrying parts having the current temperature $\theta_{Ci} \geq \theta_{0i}$, and the thermal conductivity of the layers of its conductive materials of the core (shell) and insulation on the Joule heating of the current-carrying parts of the checkpoint are neglected. It is required by calculation to determine in approximate form the critical sections S_{Ci} of current-carrying parts for uninsulated copper (aluminum) wires, as well as for insulated wires and cables with copper (aluminum) cores (shells), PVC, R and PET insulation used in power circuits of electrical equipment of general industrial applications and experiencing in emergency operation mode the direct effect of the axial SC current i $i_k(t)$ with specified ATPs. In addition, based on the calculation of the values of the critical sections S_{Ci}, it is necessary to determine the values of the critical amplitudes of the densities δ_{Ci} of AC current with frequency f = 50 Hz in the current-carrying parts of wires and cables of power circuits of electrical equipment of power industry, through which SC current $i_k(t)$ can flow.

The electrical engineering approach to the calculation of critical sections S_{Ci} and current densities δ_{Ci} in wires and cables of circuits of electrical equipment for general industrial purposes. To find critical cross-sections S_{Ci} of conductive cores (shells) of considered non-insulated and insulated with PVC, R and PET insulation electrical wires and cables in power circuits of electrical equipment with axial SC current $i_k(t)$ of specified ATPs, from the equation of their heat balance in the adiabatic Joule mode heating of the current-carrying parts of the CCP the following calculation relation follows [3]:

$$S_{Ci} = (J_{CiA})^{1/2} / D_{Ci}, \quad (1)$$

where $J_{CiA}=\int_0^{t_k} i_k^2(t)dt$ – the Joule (action) integral for the SC current $i_k(t)$ with duration t_k of its flow through the cores (shells) of the CCP, $A^2\cdot s$; $D_{Ci} = (J_{Ci}-J_{li})^{1/2}$, $A\cdot s^{1/2}/m^2$; J_{li} is the critical value of the current integral for the material of cores (shells) of wires and cables of electrical equipment circuits [2], $A^2\cdot s/m^4$; J_{li} is the value of the current integral for the material of conductors (shells) of wires and cables of electrical equipment circuits, the long-term permissible heating temperature of which with the rated current corresponds to the known value θ_{li} [4], $A^2\cdot s/m^4$.

In (1), the value of the current integral J_{li} is calculated from the following analytical expression [3]:

$$J_{li} = \gamma_{0i}\beta_{0i}^{-1}\ln\left[c_{0i}\beta_{0i}(\theta_{li}-\theta_0)+1\right], \qquad (2)$$

where c_{0i}, β_{0i} are accordingly, the specific heat attributed to the unit volume of the material of the core (shell) of the wire (cable) and the thermal coefficient of the specific conductivity of this CCP material before the SC current $i_k(t)$ flows through it at θ_0=20 °C.

It can be seen from (2) that at $\theta_{li}=\theta_0$ (the power-off mode of the CCP), the desired current integral is zeroed (J_{li}=0).

In Table 1 at θ_0=20 °C, numerical values are given for such basic characteristics of copper and aluminum conductors (shells) of wires (cables) of the studied power circuits as γ_{0i}, c_{0i}, β_{0i} and J_{Ci} [2].

Table 1

Thermophysical characteristics of copper (aluminum) cores (shells) of considered wires and cables of power circuits of electrical equipment before action on them of SC current $i_k(t)$ (at θ_0=20 °C) [2]

Material of the core (shell) of the wire (cable)	Numerical value of the characteristic			
	γ_{0i}, 10^7 $(\Omega\cdot m)^{-1}$	c_{0i}, $10^6\cdot$J/ $(m^3\cdot°C)$	β_{0i},$10^{-9}\cdot$ m^3/J	J_{Ci}, 10^{17} $A^2\cdot s\cdot m^{-4}$
Copper	5.81	3.92	1.31	1.95
Aluminum	3.61	2.70	2.14	1.09

Table 2, taking into account the use of data of (1), (2) and Table 1, shows the numerical values of the coefficient D_{Ci} necessary for calculating, according to (1), the critical cross-section S_{Ci} of the conductive core (sheath) of the considered wire (cable) in the power circuit of electrical equipment used in power industry.

Table 2

Numerical values of the coefficient D_{Ci} for non- and insulated wires (cables) with copper (aluminum) cores (shells) in general-purpose electrical equipment circuits

Type of insulation in the wire (cable) of the electrical installation	Material of the core (shell) of the wire (cable)	Numerical value of D_{Ci}, 10^8 $A\cdot s^{1/2}/m^2$	
		$J_{li}\neq0$	J_{li}=0
Without insulation	Copper	4.299	4.415
	Aluminum	3.236	3.301
PVC, R	Copper	4.299	4.415
	Aluminum	3.236	3.301
PET	Copper	4.299	4.415
	Aluminum	3.236	3.301

From the data of Table 2 it can be seen that the current mode of operation of the CCP under consideration (wires and cables of electrical circuits are fully loaded with rated current ($J_{li}\neq0$) or at J_{li}=0 are completely de-energized) slightly affects the numerical values of the calculated coefficient D_{Ci} (up to 3 %). Its quantitative values are determined mainly by the type of conductive material of the core (shell) of the considered CCP. For copper and aluminum, the difference in the numerical values of D_{Ci} is approximately 25 %.

It follows from (1) that, for the numerical values of the coefficient D_{Ci} found (see Table 2), the determination of the critical cross-sections S_{Ci} of the copper (aluminum) cores (shells) of the investigated CCP is reduced to the quantitative determination of the action integral J_{CiA} of the SC current $i_k(t)$ flowing during time t_k over the current-carrying parts of the selected wires and cables.

2.1Approximate calculation at SC integral of the action integral J_{CiA} of the emergency current. As in [7, 8], we assume that the SC current $i_k(t)$ in the circuits with the considered CCP is described by the following temporal dependence:

$$i_k(t) = I_{mk}[\exp(-t/T_a)-\cos(2\pi t/T_p)], \qquad (3)$$

where I_{mk} is the amplitude of the steady SC current $i_k(t)$ in the power circuit of the electrical equipment; T_a, T_p are, respectively, the decay time constant of the aperiodic component and the period of oscillations of the periodic component of the emergency SC current $i_k(t)$ in the circuit with the CCP.

Then, based on (1) and (3), the calculated expression for the integral of the action of the SC current $i_k(t)$ in power circuits with the CCP takes the following analytical form [7]:

$$J_{CiA} = I_{mk}^2\{0{,}5t_k + 0{,}25\pi^{-1}T_p\sin(2\pi t_k/T_p)\times$$
$$\times\cos(2\pi t_k/T_p) - 2T_a^2T_p^2(T_p^2+4\pi^2T_a^2)^{-1}[\exp(-t_k/T_a)\times \qquad (4)$$
$$\times[2\pi T_p^{-1}\sin(2\pi t_k/T_p) - T_a^{-1}\cos(2\pi t_k/T_p)+T_a^{-1}]\ ]+$$
$$+0{,}5T_a[1-\exp(-2t_k/T_a)]\}.$$

In Table 3, for the case T_a=50 ms (T_p=20 ms), the numerical values of the action integral J_{CiA} calculated by (4) for the SC current $i_k(t)$ are given for the steady SC current amplitudes I_{mk} and its durations (shutdown times) t_k in power circuits of electrical equipment for general industrial use according to the requirements of [4, 8]. Knowing the numerical values of the coefficient D_{Ci} (see Table 2) and the action integral J_{CiA} of the SC current $i_k(t)$ (see Table 3), from (1) the numerical values of the critical sections S_{Ci} of the current-carrying parts of the considered CCP in power electrical installations circuits for general industrial use can be relatively easy determined. Taking into account the assumptions made, from the relation of the form $\delta_{Ci}\approx I_{mk}/S_{Ci}$, the critical amplitudes of the AC current densities δ_{Ci} in the cores (shells) materials of the studied wires (cables) for the SC emergency fault mode can be quantified.

2.2. The results of the calculated choice of critical sections S_{Ci} and current densities δ_{Ci} in wires and cables of electrical equipment circuits for general industrial purposes. Table 4 shows the results of approximate calculation according to (1), taking into

Table 3

Numerical values of the action integral J_{CiA} for the SC current $i_k(t)$ flowing in power circuits of general-purpose electrical equipment (T_p=20 ms; T_a=50 ms) calculated by the relation (4)

The value of the amplitude I_{mk} of the steady SC current $i_k(t)$ in the power circuit of an industrial electrical installation, kA	Values of the action integral J_{CiA} for the SC current $i_k(t)$ by (4), $10^7 \cdot A^2 \cdot s$	
	t_k=100 ms	t_k=160 ms
30	6.75	9.45
50	18.75	26.25
70	36.75	51.45
100	75.00	105.00
125	117.18	164.06

account the data in Table 2, 3 of critical cross-sections S_{Ci} of copper (aluminum) cores (shells) of uninsulated (bare) wires and insulated wires (cables) of power circuits of general industrial electrical equipment (T_p=20 ms) for the case when $J_{li}\neq 0$, t_k=100 ms and T_a=50 ms, and the amplitude I_{mk} of the steady SC current $i_k(t)$ varies discretely in the range (30-100) kA. From the data of Table 4 it follows that the critical amplitudes of the densities $\delta_{Ci} \approx I_{mk}/S_{Ci}$ of the SC current $i_k(t)$ at the time of its flow (switch off) in the power circuits of electrical installations equal to t_k=100 ms for uninsulated wires and insulated wires (cables) with PVC, R and PET insulation with copper (aluminum) cores (shells) in the circuits of electrical equipment for general industrial use (T_p=20 ms; T_a=50 ms) are numerically approximately 1.57 kA/mm^2 and 1.18 kA/mm^2, respectively. It is important to note that these values of the critical amplitudes of the densities δ_{Ci} of the SC current $i_k(t)$ in the materials of the current-carrying parts of the wires (cables) of the power circuits of the electrical equipment do not depend on the level of the amplitude I_{mk} of the steady SC emergency fault current of the power frequency of 50 Hz.

Table 5 presents the results of the calculated determination according to (1), taking into account the data in Table 2, 3, of critical cross-sections S_{Ci} of copper (aluminum) cores (shells) of bare wires and insulated wires (cables) of power circuits of electrical equipment of general industrial use (T_p=20 ms) for the case when $J_{li}\neq 0$, t_k=160 ms and T_a=50 ms, and the amplitude I_{mk} of the steady SC current $i_k(t)$ varies discretely in the range (30-100) kA.

Table 4

Numerical values of critical cross-sections S_{Ci} for bare wires and insulated wires (cables) with copper and aluminum cores (shells) in power circuits of general industrial electrical equipment with amplitude I_{mk} of SC current $i_k(t)$ varying from 30 to 100 kA (for t_k=100 ms and T_a=50 ms)

Type of insulation in the wire (cable) of the electrical installation	Material of the core (shell) of the wire (cable)	Values of section S_{Ci}, mm^2			
		Amplitude I_{mk} of the steady SC current, kA			
		30	50	70	100
Without insulation	Copper	19.11	31.85	44.59	63.70
	Aluminum	25.38	42.31	59.24	84.63
PVC, R	Copper	19.11	31.85	44.59	63.70
	Aluminum	25.38	42.31	59.24	84.63
PET	Copper	19.11	31.85	44.59	63.70
	Aluminum	25.38	42.31	59.24	84.63

Table 5

Numerical values of critical cross-sections S_{Ci} for bare wires and insulated wires (cables) with copper and aluminum cores (shells) in power circuits of general industrial electrical equipment with amplitude I_{mk} of SC current $i_k(t)$ varying from 30 to 100 kA (for t_k=160 ms and T_a=50 ms)

Type of insulation in the wire (cable) of the electrical installation	Material of the core (shell) of the wire (cable)	Values of section S_{Ci}, mm^2			
		Amplitude I_{mk} of the steady SC current, kA			
		30	50	70	100
Without insulation	Copper	22.61	37.68	52.76	75.37
	Aluminum	30.04	50.06	70.09	100.13
PVC, R	Copper	22.61	37.68	52.76	75.37
	Aluminum	30.04	50.06	70.09	100.13
PET	Copper	22.61	37.68	52.76	75.37
	Aluminum	30.04	50.06	70.09	100.13

From the data of Table 5 it follows that the critical amplitudes of the densities $\delta_{Ci} \approx I_{mk}/S_{Ci}$ of the SC current $i_k(t)$ at time t_k=160 ms of its flow (switch off) in the power circuits of the electrical equipment under consideration for uninsulated wires and insulated wires (cables) with PVC, R and PET insulation with copper (aluminum) cores (shells) in the circuits of electrical equipment for general industrial use (T_p=20 ms; T_a=50 ms) numerically are approximately 1.33 kA/mm^2 and 0.99 kA/mm^2, respectively. Here, the numerical values of the critical amplitudes of the densities δ_{Ci} of the SC current $i_k(t)$ in the copper (aluminum) cores (shells) of the CCP of the industrial electric power equipment under consideration, indicated for the calculation case (t_k=160 ms; T_a=50 ms), as well as for the previous case (t_k=100 ms; T_a=50 ms), do not depend on the quantitative values of the amplitude I_{mk} of the steady SC current. In addition, from the data of Table 4, 5 it follows that the quantitative values of the critical cross-sections S_{Ci} and critical amplitudes of densities δ_{Ci} of AC SC current $i_k(t)$ for the current-carrying parts of the investigated CCP, which is widely used in power circuits of electrical equipment of general industrial use, do not depend on any type of insulation (air or solid) used in the considered electric wires and cables of electric power devices.

Conclusions.

1. The proposed electrical engineering approach allows, according to the condition of the EE in the atmospheric air of the current-carrying parts of the CCP, to approximate the critical cross-sections S_{Ci} and the amplitudes of the densities δ_{Ci} of the AC axial current for uninsulated wires with copper (aluminum) cores, as well as for insulated wires and cables with copper (aluminum) cores (shells), PVC, R and PET insulation, through which AC SC current $i_k(t)$ with given ATPs flows during emergency operation of power electrical equipment for general industrial use.

2. The used approximate calculation relations (1)-(4) made it possible for two real cases (t_k=100 ms; t_k=160 ms) at T_a=50 ms to establish for a discrete change in the amplitude I_{mk} of the steady SC current $i_k(t)$ in the range (30-100) kA specific capabilities of the proposed electrical engineering approach for the selection of critical sections S_{Ci} and density amplitudes δ_{Ci} of AC current in

the indicated wires and cables of power circuits of electrical equipment of general industrial use, in the current-carrying parts of which in emergency operating modes of the considered power electrical equipment large axial SC currents $i_k(t)$ flow.

3. It was established by calculation that the critical amplitudes of the densities $\delta_{Ci} \approx I_{mk}/S_{Ci}$ of the axial SC current $i_k(t)$ in copper (aluminum) cores of uninsulated wires and insulated wires (cables) with copper (aluminum) cores (shells), PVC, R and PET insulation at T_a=50 ms for the case of switch off time t_k=100 ms of the SC current $i_k(t)$ in the power circuits of electrical equipment numerically equal approximately 1.57 (1.18) kA/mm^2, and for a case of t_k=160 ms – 1.33 (0.99) kA/mm^2.

4. The results obtained for critical cross-sections S_{Ci} and density amplitudes δ_{Ci} of AC axial current with frequency f = 50 Hz (T_p=20 ms) can be used in electric power practice to choice thermally resistant to large SC axial currents $i_k(t)$ the CCP with copper (aluminum) cores (shells), designed to operate in power circuits of electrical equipment of power industry.

REFERENCES

1. Baranov M.I. Calculation and experimental determination of critical sections of electric wires and cables in the circuits of devices of high-voltage high-current pulse technique. *Electrical engineering & electromechanics*, 2019, no.2, pp. 39-46. **doi: 10.20998/2074-272X.2019.2.06.**

2. Knopfel' G. *Sverkhsil'nye impul'snye magnitnye polia* [Ultra strong pulsed magnetic fields]. Moscow, Mir Publ., 1972. 391 p. (Rus).

3. Baranov M.I. *Izbrannye voprosy elektrofiziki. Monografiya v 3kh tomakh. Tom 3: Teorija i praktika elektrofizicheskih zadach* [Selected topics of Electrophysics. Monograph in 3 Vols. Vol. 3. Theory and practice of electrophysics tasks]. Kharkiv, Tochka Publ., 2014. 400 p. (Rus).

4. Orlov I.N. *Elektrotehnicheskij spravochnik. Proizvodstvo i raspredelenie elektricheskoj energii. Tom 3, Kn. 1* [Electrical engineering handbook. Production and distribution of electric energy. Vol. 3, Book 1. Ed. I.N. Orlov]. Moscow, Energoatomizdat Publ., 1988. 880 p. (Rus).

5. Belorussov N.I., Saakjan A.E., Jakovleva A.I. *Elektricheskie kabeli, provoda i shnury. Spravochnik* [Electrical cables, wires and cords. Directory]. Moscow, Energoatomizdat Publ., 1988. 536 p. (Rus).

6. Baranov M.I. A choice of sections of electric wires and cables in circuits of devices of high-voltage high-current impulse technique. *Electrical engineering & electromechanics*, 2018, no.6, pp. 56-62. **doi: 10.20998/2074-272X.2018.6.08.**

7. Baranov M.I. Refined selection of allowable cross-sections of electrical conductors and cables in the power circuits of industrial electrical equipment taking into account emergency operating modes. *Electrical engineering & electromechanics*, 2019, no.3, pp. 37-43. **doi: 10.20998/2074-272X.2019.3.06.**

8. Knyazevskyi B.A., Lipkin B.Yu. *Elekrosnabzhenie promyschlennyh predpriyatij* [Power supply of industrial enterprises]. Moscow, High School Publ., 1972. 432 p. (Rus).

Received 04.02.2019

M.I. Baranov, Doctor of Technical Science, Professor,
Scientific-&-Research Planning-&-Design Institute «Molniya»,
National Technical University «Kharkiv Polytechnic Institute»,
47, Shevchenko Str., Kharkiv, 61013, Ukraine,
phone +38 057 7076841, e-mail: baranovmi@kpi.kharkov.ua

How to cite this article:
Baranov M.I. A choice of critical sections of electric wires and cables in power circuits of electrical equipment of power industry. *Electrical engineering & electromechanics*, 2019, no.5, pp. 35-39. **doi: 10.20998/2074-272X.2019.5.06.**

UDC 624.318 **doi: 10.20998/2074-272X.2019.5.07**

Yu.V. Batygin, E.A. Chaplygin, S.A. Shinderuk, V.A. Strelnikova

NUMERICAL ESTIMATES OF CURRENTS AND FORCES IN LINEAR TOOLS OF THE MAGNETIC-PULSE ATTRACTION OF METALS. PART 1: LOW ELECTRICAL CONDUCTANCE METALS

Purpose. *The electrodynamics processes study in the linear tools of magnetic-pulsed attraction, the final result of which should be the physics-mathematical dependencies for the characteristics of the flowing processes, under the conditions of intensive penetration in metal of acting electromagnetic fields, as well as numerical estimates of these processes main characteristics.* ***Methodology.*** *To carry out research, we used the fundamental statements of the electromagnetic field theory and the mathematical simulation with help of the standard codes from the Wolfram Mathematica package.* ***Results.*** *The functional dependencies for the space-temporal distributions of the currents and forces excited in the linear tools of magnetic-pulsed attraction under intensive penetration of the acting electromagnetic fields through the tool's conducting construction elements are used for the numerical estimates. From the calculation results it follows that from a physical point of view, the cause of the increase in attractive forces while decreasing the operating frequencies can be considered the intensification of penetration processes of the excited fields, which leads to increasing the magnetic pressure from the outside. Thus, the transition to low operating frequencies of the exciting currents can significantly increase the efficiency of the magnetic-pulsed attraction of the sheet metals with the linear tools.* ***Originality.*** *It was firstly determined that from the physical point of view, the reason for the increase in attractive forces with a decrease in operating frequencies can be considered the intensification of penetration processes of the excited fields, which leads to increasing the forces of magnetic pressure on the conductors from side of their external surfaces.* ***Practical value.*** *A usage of the obtained results will allow creating new, more efficient linear tools of magnetic-pulsed attraction of the low-electrical conduction sheet metals operating under conditions of intensive penetration of the electromagnetic fields being excited.* References 10, figures 9.

Key worlds: **linear tool for eliminating dents in sheet conductors, intensive penetration of the field into metals with low electrical conductance, magnetic-pulse attraction of conductors with unidirectional currents.**

Метою статті є проведення чисельних оцінок основних характеристик електродинамічних процесів в лінійних інструментах магнітно-імпульсного притягання провідників з односпрямованими струмами в умовах інтенсивного проникнення діючих електромагнітних полів в метали з низькою питомою електропровідністю. Методика. Для проведення обчислень використовувалися положення теорії електромагнітного поля, що витікають з рівнянь Максвелла, і стандартні математичні програми з пакета Wolfram Mathematica. Результати. За допомогою аналітичних виразів розраховані амплітудно-часові залежності струмів і електродинамічних зусиль в лінійних магнітно-імпульсних інструментах, дієвість яких заснована на збудженні сил взаємного притягання провідників з односпрямованими струмами. Вперше встановлено, що збільшення сил притягання, в першу чергу, можливо за рахунок інтенсифікації процесів проникнення полів, що забезпечується переходом до досить низьких робочих частот збуджуючих струмів. Практична значимість. Використання отриманих результатів дозволить створювати нові більш ефективні лінійні інструменти магнітно-імпульсного притягання заданих ділянок листових металів, що працюють в умовах інтенсивного проникнення збуджених електромагнітних полів. Бібл. 10, рис. 9.

Ключові слова: **лінійний інструмент усунення вм'ятин в листових провідниках, інтенсивне проникнення поля в метали з низькою питомою електропровідністю, магнітно-імпульсне притягання провідників з односпрямованим струмами.**

Целью статьи является проведение численных оценок основных характеристик электродинамических процессов в линейных инструментах магнитно-импульсного притяжения проводников с однонаправленными токами в условиях интенсивного проникновения действующих электромагнитных полей в металлы с низкой удельной электропроводностью. Методика. Для проведения вычислений использовались положения теории электромагнитного поля, вытекающие из уравнений Максвелла, и стандартные математические программы из пакета «Wolfram Mathematica». Результаты. С помощью аналитических выражений рассчитаны амплитудно-временные зависимости токов и электродинамических усилий в линейных магнитно-импульсных инструментах, действенность которых основана на возбуждении сил взаимного притяжения проводников с однонаправленными токами. Впервые установлено, что увеличение сил притяжения, в первую очередь, возможно за счет интенсификации процессов проникновения полей, что обеспечивается переходом к достаточно низким рабочим частотам возбуждающих токов. Практическая значимость. Использование полученных результатов позволит создавать новые более эффективные линейные инструменты магнитно-импульсного притяжения заданных участков листовых металлов, работающие в условиях интенсивного проникновения возбуждаемых электромагнитных полей. Библ. 10, рис. 9.

Ключевые слова: **линейный инструмент устранения вмятин в листовых проводниках, интенсивное проникновение поля в металлы с низкой удельной электропроводностью, магнитно-импульсное притяжение проводников с однонаправленными токами.**

Introduction. The methods of attraction of specified sections of sheet metals using the energy of pulsed magnetic fields for various kinds of processing technologies are becoming increasingly relevant in various industries [1-3]. Particular attention is paid to the development of technologies for removing dents and leveling sheet metal surfaces during the restoration of aircraft and care bodies [4].

As practice shows, more than 50 % of damages are dents in areas with difficult or completely closed reverse access [4]. In this regard, a very attractive method of magnetic-pulse attraction of thin-walled sheet metals, which can be the basis for creating an effective tool for external straightening of car bodies, is the attraction by linear tools. The physical essence of this method consists in the force interaction of unidirectional parallel currents (Ampere law [10]). The first is the current in the main current lead of a linear instrument (an analog of an inductor, in the generally accepted terminology [1]). The second is the current in the metal being processed. Both currents are excited by direct serial or parallel point connection to a power source. The main conductor is the linear tool firmly fixed. The metal being processed is deformed by attraction. An obvious obstacle to the effective excitation of electrodynamic forces can be induction effects, respectively to which the current in the main current lead induces a countercurrent in the sheet workpiece, and the current in its metal induces a countercurrent in the main current lead of a linear tool.

In general, the attractiveness of this method is due to the simplicity of technical implementation and fairly high energy performance [5, 6]. An analysis of electrodynamic processes in such a scheme will establish the requirements, the fulfillment of which will provide not only ability, but also the effectiveness of the tool of the proposed principle of action.

In fairness, it should be noted that a similar problem has already been considered previously by the authors [7, 8]. However, the direct use of the obtained formulas and relations obtained in the cited works for practical calculations is not possible, due to the limited results found by the conditions for the formulation and solution of this problem.

The goal of the work is an analysis of the temporal characteristics of electrodynamic processes in linear instruments of magnetic-pulse attraction of sheet metals, the final result of which should be physical and mathematical dependencies for the excited currents and forces under conditions of intensive penetration of electromagnetic fields into the conducting elements of tools.

Physico-mathematical model, assumptions and problem definition. For the analysis of electromagnetic processes in the considered metal processing scheme, we adopt a calculation model (Fig. 1) corresponding to the cross section of the studied electromagnetic system with currents J_1 and J_2 [9].

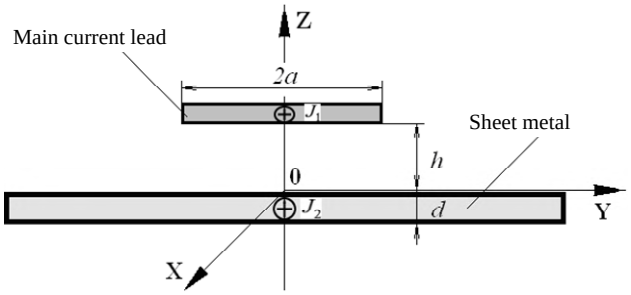

Fig 1. Calculation models ($J_{1,2}$ – flowing currents)

The workpiece being processed is a rather thin sheet metal of thickness d with rather large transverse dimensions and electrical conductance of the material γ.

The main current lead is also «transparent» to the existing fields, so that its metal does not affect the flowing electromagnetic processes. There is a geometric symmetry of the system relative to the ZOX coordinate plane. Along the abscissa axis OX, the system has a sufficiently large extent, so that the differentiation operator $\partial/\partial x = 0$. In the main current lead in the direction of the OX axis, an exciting current uniformly distributed along OY with linear density $j(t)=j_m \cdot j_t(t)$ flows, where $j_m = I_m/2a$ is the amplitude of the current density (I_m is the maximum of the current), and $j_t(t)$ is the time dependence of the current.

The frequency characteristics of the exciting current are such that the condition of quasistationarity according to Landau – $\frac{\omega}{c} \cdot b << 1$ [10], where ω is the cyclic frequency of the process; c is the speed of light in vacuum; b is the arbitrary characteristic size of the considered electromagnetic system. Let an electromagnetic field with nonzero strength components $E_x \neq 0$; $H_{y,z} \neq 0$ be excited in the system. It is required to estimate the currents and forces in the electromagnetic system under consideration.

Calculation relations. For further calculations, we use the analytical expressions obtained by the authors of [9]. According to the cited publication, on the assumption that the main current lead and the given section of the deformed metal are parallel, the excited currents taking into account induction effects can be described by the following relationship. Total current in the main lead:

$$I_x^{(s)}(t) = I_m \left[\begin{array}{l} j_t(t) - \left(\frac{4a}{\pi d}\right) \int_0^\infty \left(\frac{\sin\left(\alpha \frac{a}{d}\right)}{\left(\alpha \frac{a}{d}\right)} \right) \times \\ \times e^{-\alpha \frac{h}{d}} \sum_{k=0}^{\infty} \delta_k \frac{G(\beta_k,\alpha)}{\Phi(\beta_k,\alpha)} \left(\frac{dj_t(t)}{dt} \cdot e^{p_k t} \right) \alpha \partial \alpha \end{array} \right] \quad (1)$$

where

$$G(\beta_k,\alpha) = \left[(1-\cos\beta_k) + \left(\frac{\beta_k}{\alpha}\right) \right] \cdot \sin\beta_k;$$

$$\Phi(\beta_k,\alpha) = \cos\beta_k \cdot \left[\alpha^2 + 2\alpha - \beta_k^2\right] + 2\beta_k \sin\beta_k \cdot [\alpha + 1];$$

δ_k is the Kronecker symbol; β_k are the roots of the equation:

$$\operatorname{ctg}\beta_k = 0{,}5 \cdot \left(\frac{\beta_k}{\alpha} - \frac{\alpha}{\beta_k} \right); \; p_k = -\frac{1}{\left(\mu_0 \gamma d^2\right)} \cdot \left(\beta_k^2 + \alpha^2\right),$$

$k = 0, \pm 1, 2\ldots$; $\left(\frac{dj_t(t)}{dt} \cdot e^{p_k t} \right)$ is the convolution of functions.

The integral force of attraction, excited by the interaction of identical unidirectional parallel currents for the same conductors – the main current lead and the given section of sheet metal, is written in the form [5]:

$$F_{attr}(t) = \frac{\mu_0}{2\pi} \cdot \left(I_x^{(s)}(t) \right)^2 \frac{l}{h}, \qquad (2)$$

where μ_0 is the magnetic constant; l is the conductor length; h is the distance between the main current lead and sheet metal.

We carry out **numerical estimates** for the following initial data. Sheet metal – d = 0.001 m, $\gamma = 0.4 \cdot 10^7$ $(\Omega \cdot м)^{-1}$ (steel). The main current lead is made of the same metal and the same thickness as the object being processed (the electrodynamic system «steel –steel» is considered). The geometry of the system is l = 0.06 mm, $2a$ = 0.01 ... 0.06 m, h = 0.002 m, the working area of the tool is the region $l \times (2a)$. The main current lead and the given section of the metal being processed are parallel and identical, so that the currents flowing in the circuit of each of them are the same.

The parameters of current pulses are determined by the characteristics of the power source – magnetic pulse installation МИУС-2 [2], developed and created at the Laboratory of Electromagnetic Technologies of Kharkiv National Automobile and Highway University.

The maximum voltage at the capacitive storage is U = 2000 V. The maximum operating frequency when connected directly to the МИУС-2 electrical output is f_{max} = 7000 Hz (relative attenuation coefficient is δ/ω = = 0.3). The operating frequency in the discharge circuit of the installation is f_p = 1000 ... 1500 Hz (relative attenuation coefficient is δ/ω = 0.3) when it is connected through a matching device with a coefficient of energy transfer to the instrument working area $K \approx 4$. Magnetic-pulse installation МИУС-2 allows to operate in 2 modes. The first mode is the generation of exponentially decaying (oscillating) current pulses. The second mode is the generation of current pulses of an aperiodic (unipolar) time shape. It should be noted that the latter mode is more preferable for practice, since the operation of thyristor switches of this installation with unipolar signals is characterized by a longer term of their operation.

The calculations were carried out using the standard Wolfram Mathematica software package. The approximate interval of variation of the integration variable $\alpha \in [0; \alpha_{max}]$ is determined by the functional form of the Fourier image of the transverse distribution of the exciting current. For values $\alpha \in [0; \alpha_{max}]$ the modulus of the distribution function must be nonzero. As shown by numerical estimates for the maximum $\alpha \in [0; 1]$. In the general case, the calculated dependence $\beta_k = \beta_k(\alpha)$ can be approximated by the totality of the sequence of linear functions. Numerical estimates showed that for the adopted geometry of the main current lead (inductor), the approximation of $\beta_k(\alpha)$ by the analytical dependence $\beta_k \approx \sqrt{2\alpha} + k \cdot \pi$, k = 0, ±1, ±2… seems to be quite satisfactory. The found dependence $\beta_k = \beta_k(\alpha)$ is substituted into the integrand expression of the dependence (1).

The improper integrals and the sums of the series in them are calculated using the standard NIntegrate and NSum programs. Summation in rows is performed for different numbers of higher harmonics. Their number taken into account is considered sufficient if an increase in the limiting value of «k» per unit does not lead to a result different from the previous one by more than 5 ... 10 %. Correction of the integration interval $\alpha \in [0; \alpha_{max}]$ is made for the condition $\alpha < \alpha_{max}$ accepted a priori by comparing the final results of the calculations. Their discrepancy is allowed ~ 5 ... 10 %.

The graphs of the characteristic calculated dependencies are grouped below by the type of current pulses generated by the magnetic pulse installation.

Graphic illustrations. In accordance with the capabilities of the power source in terms of generating current signals of various time shapes, numerical estimates of the parameters under consideration were performed initially for oscillating current pulses (Fig. 2-5).

Option No. 1. Operating frequency is f = 7000 Hz, voltage is U = 2000 V, working area: $l \times (2a)$ = 0.06 m × 0.06 m.

From the results of calculations for high operating frequencies (f = 7000 Hz) it follows that in the mode of oscillating pulses of the exciting current, the maximum potential of the power source corresponds to a maximum of the attractive force of ~ 1000 N. The transition to the unipolar pulse of the exciting current leads to a decrease in the amplitude of the attractive force by almost ~ 2 times, i.e. up to ~ 500 N.

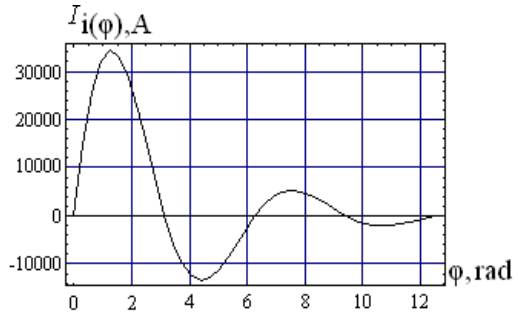

Fig. 2. Exciting current

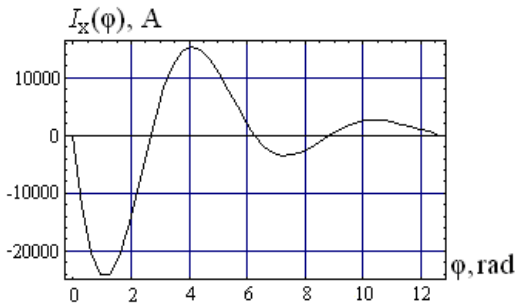

Fig. 3. Induced current

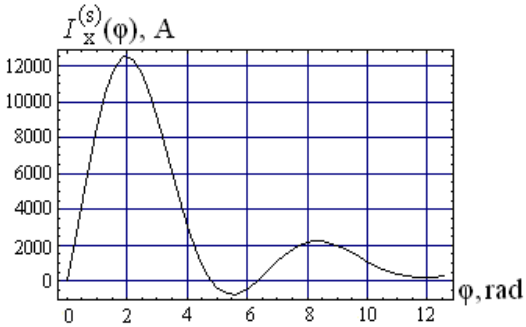

Fig. 4. Total current in the circuit of each of the interacting conductors

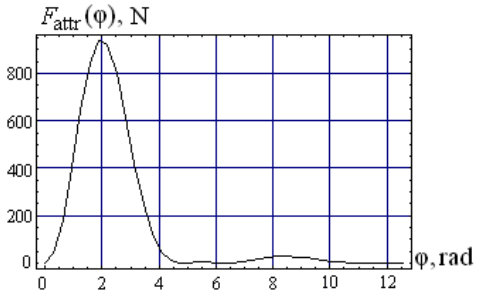

Fig. 5. Excited attractive force

From a physical point of view, as the reason for a decrease in the attractive force with an aperiodic shape of the exciting current, a decrease in its temporal duration in comparison with an oscillating and exponentially decaying harmonic signal can be considered (see Fig. 2, where $\varphi \in [0, (4\cdot\pi)]$). This, obviously, leads to a reduction in the development time of electrodynamic processes in the processed object. All further calculations were performed for the unipolar shape of the exciting current, as more preferable for practice (increase in the operating life of the thyristor switches of the installation) (Fig. 6-9).

Option No. 2. Working frequency is f = 1500 Hz, voltage is U = 2000 V, working area: $l\times(2a)$ = 0.06 m × × 0.06 m.

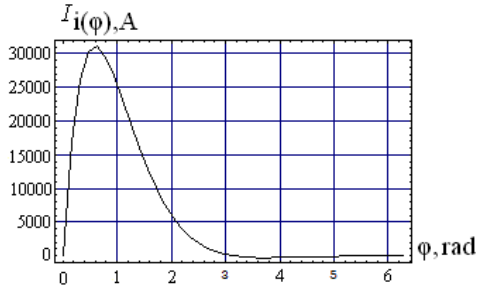

Fig. 6. Exciting current

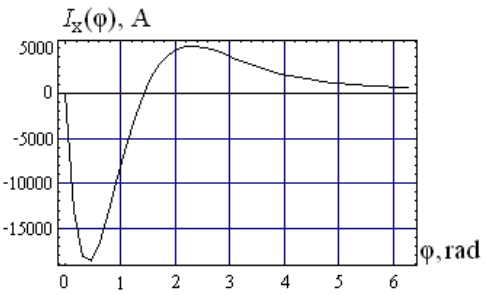

Fig. 7. Induced current

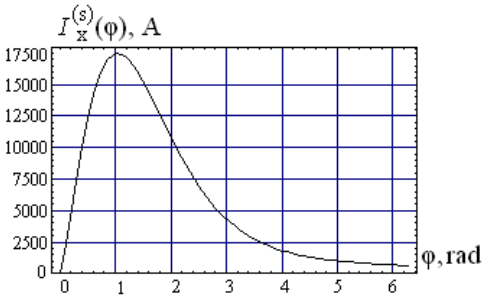

Fig. 8. Total current in the circuit of each of the interacting conductors

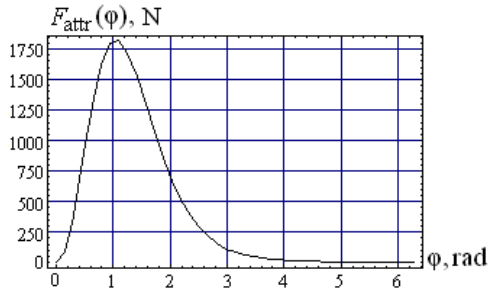

Fig. 9. Excited attractive force

From the results of calculations for low operating frequencies (f = 1500 Hz) it follows that:

- the maximum potential of the power source corresponds to the maximum of the attractive force ~ 1800 N, which is approximately 2 times higher than the similar maximum for high frequencies (f = 7000 Hz) of the exciting current;
- from a physical point of view, as the reason for the increase in attractive forces with a decrease in working frequencies, the intensification of the processes of penetration of excited fields into the workpiece metal and tool can be considered, which leads to an increase in magnetic field strengths from the outside of the system conductors and, accordingly, to an increase in magnetic pressure forces them from the outside.

Conclusions.

1. The amplitude-temporal dependencies of the characteristics of electromagnetic processes in linear instruments of magnetic-pulse attraction of sheet metals with low electrical conductance at the intense penetration of the excited magnetic fields into the conductive elements of the tools and the processed objects are calculated.

2. It has been established that the transition to low operating frequencies of exciting currents can significantly increase the amplitudes of the attractive forces of metal (for example, at f = 1.5 kHz, the force indicators for the steel being processed increase by about 2 times compared with the case when f = 7 kHz) .

3. It is shown that as the physical reason for the increase in attractive forces with a decrease in working frequencies, the intensification of the processes of penetration of the excited fields through the metal of the tool and the workpiece can be considered, which leads to an increase in the magnetic pressure forces on the conductors from the outside.

Acknowledgment. The work was carried out by the Department of Physics of Kharkiv National Automobile and Highway University in the framework of the Research Project «Energy-saving low-cost technologies of power supply and repair of vehicles» No. 08-53-19, funded by the Ministry of Education and Science of Ukraine.

REFERENCES

1. Psyk V., Risch D., Kinsey B.L., Tekkaya A.E., Kleiner M. Electromagnetic forming – A review. *Journal of Materials Processing Technology*, 2011, vol.211, no.5, pp.787-829. **doi: 10.1016/j.jmatprotec.2010.12.012**.

2. Batygin Yu.V., Chaplygin E.A., Sabokar O.S. Magnetic pulsed processing of metals for advanced technologies of mod-

ernity – a brief review. *Electrical engineering & electromechanics*, 2016, no.5, pp. 35-39. **doi: 10.20998/2074-272X.2016.5.05**.

3. Hnatov A., Arhun S., Ponikarovska S. Energy saving technologies for urban bus transport. *International journal of automotive and mechanical engineering*, 2017, vol.14, no.4, pp. 4649-4664. **doi: doi:10.15282/ijame.14.4.2017.5.0366.**

4. *Welcome to BETAG Innovation*. Available at: http://www.betaginnovation.com (accessed 17 June 2018).

5. Bondarenko A.Yu., Finkelishteyn V.B., Gavrilova T.V. External straightening basket of the motor transport by means of electro dynamic of the systems at direct drive pulsed current. *Bulletin of NTU «KhPI». Series: Car- and tractorbuilding*, 2014, no.9(1052), pp. 66-72. (Rus).

6. Batygin Yu.V., Chaplygin E.A., Sabokar O.S. Estimating the limit possibilities of the step charging system for capacitive energy storage. *Electrical engineering & electromechanics*, 2016, no.2, pp. 35-37. **doi: 10.20998/2074-272X.2016.2.06**.

7. Shneerson G.A. *Polja i perehodnye processy v apparature sil'nyh tokov. 2-e izd., pererab. i dop.* [Fields and transients in the equipment of strong currents. 2nd edition]. Moscow, Energoizdat Publ., 1992. 413 p. (Rus).

8. Batygin Yu.V., Chaplygin E.A., Shinderuk S.A. Calculation of fields and currents in the induction system with the attractive screen and the additional coil as a tool for the straightening. *Electrical engineering & electromechanics*, 2015, no.1, pp. 57-62. (Rus). **doi: 10.20998/2074-272X.2015.1.11**.

9. Batygin Yu.V., Yeryomina O.F., Chaplygin E.A., Strelnikova V.A. Electrodynamic processes in instruments of magnetic pulse attract at «direct current passing» through the handled metal. *Bulletin of NTU «KhPI». Series: Mathematical modeling in engineering and technologies*, 2019, no.8(1333), pp. 207-213. (Rus).

10. Landau L.D., Lifshits E.M. *Elektrodinamika sploshnyh sred T. 8* [Continuum Electrodynamics. Vol.8]. Moscow, Fizmatlit Publ., 2005. 656 p. (Rus).

Received 16.04.2019

Yu.V. Batygin[1], *Doctor of Technical Science, Professor,*
E.A. Chaplygin[1], *Candidate of Technical Science, Associate Professor,*
S.A. Shinderuk[1], *Candidate of Technical Science, Associate Professor,*
V.A. Strelnikova[1], *Postgraduate Student,*
[1] Kharkiv National Automobile and Highway University,
25, Yaroslava Mudrogo Str., Kharkov, 61002, Ukraine,
phone +380 57 7003852,
e-mail: yu.v.batygin@gmail.com; chaplygin.e.a@gmail.com;
s.shinderuk.2016102@ukr.net; v.strelnikova91@gmail.com

How to cite this article:
Batygin Yu.V., Chaplygin E.A., Shinderuk S.A., Strelnikova V.A. Numerical estimates of currents and forces in linear tools of the magnetic-pulse attraction of metals. Part 1: Low electrical conductance metals. *Electrical engineering & electromechanics*, 2019, no.5, pp. 40-44. **doi: 10.20998/2074-272X.2019.5.07.**

UDC 621.314.228 **doi: 10.20998/2074-272X.2019.5.08**

A.G. Gurin, I.A. Kostiukov

THE EFFECT OF THE ACTIVE RESISTANCE OF THE PULSE TRANSFORMER WINDINGS ON THE PARAMETERS OF VOLTAGE PULSES GENERATED ON A CAPACITIVE LOAD

Goal. Analysis of the influence of the active resistance of the primary and secondary windings of a pulse transformer on the voltage at the load capacitance based on the developed methodology for the analysis of transients caused by the discharge of the storage capacitance in the primary winding. Methodology. A model for calculating transients is developed using the Laplace transform. Transient modeling is carried out in the MATLAB software package. The results of transient calculations are compared with experimental results. Results. A method for calculating transients in test installations with pulse transformers has been developed, which allows taking into account the effect of power losses in the primary and secondary windings on the voltage at the load capacitance. The calculated relations are obtained, allowing to take into account the influence of the active resistance of the primary and secondary windings of the transformer on the voltage at the load capacitance, the currents in the primary and secondary windings of the transformer, as well as on the voltage drop on the inductance of the primary winding of the transformer. Scientific novelty. A mathematical model is developed for calculating transients in the primary and secondary windings of a pulse transformer, taking into account the influence of the active resistance of the windings when it changes over a wide range of possible values. Practical value. Using the proposed technique, it is possible to determine the parameters of the discharge circuit at which test voltage pulses are formed on the load capacitance without distorting the shape of the pulse front. References 14, figures. 5.

Key words: **pulse transformer, capacitive load, winding active resistance, test voltage pulse, electrical insulation test.**

Мета. Аналіз впливу активного опору первинної та вторинної обмоток імпульсного трансформатору на напругу на навантажувальній ємності на основі розробленої методики аналізу перехідних процесів, що обумовлені розрядом накопичувальної ємності в первинній обмотці. Методика. Модель для розрахунку перехідних процесів розроблена із використанням перетворення Лапласа. Моделювання перехідних процесів проведено в програмному пакеті MATLAB. Результати розрахунку перехідних процесів порівняно із експериментальними результатами. Результати. Розроблено методику розрахунку перехідних процесів у випробувальних установках з імпульсними трансформаторами, що дає можливість враховувати втрати потужності в первинній та вторинній обмотках на напругу на навантажувальній ємності. Отримані розрахункові співвідношення, що дозволяють враховувати вплив активного опору первинної та вторинної обмоток трансформатору на напругу на навантажувальній ємності, струми у первинній та вторинній обмотках трансформатору, а також на напругу на індуктивності первинної обмотки трансформатору. Наукова новизна. Розроблена математична модель для розрахунку перехідних процесів в первинній та вторинній обмотках трансформатору із врахуванням впливу активного опору обмоток при його зміні в широкому діапазоні можливих значень. Практичне значення. Використання розробленої методики дозволяє визначати параметри розрядного кола, при яких на навантажувальній ємності відбувається формування імпульсів напруги без зміни форми фронту імпульсу. Бібл. 14, рис. 5.

Ключові слова: **імпульсний трансформатор, ємнісне навантаження, активний опір обмоток, імпульс випробувальної напруги, випробування електричної ізоляції.**

Цель. Анализ влияния активного сопротивления первичной и вторичной обмоток импульсного трансформатора на напряжение на нагрузочной емкости на основании разработанной методики анализа переходных процессов, вызванных разрядом накопительной емкости в первичной обмотке. Методика. Модель для расчета переходных процессов разработана с применением преобразования Лапласа. Моделирование переходных процессов проводилось в программном пакете MATLAB. Результаты расчетов переходных процессов сравнивались с экспериментальными результатами. Результаты. Разработана методика расчета переходных процессов в испытательных установках с импульсными трансформаторами, позволяющая учитывать влияние потерь мощности в первичной и вторичной обмотках на напряжение на нагрузочной емкости. Получены расчетные соотношения, позволяющие учитывать влияние активного сопротивления первичной и вторичной обмоток трансформатора на напряжение на нагрузочной емкости, токи в первичной и вторичной обмотках трансформатора, а также на падение напряжения на индуктивности первичной обмотки трансформатора. Научная новизна. Разработана математическая модель для расчета переходных процессов в первичной и вторичной обмотках импульсного трансформатора с учетом влияния активного сопротивления обмоток при его изменении в широком диапазоне возможных значений. Практическое значение. Использование предложенной методики позволяет определять параметры разрядной цепи, при которых на нагрузочной емкости происходит формирование тестовых импульсов напряжения без искажений формы фронта импульсов. Библ. 14, рис. 5.

Ключевые слова: **импульсный трансформатор, емкостная нагрузка, активное сопротивление обмоток, импульс испытательного напряжения, испытания электрической изоляции.**

Introduction. The problem of controlling the stability of insulation of electric power equipment in relation to overvoltages due to various causes is usually solved by using pulse voltage generators. Such generators can be developed using the widespread Arkadyev-Marx scheme [1], which, when applied, implies the charge of electric capacitors when they are connected in parallel, followed by discharge when connected in series. An example of the practical application of the mentioned

method for generating test pulses is given in [2], which describes a generator with stored energy up to 0.48 MJ, for generating voltage pulses with amplitude of up to 3 MV. This approach allows to simulate overvoltage pulses that occur as a result of lightning strikes, as well as switching overvoltages. A detailed description of the metrological equipment used in the practice of forming high-voltage voltage pulses is given in [3]. Although the use of Marx generators allows the generation of voltage pulses with sufficient amplitude levels and time characteristics that are satisfactory for practical purposes, the practical implementation of such schemes leads to certain difficulties, primarily due to the need to use a significant number of arresters [4].

Another widespread approach that is used in the practice of generating high-voltage pulses is based on the implementation of various circuits, which involve amplifying voltage pulses to the required level using pulse transformers. A typical example is the pulse transformer with a magnetic core consisting of 68 ferrite rods described in [5]. In some technical applications, certain advantages can be obtained by using air transformers, since transformers of this type do not require additional demagnetization circuits, which are usually used to ensure maximum magnitude of magnetic flux density in the core [6].

One of the most common problems for high-voltage installations with pulse transformers is the need to determine the voltage at the load capacitance in a wide range of its values. In the case of using pulse transformers with magnetic cores, relatively small values of the open circuit current in some cases allow mathematical analysis of the discharge of the storage capacitor, neglecting the value of the magnetization inductance. The results of mathematical modelling of discharge processes of a storage capacitor on the primary circuit of a pulse transformer with a magnetic core, performed in [4], showed that an increase in the load capacitance leads to a decrease in the voltage across it. In the case of using an air transformer, its analysis is often carried out without taking into account the active resistance of the primary and secondary windings. A detailed analysis of the transient in a pulse transformer, taking into account the influence of energy losses in the primary and secondary windings on the voltage value at the load capacitance, was performed in [8]. However, the solution of a differential equation of the 4^{th} order, which determines the shape of the current in the primary and secondary windings, was obtained in the form in which the existence of only complex conjugate roots of the characteristic equation is implied. These types of roots usually occur in the case of analysis of circuits with a sufficiently high quality factor. Therefore, the scope of the mentioned analysis is limited by the range of problems that occur in the case of rather insignificant losses in the primary and secondary windings. Although such an analysis is sufficient for the vast majority of practical cases, an increase in losses in the primary and secondary windings can lead to other solutions of the characteristic equation. Obviously, such pulse transformers will have degraded technical characteristics compared to transformers with reduced losses. Nevertheless, if it is necessary to generate voltage pulses with certain requirements for the duration of the front and the cutoff of the pulse, for example, when forming voltage pulses in a shape close to aperiodic, circuits with a reduced quality factor may be of some interest. The increase in active resistance allows to reduce or completely eliminate the distortion of voltage pulses, which are caused by oscillatory processes in electrical circuits with high quality factor. Therefore, for some cases, it is preferable to develop a more universal solution that allows to analyze transients in the primary and secondary windings of a pulse transformer for a wider range of power losses in the windings. Such a problem was also considered in [9]; however, the presented solutions, similarly to the results of [8], describe the case of weakly damped oscillations, which usually occur in the case of relatively insignificant losses in the primary and secondary windings. In addition, issues related to determining the voltage across the capacitance of the tested object are not addressed in [9]. The expression for the voltage at the load capacitance in operator form and general form is given in [10]. However, the original of this expression was determined for its simplified form, in which the value of the active resistance of the windings was not taken into account. The solutions given in [11] take into account the influence of the secondary active resistance on the voltage on the capacitance of the secondary circuit, but the analysis was carried out for the case of primary circuit excitation by harmonic voltage. In this paper, attention is focused on the case of primary circuit excitation by discharging the storage capacitance. A detailed analysis of the conditions for obtaining maximum voltages on the capacitance of the secondary circuit without taking into account the influence of the active resistance of the windings of the primary and secondary circuits on the temporal characteristics of the voltage was performed in [12]. There are no publications that take into account the attenuation of the voltage at the load capacitance associated with the parameters of the primary and secondary circuits [13]. The relations given in [13] for the voltage on the electric capacitance of the secondary winding obtained after such an analysis are also based on the consideration of the oscillation voltage on it. Thus, the issues of the formation of test voltage pulses at the load capacitance close to the aperiodic shape are closely related to the results given in [8, 13]. Nevertheless, if it is necessary to form such pulses, the analysis should be carried out for the case of more significant values of the active resistance of the windings, which lead to a different type of roots of the characteristic equation.

The goal of the work is an analysis of the influence of the active resistance of the primary and secondary windings of a pulse transformer on the voltage at the load capacitance based on the developed technique for the analysis of transients caused by the discharge of the storage capacitance in the primary winding.

Analysis of the equivalent circuit of a pulse transformer. Transient analysis is performed for the transformer's equivalent circuit shown in Fig. 1.

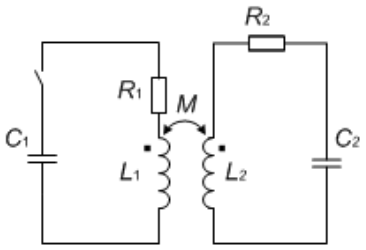

Fig. 1. Equivalent circuit for determining effect of the test object on the voltage pulse parameters at the load capacitance [8]

In the equivalent circuit in Fig. 1, C_1, C_2 represent the capacitances of the capacitor in the primary winding (storage capacitor) and the load capacitance of the test object in the secondary winding, respectively; R_1, R_2 are the resistances of the primary and secondary circuit, respectively; M is the mutual induction coefficient between the primary and secondary windings; L_1, L_2 are the inductances of the primary and secondary windings, respectively.

The analysis is carried out under the assumption of an insignificant parasitic capacitance of the primary and secondary windings (see Fig. 1). In resonance mode, the equality holds

$$L_1C_1 = L_2C_2 . \quad (1)$$

In this case, the equivalent circuit (Fig. 1) is actually a Tesla transformer's equivalent circuit. For the case of negligibly small active resistances of the primary and secondary windings and the previously given equality (1), which determines the relationships between the inductances L_1, L_2 and capacitances C_1, C_2, the voltage at the load capacitance C_2 can be determined using the following expression [14]:

$$U_2 = \frac{U_1}{2}\sqrt{\frac{C_1}{C_2}}\left[\cos\left(\left(\frac{\omega_0}{\sqrt{1-k}}\right)t\right) - \cos\left(\left(\frac{\omega_0}{\sqrt{1+k}}\right)t\right)\right], \quad (2)$$

where k is the coupling coefficient between primary and secondary windings, ω_0 is the natural frequency of oscillations of the primary and secondary windings [14]:

$$\omega_0 = \frac{1}{\sqrt{L_1C_1}} = \frac{1}{\sqrt{L_2C_2}}. \quad (3)$$

Applying the Laplace transform to the expressions for the voltage drop across the elements of the equivalent circuit (Fig. 1), we can obtain relations for determining the current in the secondary winding in the operator form:

$$(pL_1 + R_1 + \frac{1}{pC_1})i_1 - pMi_2 = \frac{u_{c_1}}{p}, \quad (4)$$

$$(pL_2 + R_2 + \frac{1}{pC_2})i_2 - pMi_1 = 0, \quad (5)$$

where u_{c1} is the voltage across the storage capacitor at the beginning of the transient.

Taking the expressions (4), (5), we can write the expressions for the current in the secondary winding:

$$i_2(p) = \frac{p^2Mu_cC_1C_2}{ap^4 + bp^3 + cp^2 + dp + 1}, \quad (6)$$

where constants a, b, c, d can be determined using the following expressions:

$$a = L_2C_2L_1C_1 - M^2C_1C_2, \quad (7)$$

$$b = L_2C_2R_1C_1 + R_2C_2L_1C_1, \quad (8)$$

$$c = L_2C_2 + R_2C_2R_1C_1 + L_1C_1, \quad (9)$$

$$d = R_2C_2 + R_1C_1. \quad (10)$$

In accordance with the usual scheme of applying the Laplace transform, the expression for the dependence of the current in the secondary circuit on time can be written in the general form:

$$i_2(t) = \sum_{n=1}^{4}\frac{N(p_n)}{M'(p_n)}e^{p_nt}, \quad (11)$$

where all $N(p_n)$ are the numerator values in formula (6) at the points that correspond to the roots of the polynomial in the denominator of (6), and all $M'(p_n)$ are the values of the derivative of the polynomial in the denominator of the expression (6) at the points corresponding to the zeros of this denominator.

Thus, assuming that the load capacitance at the beginning of the transient is not charged, the voltage on it can be found using the following expression:

$$u_{c_2}(t) = \frac{1}{C_2}\int_0^t i_2(t)dt = \frac{1}{C_2}\sum_{n=1}^{4}\frac{N(p_n)}{M'(p_n)}\cdot\left(\frac{e^{p_nt}}{p_n} - \frac{1}{p_n}\right). \quad (12)$$

Since the transfer of energy from the primary circuit to the secondary one is made by inductive coupling, the analysis of transients must be performed taking into account the time dependence of the voltage on the inductance of the primary winding. Taking into account relations (4), (5), the expression for the current in the primary circuit can be written in the form:

$$i_1(p) = \frac{u_cC_1(p^2L_2C_2 + pR_2C_2 + 1)}{ap^4 + bp^3 + cp^2 + dp + 1}. \quad (13)$$

The currents in the primary and secondary circuits are determined by expressions in which the denominator is the same (compare (6) and (13)). This circumstance makes it possible to simplify the simulation of transients caused by the discharge of capacitor C_1. Taking into account (13), the expression for the dependence of the current in the primary winding on time can be written in the form:

$$i_1(t) = \sum_{n=1}^{4}\frac{W(p_n)}{M'(p_n)}e^{p_nt}, \quad (14)$$

where $W(p_n)$ represent the values of the numerator from (13) at the points that correspond to the roots of the polynomial from the denominator (6) and (13).

Taking into account the expression (14), the voltage drop across the inductance of the primary winding L_1 can be determined using the following expression:

$$u_{L_1}(t) = L_1\sum_{n=1}^{4}\frac{W(p_n)}{M'(p_n)}p_ne^{p_nt}. \quad (15)$$

Taking into account (11), (14), as well as (4), (5), the expressions for the voltages on the load capacitance (12) and the inductance of the primary winding (15) can be written in the form:

$$u_{C_2}(t) = M\frac{di_1}{dt} - L_2\frac{di_2}{dt} + Ri_2(t), \quad (16)$$

$$u_{L_1}(t) = u_{c1} + M\frac{di_2(t)}{dt} - i_1(t)R_1 - \frac{1}{C}\int_0^t i_1(t)t. \quad (17)$$

Expressions (16), (17) can also be used to partially verify the previously given formulas for the voltage at the load capacitance and inductance of the primary winding.

Simulation results of transients in the primary and secondary windings caused by the discharge of the storage capacitor. Figures 2-5 show the results of transient calculations in the described model of the pulse transformer during its operation on the capacitive load. All calculations and measurements were carried out with the mutual induction between the primary and secondary windings M = 1.133·10^{-4} H. The inductance of the primary winding is taken equal to L_1 = 186·10^{-6} H. Secondary winding inductance: L_2 = 126·10^{-6} H. Despite the fact that in practical applications such circuit parameters do not provide certain advantages from the point of view of technical characteristics, they can be used both to verify the described solutions and to determine the general trends of transients in the primary and secondary windings.

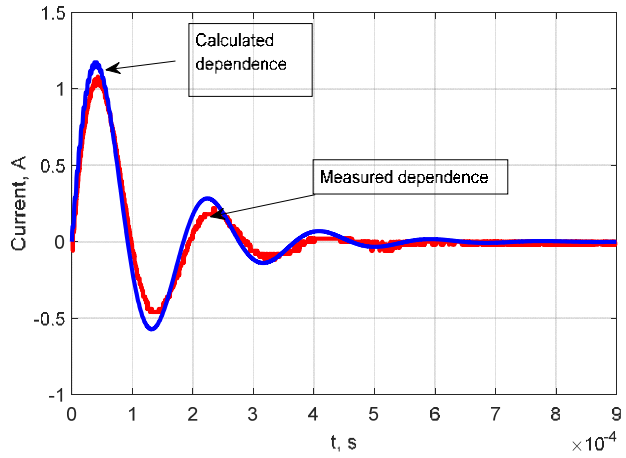

Fig. 2. Results of simulation and measurement of the current in the primary winding for C_2 = 6.128·10^{-9} F, C_1 = 4.5·10^{-6} F, R_2 = 1.57 Ω, R_1 = 2.79 Ω

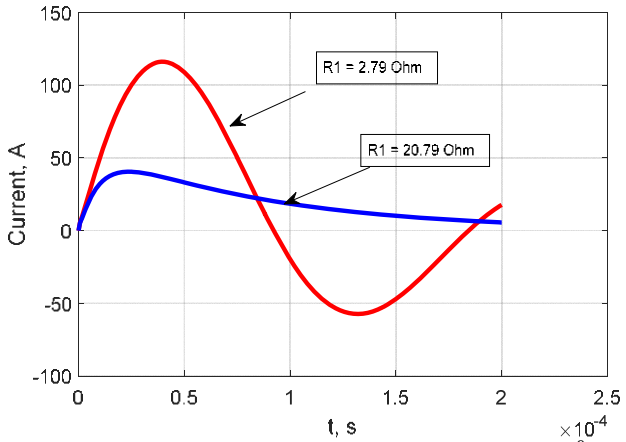

Fig. 3. Currents in the primary winding for C_2 = 6,128·10^{-9} F, C_1 = 4.5·10^{-6} F and charge voltage 1000 V

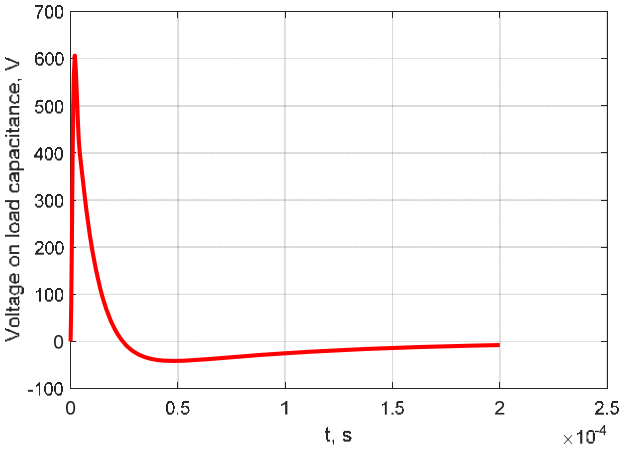

Fig. 4. Voltage at the load capacitance with the active resistance of the primary winding 20.79 Ω and the resistance of the secondary winding 100.57 Ω

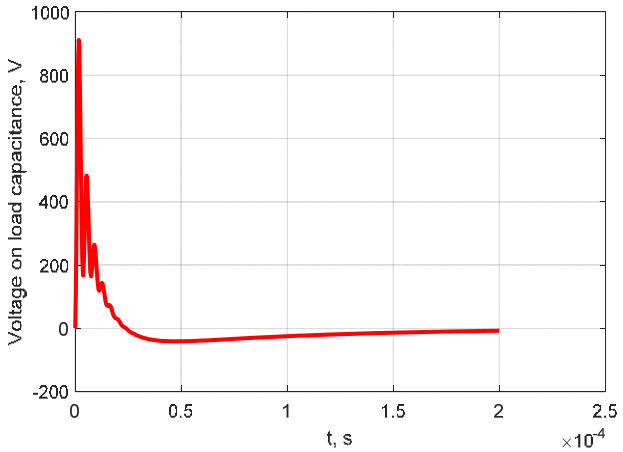

Fig. 5. Voltage at the load capacitance with the active resistance of the primary winding 20.79 Ω and the resistance of the secondary winding 20.57 Ω

It can be seen from the above results that even in the case of the aperiodic discharge mode of the storage capacitor C_1 (calculation results in Fig. 3), which can be achieved by increasing the primary active resistance, the mathematical simulation does not allow the aperiodic shape of the voltage across the load capacitance to be obtained (results calculation in Fig. 4). In this case, at the aperiodic discharge mode of the storage capacitor, the absence of jumps that distort the shape of the voltage at the load capacity of the test object, which are clearly visible in Fig. 5 is not provided. Elimination of the illustrated distortions can be achieved by increasing the time constant of the *RC* circuit in the secondary circuit of the transformer, whose action on the shape of the voltage pulse is seen in Fig. 4.

Conclusions.

1. The described solutions obtained using the Laplace transform can be used if it is necessary to generate voltage pulses on the capacitive load that are close in shape to aperiodic by adjusting the active resistance values of the primary and secondary transformer windings.

2. An increase in the active resistance of the primary winding allows achieving an aperiodic discharge mode of the storage capacitor. However, even with such a discharge mode, it is not possible to provide an aperiodic

shape of voltage at the load capacitance. One of the possible ways to obtain voltage pulses at a capacitive load that is as close as possible to the aperiodic shape is to increase the active resistance of the primary winding to values providing an aperiodic discharge of the storage capacitance, followed by an increase in the active resistance of the secondary winding, to eliminate jumps that distort the shape of the voltage.

3. A negative consequence of the described approach to the formation of voltage pulses is the fact that the elimination of jumps that distort the shape of the voltage due to an increase in the active resistance of the windings is accompanied by an inevitable decrease in the amplitude of the voltage pulse at the capacitive load.

4. Using the above methodology for calculating transients allows controlling the active resistance of the windings in order to eliminate distortion of the front of the voltage pulse, generated at the capacitive load, by high-frequency oscillations.

REFERENCES

1. Baranov M. I., Koliushko G. M., Kravchenko V. I. Generation of standard switching aperiodic impulses of high and superhigh voltage for full-scale tests of electrical power objects. *Electrical engineering & electromechanics*, 2013, no.2, pp. 52-56. (Rus). **doi: 10.20998/2074-272X.2013.2.10.**

2. Baranov M.I., Bocharov V.A., Ignatenko N.N., Kolobovsky A.K. Powerful generators of pulse voltages and currents with top parameters for testing of power electroenergetic equipment. *Electrical engineering & electromechanics*, 2003, no.2, pp. 75-80. (Rus).

3. Baranov M.I., Buriakovskyi S.G., Rudakov S.V. The metrology support in Ukraine of tests of objects of energy, aviation and space-rocket engineering on resistibility to action of pulses of current (voltage) of artificial lightning and commutation pulses of voltage. *Electrical engineering & electromechanics*, 2018, no.5, pp. 44-53. **doi: 10.20998/2074-272X.2018.5.08.**

4. Ivanov V.M. High voltage pulsed transformers with low leakage inductance. *Electrical engineering & electromechanics*, 2010, no.5, pp. 17-20. (Rus). **doi: 10.20998/2074-272X.2010.5.04.**

5. Liu Z., Winands G.J.J, Van K., Pemen A.J.M., van Heesch E.J.M. A high-voltage pulse transformer with a modular ferrite core. *Review of Scientific Instruments*. 2008, vol.79, no.1. pp. 625-630. **doi: 10.1063/1.2830943**.

6. Bortis D., Biela J., Kolar J. W. Optimal design of a DC reset circuit for pulse transformers. *Proceedings of the IEEE Twenty-Second Annual IEEE Applied Power Electronics Conference and Exposition APEC 07 (Cat. No.99TH8475)*, 2007, pp. 1171-1177. **doi: 10.1109/APEX.2007.357663.**

7. Lee Li, Chaobing Bao, Xibo Feng, Yunlong Liu, Lin Fochan. Fast switching thyristor applied in nanosecond-pulse high-voltage generator with closed transformer core. *Review of Scientific Instruments*. 2013, vol.84, no.2. pp. 425-432. **doi: 10.1063/1.4792593**.

8. Corum J., Daum J. Moore H. L. *Tesla coil research*. New Jercey, US army armament research, development and engineering center Publ., 1992, 38 p.

9. Kontorovich M.I. *Operatsionnoe ischislenie i nestatsionarnye iavleniia v elektricheskikh tsepiakh* [Operational calculus and non-stationary phenomena in electrical circuits]. Moscow, Gostekhizdat Publ., 1955. 277 p. (Rus).

10. Smith P.W. *Transient electronics. Pulsed circuit technology*. New-York, John Wiley & Sons Publ, 2011. 288 p.

11. Batygin Yu.V., Chaplygin E.A., Shynderuk S.A., Sobokar O.S. Resonance in the secondary circuit of the Tesla transformer excited by the harmonic voltage. *Bulletin of NTU «KhPI»*, 2017, no.30(1252), pp. 21-27. (Rus).

12. Denicolai M. Optimal performance for Tesla transformers. *Review of Scientific Instruments.* 2002, vol.73, no.9. pp. 3332-3336. **doi: 10.1063/1.1498905.**

13. Reed J.L. Note: Tesla transformer damping. *Review of Scientific Instruments*. 2012, vol.83, no.7. pp. 76101-76103. **doi: 10.1063/1.4732811.**

14. Vavriv L.V., Ivanov V.M., Martsenyuk V.E., Mirzoev R.S. Devices for obtaining high voltage pulses in electrotechnologies. *Bulletin of NTU «KhPI»*, 2017, no.15(1237), pp. 23-30. (Ukr).

Received 25.04.2019

A.G. Gurin[1], *Doctor of Technical Science, Professor,*
I.A. Kostiukov[1], *Candidate of Technical Science,*
[1] National Technical University «Kharkiv Polytechnic Institute», 2, Kyrpychova Str., Kharkiv, 61002, Ukraine,
e-mail: iakostiukow@gmail.com

How to cite this article:
Gurin A.G., Kostiukov I.A. The effect of the active resistance of the pulse transformer windings on the parameters of voltage pulses generated on a capacitive load. *Electrical engineering & electromechanics*, 2019, no.5, pp. 45-49. **doi: 10.20998/2074-272X.2019.5.08.**

UDC 629.1.032 **doi: 10.20998/2074-272X.2019.5.09**

V.V. Dushchenko, V.G. Masliev, R.A. Nanivskyi, A.O. Masliev

APPLICATION OF MAGNETORHEOLOGICAL ELASTOMERS FOR PERFORMANCE CONTROL OF CUSHIONING SYSTEMS FOR WHEELED VEHICLES

The purpose of the work is to study the influence of the control of the elastic and damping characteristics of the cushioning system based on the use of magnetorheological elastomers on the smoothness of the course of wheeled transport vehicles. The technique. The research used the methods of: magnetic field theory, the theory of vehicle suspension, experiment theory planning, and the FEMM code for studying magnetic field characteristics and mathematical modeling of wheeled vehicle movement along roughness in the Delphi environment. Results. Designed, researched and patented designs of elastic hinges of the suspension arms with magnetorheological elastomers. The relative boundaries of changes in the elastic modules and losses of these hinges are determined when controlling the characteristics of the suspension in order to improve the smoothness of the wheeled vehicle. Scientific novelty. For the first time, the feasibility of using magnetorheological elastomers to control the elastic and damping characteristics of the cushioning system of wheeled vehicles has been investigated, and the requirements for control laws have been determined, which make it possible to increase smoothness by more than 40 %; it is established that the control of the loss modulus has a greater effect on the improvement of smoothness of motion than the control of the elastic modulus. Practical value. The design has been developed and the relative boundaries of changes in the modules of elasticity and loss of hinges with magnetorheological elastomers during their control have been determined, which will make it possible to formulate requirements for elastomers when developing promising hinge designs for vehicle suspension systems. References 21, figures 18.
Key words: **magnetorheological elastomer, control magnetic field, modulus of elasticity, loss modulus, wheeled vehicle, cushioning system, elastic hinges, suspension performance control.**

Метою роботи є дослідження впливу керування пружними та демпфіруючими характеристиками системи підресорювання на основі використання магнітореологічних еластомерів на плавність ходу колісних транспортних засобів. Методика. При дослідженнях використано методи: теорії магнітного поля, теорії підресорювання транспортних засобів, теорії планування експерименту, а також пакет Femm для дослідження характеристик магнітного поля та математичне моделювання руху колісних транспортних засобів по нерівностям у середовищі Delphi. Результати. Розроблено, досліджено та запатентовано конструкції пружних шарнірів важелів підвіски з магнітореологічними еластомерами. Визначено відносні межі зміни модулів пружності та втрат даних шарнірів при здійсненні керування характеристиками підвіски для забезпечення підвищення плавності ходу колісного транспортного засобу. Наукова новизна. Вперше досліджено доцільність застосування магнітореологічних еластомерів для керування пружними та демпфіруючими характеристиками систем підресорювання колісних транспортних засобів та визначено закони керування, які дозволяють підвищити плавність ходу більше ніж на 40 %; встановлено, що керування модулем втрат в більшій мірі впливає на підвищення плавності ходу, ніж керування модулем пружності. Практична цінність. Розроблено конструкції та визначено відносні межі змін модулів пружності та втрат шарнірів із магнітореологічних еластомерів при здійсненні їх керування, що дозволить формулювати вимоги до еластомерів при розробці перспективних конструкцій шарнірів для систем підресорювання транспортних засобів. Бібл. 21, рис. 17.
Ключові слова: **магнітореологічний еластомер, керуюче магнітне поле, модуль пружності, модуль втрат, колісний транспортний засіб, система підресорювання, пружні шарніри, керування характеристиками підвіски.**

Целью работы является исследование влияния управления упругими и демпфирующими характеристиками системы подресорювання на основе использования магнитореологических эластомеров на плавность хода колесных транспортных средств. Методика. При исследованиях использованы методы: теории магнитного поля, теории подрессоривания транспортных средств, теории планирования эксперимента, а также пакет Femm для исследования характеристик магнитного поля и математическое моделирование движения колесных транспортных средств по неровностям в среде Delphi. Результаты. Разработаны, исследованы и запатентованы конструкции упругих шарниров рычагов подвески с магнитореологическими эластомерами. Определены относительные границы изменения модулей упругости и потерь данных шарниров при осуществлении управления характеристиками подвески для обеспечения повышения плавности хода колесного транспортного средства. Научная новизна. Впервые исследованы целесообразность применения магнитореологических эластомеров для управления упругими и демпфирующими характеристиками систем подрессоривания колесных транспортных средств и определены требования к законам управления, которые позволяют повысить плавность хода более чем на 40 %; установлено, что управление модулем потерь в большей степени влияет на повышение плавности хода, чем управление модулем упругости. Практическая ценность. Разработана конструкция и определены относительные границы изменений модулей упругости и потерь шарниров с магнитореологическими эластомерами при осуществлении их управления, что позволит сформулировать требования к эластомерам при разработке перспективных конструкций шарниров для систем подрессоривания транспортных средств. Библ. 21, рис. 17.
Ключевые слова: **магнитореологический эластомер, управляющее магнитное поле, модуль упругости, модуль потерь, колесное транспортное средство, система подрессоривания, упругие шарниры, управление характеристиками подвески.**

Problem definition. One of the promising directions for further enhancing the smoothness of vehicles when driving on rough terrain at high speeds is to control the characteristics of their cushioning systems (CS). However, well-known traditional solutions of controlled

CS joints are characterized by complexity, high cost and unreliability, which significantly impedes their implementation on serial models of vehicles. One of the main reasons for this is the invariance of the physicochemical properties and characteristics of the traditional materials used at the CS joints as a working body. A possible solution to this problem is to apply new, alternative, so-called *smart materials*, which can change their properties under the influence of external control influences. In particular, these include magnetoreological elastomers (MREs), the modulus of elasticity and loss modulus of which may change under the influence of a control magnetic field. The development of new technical solutions for the controlled CS joints with the aim of improving the smooth running of the vehicle, simplifying their design, providing the required speed of control at moderate power consumption is an urgent scientific problem to which the presented research is directed.

Analysis of scientific publications. In [1-3], the technology of MRE production is presented: to the matrix (of ordinary or silicone rubber, polyurethane, etc.), they add a certain amount (up to 40 % by volume) of the filler – ferromagnetic particles, for example, carbonyl iron, of size from 5 to 40 microns. The mixture is polymerized at temperature of about 150 °C. If this process occurs under the action of a magnetic field, then a MRE with anisotropic properties is obtained. Without field an isotropic MRE is obtained.

In [4], it was experimentally proved that at harmonic deformations of samples of MRE with frequencies of 1 … 50 Hz, the application of the magnetic field increases their damping properties in times.

In [5], the influence of the magnetic field on samples of MRE at a strain rate of 10 Hz is investigated. The damping properties increased from 4 to 18 times, depending on the size and concentration of the magnetic particles and the value of the flux density of the imposed magnetic field. Saturation of MRE occurred at 600…800 mT.

The work [6] investigates a damper created on the basis of MRE and intended for vibration protection of precision equipment. It is proved that the damper performance, which was 0.5 s, depends on the time of transients in MRE. The speed can be adjusted by changing the current in the control coil.

In [7], a comparative evaluation of different types of dampers for precision equipment, including ones on the basis of MRE, was carried out and its advantages were proved. The damping efficiency increases with the increase in the volume concentration in the MRE of the magnetic particles.

In [8], samples of MRE were investigated, a matrix of which made of natural rubber, and carbonyl iron (11 % by volume) with 3.5 μm particles was selected as the filler. The matrix was polymerized under the action of an external magnetic field up to 1 T to obtain the anisotropic properties of MRE. A sample with isotropic properties was also investigated. In samples with more anisotropic properties, the increase of the shear modulus when applying a control magnetic field (0… 600 mT) increased faster.

In [9], an increase of the shear modulus in natural-rubber-based MRE samples was found to be up to 130 %, and much more on silicone rubber.

In [10], samples of IRE with carbonyl iron content up to 40 % (by volume) with a particle size of 1… 10 μm were investigated. It is proved that with increasing volume concentration of filler particles the absorption efficiency of vibration energy by the damper increases. The control of the damper stiffness of MRE by means of control current is confirmed.

The analysis of the presented works shows that the range of changes in the modulus of elasticity and loss modulus of MRE under the action of a magnetic field gives the prospect of their application in the control systems of characteristics of CS wheeled vehicles, but studies of the magnetic and mechanical properties of MRE are still in their infancy:

- samples of mainly small sizes and their small deformations were investigated: since a magnetic field of about 1 T is required to obtain the desired effect, samples of the MRE were executed with a size in the direction of the magnetic flux density vector not exceeding 1 mm. Accordingly, characteristics studies are consistent with samples with such parameters;
- the performance of control processes is poorly researched and depends on the correlation of the viscosity and elastic properties of the MRE;
- the relationship of the growth of the modulus of elasticity and the loss modulus on the action of the magnetic field has not been sufficiently investigated.

Therefore, **the goal of the work** is to study the influence of the control of the elastic and damping characteristics of the CS based on the use of MRE on the smooth running of wheeled vehicles.

Tasks that need to be accomplished to achieve this goal:

- to produce samples of the MRE with parameters that are suitable for research and use in the CS;
- to develop and create a stand for magnetic field influence studies on elastic and damping characteristics of IRE specimens;
- to develop and create up-to-date measuring instruments for research;
- to carry out experimental researches in the conditions of the stand of influence of the magnetic field on the static and dynamic characteristics of the samples of MRE, including on the control speed and the ratio of the modulus of elasticity and loss modulus during the action of the control magnetic field;
- to develop the design of the joint with the control device on the basis of MRE for the hinge of the CS lever;
- to carry out, by computer simulation, comparative studies of the smooth running of a serial wheeled vehicle with one equipped with a control system based on the use of MRE in the CS;
- to develop recommendations for the use of MRE to control the elastic and damping characteristics of CS of wheeled vehicles.

Research methodology. In the general case, the CS of wheeled vehicles is composed of elastic elements, damping devices (shock absorbers) and guides in the form

of levers that connect the wheels through the elastic rubber hinges with the body of the vehicle. The rigidity and damping properties of these hinges affect the suspension characteristics, and therefore the smooth running of the vehicle.

Thus, by replacing in the hinges of rubber with MRE, it is possible to implement control of the elastic and damping characteristics of the suspension as a whole.

The scheme of two-lever suspension of wheeled vehicle is shown in Fig. 1, where the elastic hinges 4 of levers are made of MRE. In order to control their elastic and damping properties, electromagnets are placed at the ends of the hinges, which create a control magnetic field.

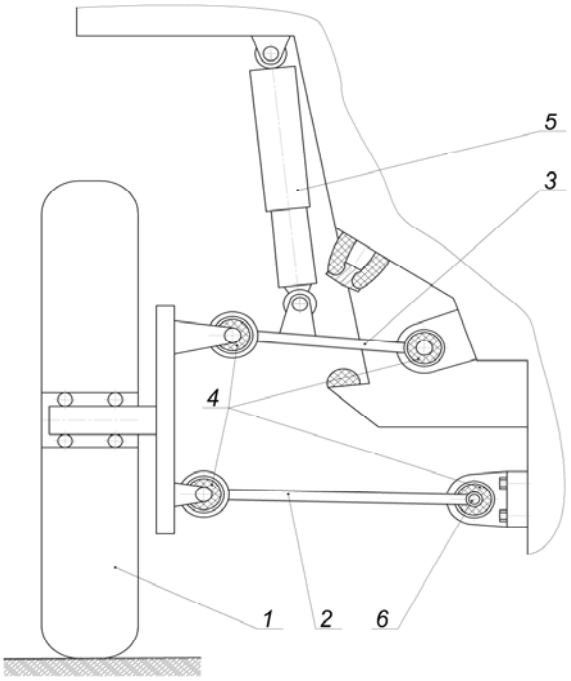

Fig. 1. Scheme of two-lever suspension of the vehicle: 1 – wheel; 2 – lower lever; 3 – upper lever; 4 – elastic hinges of MRE with control electromagnets; 5 – damping device (shock absorber); 6 – elastic element (torsion)

To calculate the magnetic flux density, to study the uniform distribution of the magnetic field in the sleeves of MRE of hinges 4, and to choose their rational design, a software package FEMM was used. The finite element mesh was created in automatic mode, with the possibility of adjusting it to refine the results of the studies.

The initial data for the research were the drawings of the elastic sleeve, the physical characteristics of the materials of the components of the magnetic circuit, and the magnetomotive force created by the current that feeds the coil. The magnetization curves for selected commercially available grades of steel and MRE are shown in Fig. 2, 3 according to [11, 12].

To prevent overheating, a current density in the coil wire of < 10 A/mm^2 was limited, with action time of <10 s.

Several variants of the design of an elastic hinge of MRE have been considered and investigated [10, 13-15]. The most rational in terms of manufacturing technology, placement and maintainability option was chosen [15], which is shown in Fig. 4.

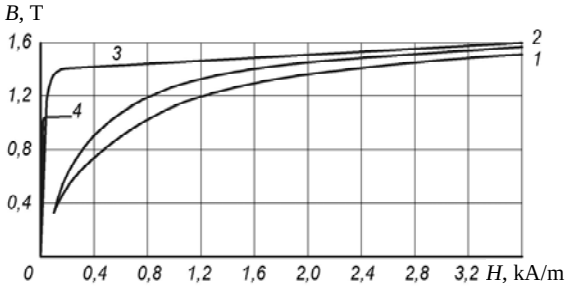

Fig. 2. Magnetization curves: 1 – cast steel; 2 – electrical steel E11; 3 – sheet steel, 4 – perm

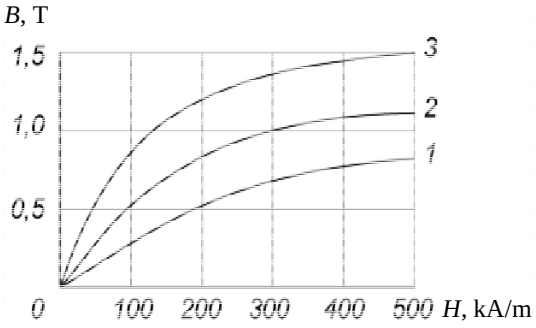

Fig. 3. Magnetization curves: 1 – MRE with a content of 20 % carbonyl iron by volume; 2 – MRE containing 40 % by volume of carbonyl iron; 3 – pure carbonyl iron powder

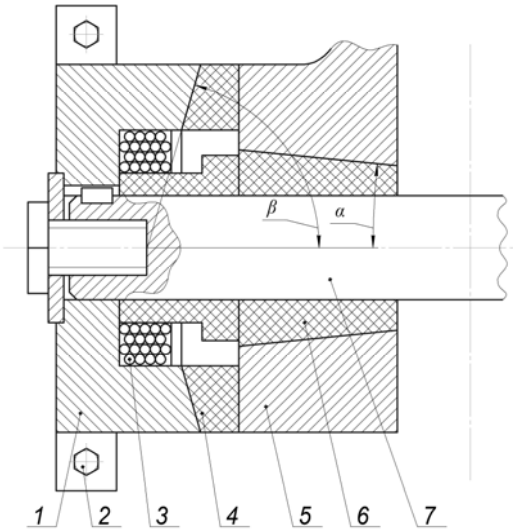

Fig. 4. Design of the hinge of MRE: 1 – bracket; 2 - bolts of fastening to the case of the vehicle; 3 – coil; 4 – end elastic element of MRE; 5 – suspension lever; 6 – radial elastic element of MRE; 7 – torsion

The results of the study using the FEMM software package proved that in order to ensure the most uniform distribution of magnetic flux density in the end 4 and radial 6 elastic elements made of MRE (Fig. 4), one of the surfaces in each of them must be made in the shape of a cone.

Variation of the angle of inclination of the cones to the axis of the torsion 7 allowed to obtain their rational values, in which the magnetic flux density in the end 1 and radial 2 elastic elements of MRE was distributed fairly uniformly, and the deviation from the average within 10 % (Fig. 5).

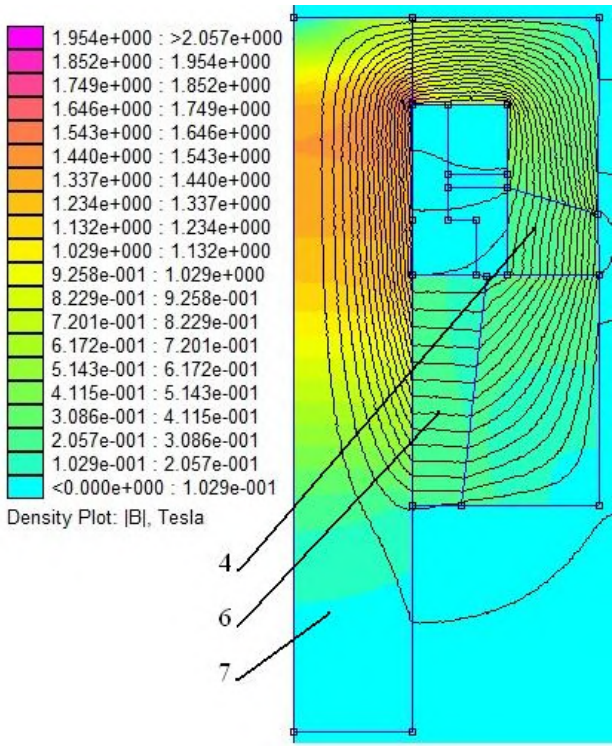

Fig. 5. Results of magnetic field distribution studies: 4 – end elastic element of MRE, 6 – radial elastic element of MRE; 7 – torsion (numbering of positions according to Fig. 4)

According to the acceptable overall parameters of the hinge and its coil 3 (Fig. 4), the value of the allowable (by heating) magnetomotive force was F = 1500 A. This allowed to obtain magnetic flux density in the elastic elements 4 and 6 within B = 0.5…0.6 T (Fig. 5). According to [18], the modulus of elasticity and the coefficient of rigidity should increase by 25 % and the damping factor by 18 %, which is insufficient to achieve the stated research objective. However, other sources claim that this increase can be significantly higher [4, 9]. The reason for this contradiction is that the relative magnetic permeability of MRE is small: at 40 % of carbonyl iron by volume and B = 0…0.5 T, $\mu_r \approx 10$, and at B = 0.5…1 T it is still decreases to $\mu_r \approx 4$ (Fig. 3).

In turn, in [19] it is recommended to increase the magnetic permeability for practical use of MRE. Thus, this contradiction requires careful experimental verification, which was carried out at a specially designed stand, shown in Fig. 6 [16, 17].

This stand allows to carry out a wide range of studies of the influence of the magnetic field on the modulus of elasticity, displacement and loss of samples of MRE. The influence of such external factors as gravity and pull force of electromagnets is practically excluded, and the closed magnetic circuit of ferromagnetics increases the magnetic flux density (Fig. 7). Electrotensometry method was used for research, measuring devices were created on the basis of modern microprocessor technologies (Fig. 8).

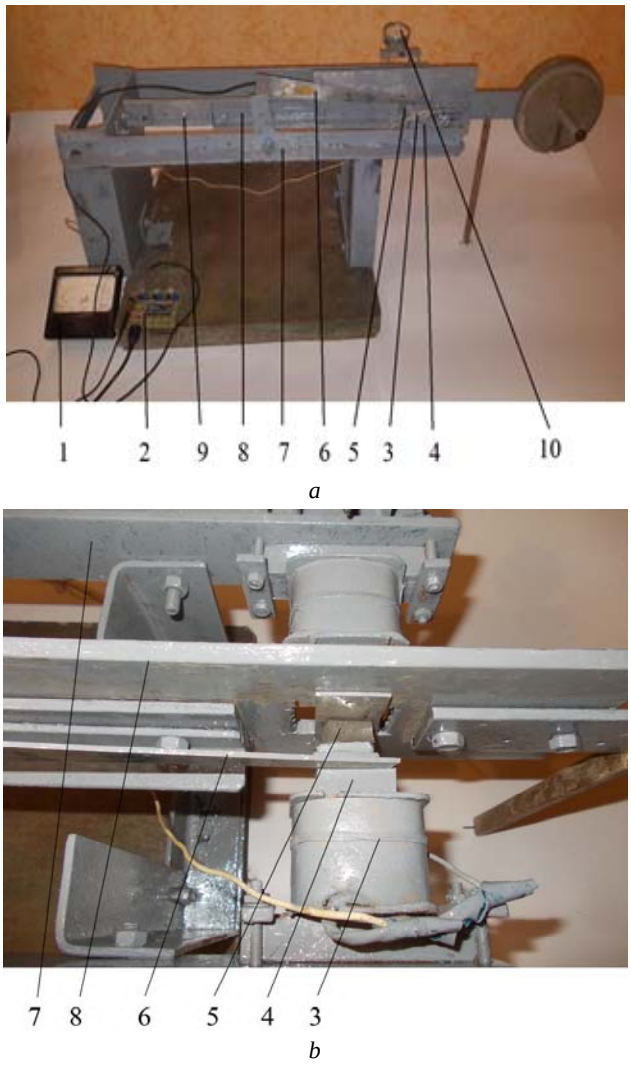

Fig. 6. Stand for investigation of mechanical characteristics of samples of MRE (*a*) and the joint where samples of MRE are installed (*b*): 1 – ammeter; 2 – strain gauge with analog-to-digital converter (ADC); 3 – coils for excitation of magnetic flux; 4 – cores of the coils; 5 – elastic samples of IRE under study; 6 – deflection meter with strain gauges; 7 – magnetic core; 8 – rigid range; 9 – flexible plate made of non-magnetic material; 10 – hour indicator

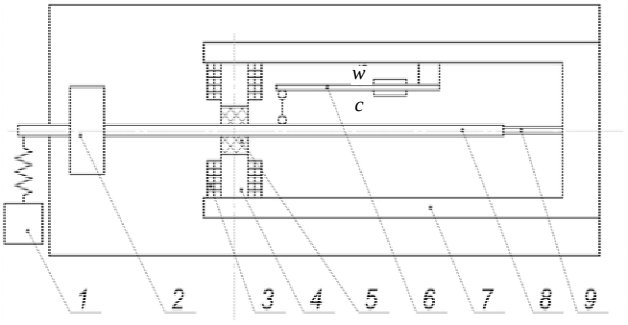

Fig. 7. Scheme of stand for research of samples of MRE: 1 – mechanical eccentric vibrator (frequency range 0… 20 Hz; oscillation amplitude 1 mm); 2 – oscillating mass; 3 – coils for excitation of magnetic flux; 4 – cores of the coils; 5 – elastic samples of MRE under study; 6 – deflection meter with strain gauges (w – working, c – compensation); 7 – magnetic core; 8 – rigid range; 9 – flexible plate made of non-magnetic material

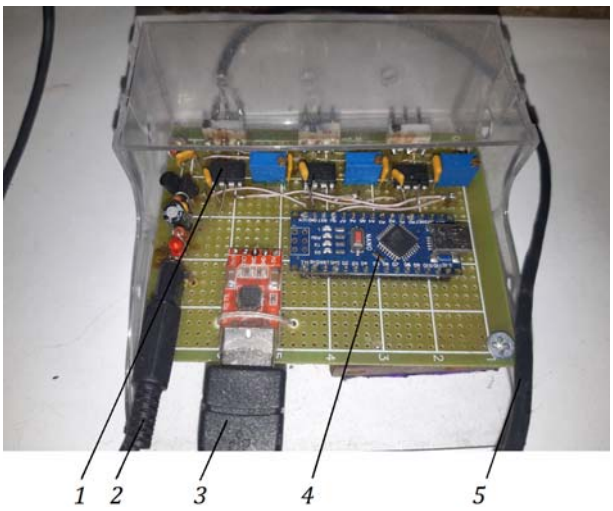

Fig. 8. Measuring device: 1 – analog current amplifiers from strain gauges; 2 – calculator; 3 – shielded cable; 4 – USB connector of the digital signal output to the computer; 5 – power cable

The frequency range of the measuring device within which the gain had a deviation within ± 1.5 % was 0… 20 Hz. The circuit of the measuring channel is shown in Fig. 9.

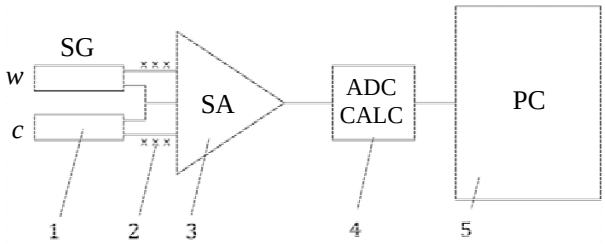

Fig. 9. Circuit of the measuring channel: 1 – SG – strain gauges of deflection meter (w – working, c – compensation); 2 – shielded cable; 3 – analog strain amplifier AD 625; 4 – ATMEGA 328 calculator with ADC; 5 – personal computer

Samples 5 (Fig. 7) were studied in the shape of rings with an outer diameter of 20 mm, a thickness of 10 mm and a central hole with a diameter of 6 mm, which were made of MRE by known technology [6].

Silicone rubber was used as the MRE matrix. The carbonyl iron content by volume is 40 %, the size of the magnetic particles is 5… 10 microns.

To create the anisotropic MRE structure, the polymerization of the sample material was carried out in a thermal cabinet at 160 °C for 2 hours and in the presence of a magnetic field B = 0.6 T, the vector of which was directed to the surfaces of the samples in the same direction as the magnetic flux density vector of the control magnetic field would be directed (in order to obtain its greater influence on the characteristics [6]).

Before and after the measurements, a direct calibration of the measuring channel was carried out by displacing the rigid range 8 one way and the other with the help of an elastic dynamometer, which caused deformation of the samples 5, which were measured by the clock indicator 10 (Fig. 6). Scale factor K = 0.067 was obtained.

Analysis of the static characteristics showed that the flux density of the control magnetic field B = 0.6 T caused an increase in the stiffness coefficient of 1.75 times and in the damping factor of 4.4 times (the stiffness coefficient was calculated at the highest values of F and x, and the damping coefficient by hysteresis loops areas). Therefore, the damping in the samples increased almost four times faster than their rigidity (Fig. 10).

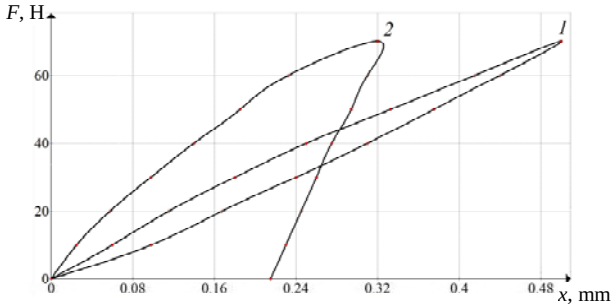

Fig. 10. Static loading characteristics of MRE specimens: 1 – without magnetic field; 2 – magnetic field B = 0.6 T

Thus, the results obtained are different from those given in [18], but do not contradict known studies, but refine them. This confirms that we have chosen the right MRE production technology and research direction.

When performing dynamic tests, the vibrations were excited by the mechanical vibrator 1, which through the spring transmitted a harmonic force to the rigid range 8 and rocked it together with the mass 2 to obtain resonance amplitudes.

Figures 11, 12 show the oscillograms of the eigen oscillations of mass 2 on elastic specimens 5 of MRE.

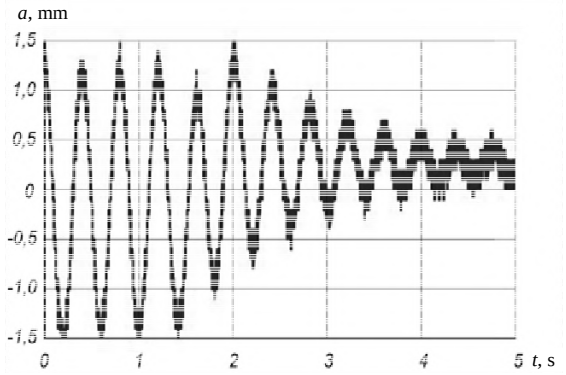

Fig. 11. The oscillogram of vibrations of mass *2* on samples *6* in the absence of a control magnetic field

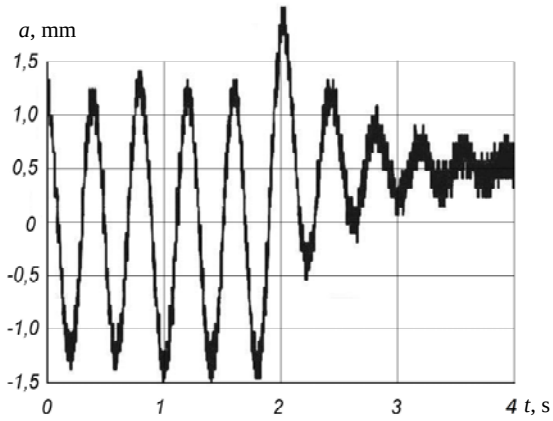

Fig. 12. The oscillogram of vibrations of mass *2* on samples *6* in the presence of a control magnetic field B = 0.6 T

The analysis of the oscillograms showed that when the control magnetic field was switched on, the time constant decreased from 1.48 s to 0.78 s, i.e. the speed of oscillation damping improved. The transient was practically completed in 3·0.78 = 2.34 s.

At the same time, there was an increase in the coefficient of rigidity of the samples by about 25 %, which caused an increase in the frequency of natural oscillations from 2.5 to 2.7 Hz, i.e. by 8 %. The damping factor increased by 118 % (from 0.038 to 0.083), i.e. 4.7 times higher than the stiffness factor. This is close to the results of static tests and well-known studies [4, 18].

Figure 13 shows a sample oscillogram of forced (close to resonant) vibrations of mass 2.

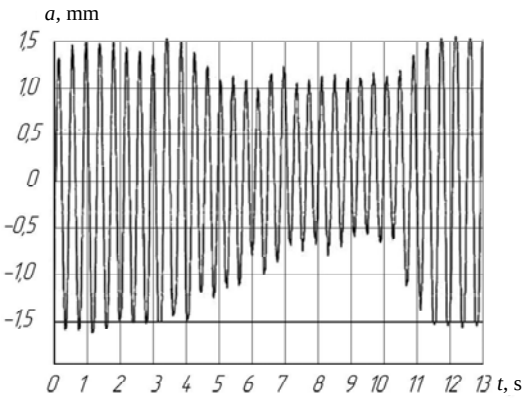

Fig. 13. The oscillogram of the forced vibrations of mass *2* on elastic specimens *5* of MRE at the modes «absence – switching on – absence» of the control magnetic field

With the help of the vibrator 1, the system was introduced into the mode of resonant vibrations, and then a current was supplied to the coils 3 (Fig. 7), which created a control magnetic field with flux density B = 0.6 T. The vibration amplitudes were halved due to the increase in damping in elastic specimens 5 of MRE.

After switching off the magnetic field, the system returned to resonant vibrations mode, and their amplitudes doubled, i.e. to the initial value. The duration of transients was about 2.3 s.

To further reduce the amplitude of the oscillations, it is necessary to increase the magnetic flux density of the control field. To prevent the increase of heat losses, it is advisable not to increase the current in the coils, but to create an MRE with increased magnetic permeability.

According to the results of studies of hinges of MRE, 4 patents of Ukraine are received [14, 15, 17, 20].

For the theoretical substantiation of the recommendations for practical application of the obtained results, comparative studies of the smoothness of the running of two wheeled vehicles were carried out: serial and the same, but equipped with the system of control of SC characteristics based on the use of hinges of MRE in suspension levers (Fig. 1, 4).

The smoothness of the running of these vehicles was investigated by the method of computer simulation of their motion on sinusoidal road profiles of bumps, in accordance with the accepted methodology in the field, by calculating and constructing the speed characteristics of the vehicles [21]. These characteristics represent the dependence of the height of the bumps h (passage height), which the vehicle is able to overcome with vertical acceleration in the locations of people not exceeding 3 g, (29.43 m/s^2), due to ergonomic requirements, on the speed of movement. Speed characteristics are calculated for three bumps lengths: 1.5L, 2L, and 2.5L, where L is the vehicle's base.

The resonance bands are characteristic of the speed characteristics, when the frequencies of the eigen oscillations of the cushioned body of the vehicle coincide with the frequency of perturbations from bumps. The passage height of the bumps corresponding to the resonance has the least value and is called the minimum passage height of the bumps. In accordance with the current requirements for smooth running of the vehicle of high passability, the level of minimum passage heights of bumps should be not less than 0.19 ... 0.24 m, depending on the given average speed of movement on the terrain.

To prevent overheating of the electromagnets, the control of the characteristics of the CS will be applied only when overcoming sections of terrain with difficult road conditions, which usually have a length of 30 ... 50 m, and overcoming which will take time no more than 10 s, while maintaining the speed of movement.

An experimentally verified mathematical model of wheeled vehicle motion was used for the research [21], which was refined in accordance with the control system utilization and implemented in the Delphi environment.

Let us evaluate the influence of the characteristics of the elastic hinges of the CS of the serial vehicle on the smoothness of the running. From Fig. 14 the following follows. In the case where the hinge loss modulus is zero, curves *2*, there is a decrease in the minimum passage heights of bumps at all resonant speeds of motion approximately equal to 6.6 m/s, 8.9 m/s, and 11 m/s, respectively, for bumps of 1.5L, 2L, and 2.5L length. This decrease occurs from the level of 0.12… 0.14 m to the level of 0.09 m, i.e. the smoothness of the running deteriorates at 25… 36 %.

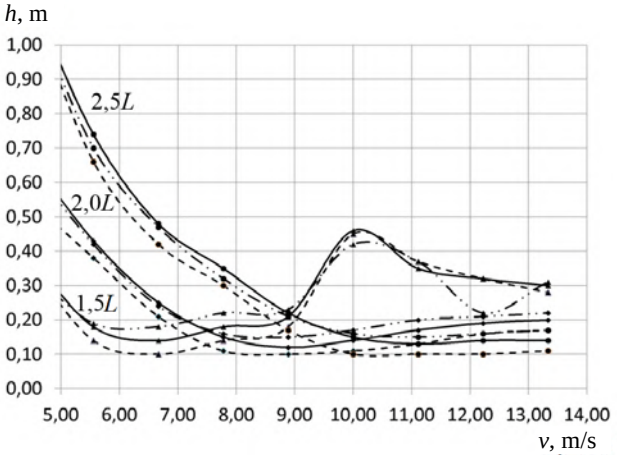

Fig. 14. CS speed features: impact assessment of elastic suspension rubber hinges:
1 – hinges with original characteristics;
2 – the hinge loss modulus is zero;
3 – the hinge elastic modulus is zero

Worsening also occurs at pre-resonance speeds for all bump lengths. At resonance speeds, the smoothness of motion deteriorates at bumps of lengths of 2*L* and 2.5*L* and remains unchanged at bumps of length of 1.5*L*.

In turn, the variant «modulus of elasticity of the hinges is zero», curves *3*, leads to an increase in the minimum passage heights of bumps at resonant speeds of movement from the level of 0.12 ... 0.14 m to the level of 0.14 ... 0.17 m, i.e., smoothness of running improves by 17… 21 %. At the same time, at pre-resonance speeds, the smoothness of running slightly decreases, and at resonance speeds it improves, at bumps of length of 2*L* and 2.5*L*, and worsens at 1.5*L*.

Thus, the characteristics of the elastic hinges of the vehicles CS levers significantly influence its smooth running, and by applying control of their loss and elasticity modules based on the use of MRE, it is possible to significantly improve the quality of cushioning.

In order to reduce the number of control electromagnets and simplify the design of the suspension, in further studies the use of the control of the characteristics of the hinges of MRE only of the lower levers of the suspension, which are coupled with the torsions are considered.

Figure 15 shows the results of the study of the influence of the control of modulus of elasticity of these hinges of MRE. From the graphs it follows that in the variant «modulus of elasticity is zero», curves *2*, at resonant speeds of movement, the minimum passage heights of bumps increase from the level of 0.12 ... 0.14 m to the level of 0.13 ... 0.15 m. Here, the smoothness of running at pre-resonance speeds does not practically change for all lengths of bumps, and at post-resonance speeds the smoothness of running is slightly improved at bumps of length of 2*L* and 2.5*L* and worsens at 1.5*L*.

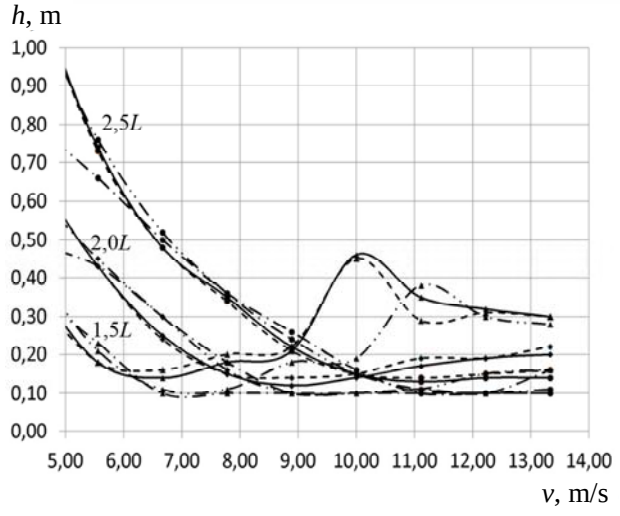

Fig. 15. CS speed features: impact assessment of the control of the modulus of elasticity of hinges of MRE (loss modulus has original value):
1 – original modulus value;
2 – modulus is zero;
3 – modulus is enlarged 5 times;
4 – modulus is enlarged 10 times

In the case of increasing the modulus of elasticity of these hinges by 5 times (curves *3*), the minimum passage heights of bumps at resonant speeds of movement decrease from the level of 0.12… 0.14 m to the level of 0.09 m. Here, the smoothness of the running at the pre-resonance speeds increases for all lengths of bumps, and at the post-resonance speeds it deteriorates at all bumps, and especially of the length of 1.5*L*. At increasing the modulus of elasticity by 10 times (curves *4*), the smoothness of the running deteriorates at almost all speeds and lengths of bumps.

Figure 16 shows the results of the study of the effect of control of loss modulus of hinges of MRE, from which it follows that in the case where the loss modulus is equal to zero, curves *2*, the minimum passage heights of bumps, at resonant speeds of movement decrease from the level of 0.12… 0.14 m to the level 0.10… 0.11 m. Here, the smoothness of the running deteriorates at all speeds of motion and lengths of bumps.

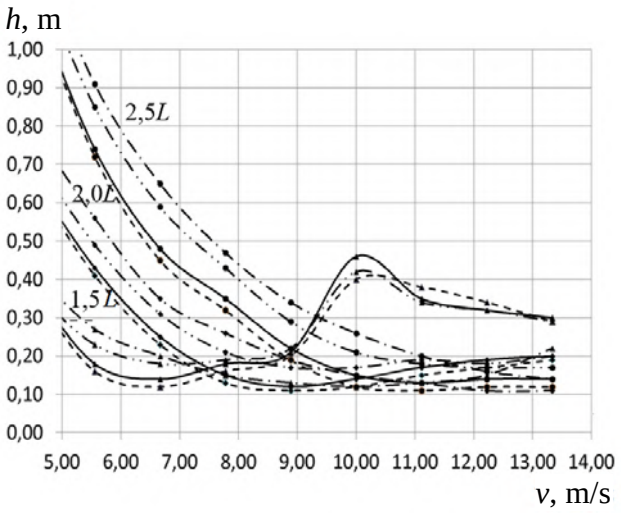

Fig. 16. CS speed features: impact assessment of the control of the loss modulus of hinges (modulus of elasticity has original value):
1 – original modulus value;
2 – modulus is zero;
3 – modulus is enlarged 5 times;
4 – modulus is enlarged 10 times

At increase of the loss modulus of these hinges in 5 times (curves *3*) the minimum pass heights of bumps at resonant speeds of movement increase from the level 0.12… 0.14 m to the level 0.17… 0.18 m, i.e. by 28.6… 41.7 %, which is close to the level of modern requirements (0.19 ... 0.24 m). At pre-resonance speeds, the smoothness of the running is improved at all lengths of bumps, and at the post-resonance ones it improves on bumps of lengths of 2*L* and 2.5*L* and slightly decreases on bumps of length of 1.5*L*.

When the loss modulus is increased by 10 times (curves *4*) at the resonant speeds of movement, the minimum passage heights of bumps decrease slightly from the level of 0.12… 0.14 m to the level of 0.12… 0.13 m. At pre-resonance speeds, the smoothness of the running is significantly improved at all lengths of bumps, at the post-resonance speeds the smoothness of running is slightly impaired at the bumps of lengths of 2*L* and 2.5*L* and significantly worsens on the bumps of length of 1.5*L*.

Figures 17, 18 present the results of the study of the effect of joint control of loss modulus and modulus of elasticity of the hinges of MRE of the lower suspension levers on the smooth of running of the vehicle.

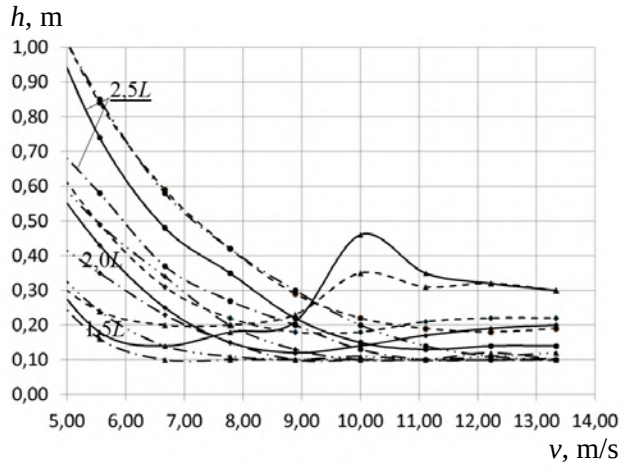

Fig. 17. CS speed features: impact assessment of the joint control of loss modulus and modulus of elasticity of lower levers hinges:
——— *1* – original value of loss and elasticity modules;
– – – – – *2* – loss modulus is increased by 5 times, modulus of elasticity is zero;
— · · — · *3* – loss and elasticity modules increased by 5 times;
— · — · – – *4* – loss modulus is increased by 5 times, modulus of elasticity is increased by 10 times

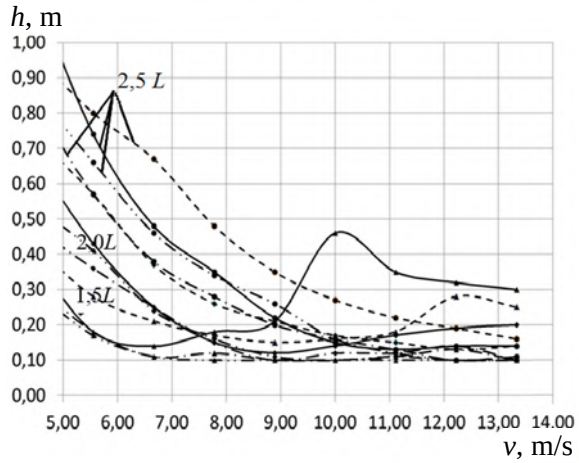

Fig. 18. SC speed features: impact assessment of the joint control of loss and elasticity modules of lower levers hinges:
——— 1 – original value of modules;
– – – – – 2 – loss modulus is increased by 10 times, modulus of elasticity is zero;
— · · — · 3 – loss modulus increased by 10 times, modulus of elasticity increased by 5 times;
— · — · – – *4* – loss and elasticity modules increased by 10 times

According to Fig. 17, for the variant «loss modulus is increased by 5 times, the modulus of elasticity is zero», curves *2*, the minimum passage heights of bumps increase from the level of 0.12 ... 0.14 m to the level of 0.17 ... 0.19 m, i.e. by 35.7… 41.7 %, which is close to the level of modern requirements (0.19 ... 0.24 m).

The option «loss and elasticity modules increased by 5 times» (curves *3*) allows to significantly (up to 43 %) increase the smoothness of running at pre-resonant speeds of motion at all lengths of bumps.

The option «loss modulus is increased by 5 times, the modulus of elasticity is increased by 10 times» (curves *4*) leads to a deterioration of smooth running in the entire speed range, at all lengths of bumps.

From the graphs shown in Fig. 18, it follows that an increase in the loss modulus by 10 tomes (graph 2) leads to an improvement in the smoothness of running at bumps of 1.5*L* in length at pre-resonance speeds and to a deterioration at post-resonance speeds of motion. This option ensures an increase in the minimum passage heights of bumps (at a speed of 9 m/s) from the level of 0.12 ... 0.14 m only to the level of 0.13 ... 0.14 m, i.e. worse than in the previous case.

The variants of «loss modulus increased by 10 times, elastic modulus increased by 5 times» (graph 3) and «loss and elastic modules increased by 10 times» (graph 4) show that such increase of modules leads to a significant deterioration of the smooth of running throughout the speeds and bumps range.

Discussion of results. Analysis of the graphs shown in Fig. 14, proves that the characteristics of the elastic hinges of levers of the vehicles' SC significantly influence its smooth of running, and control of their loss and elasticity modules is expedient to be implemented on the vehicles. In order to reduce energy consumption and prevent overheating of the joints, this control is advisable at resonant speeds of movement when overcoming sections of terrain with difficult road conditions, without reducing the speed of movement.

It is advisable to control the loss modulus more than the elastic modulus, since increasing the latter can lead to a deterioration of the smooth of running. It is necessary to create MRE with properties where, in the case of control, an increase in the loss modulus is not accompanied by an increase in the elastic modulus.

The experimental studies carried out made it possible to increase the losses modulus in MRE samples only twice, but the calculation investigation showed the desirability of its increase by 5 times. It is possible to solve this problem either by increasing the number of controlled hinges, installing them also on the upper suspension levers, or by applying another MRE fabrication technology, which will provide a fivefold increase in the loss modulus under the action of the magnetic field with flux density of up to 1.5 T.

The obtained values of increase (relative to serial vehicle) of loss and elasticity modules and constructed speed characteristics of vehicles allow to develop requirements for the laws of control of characteristics of hinges of MRE, depending on the mode of motion (pre-resonant, resonant or post-resonant) and length of bumps.

We formulate these requirements for the laws of control of the characteristics of elastic hinges of MRE in vehicles:

- control should be implemented only at resonant speeds of the vehicle;
- control is only expedient for the losses modulus of MRE of hinges of the levers of vehicles;

- it is recommended to increase the loss modulus no more than 5 times;
- control processes must be no longer than 10 s and have acceptable intervals between them.

Conclusions and recommendations.

1. For the first time, samples of magnetorheological elastomers with parameters suitable for use in the hinges of levers of vehicles' cushioning systems have been manufactured.

2. The original stand was developed, the static characteristics of the stiffness and damping of the made samples are investigated on which. It is found that the control magnetic field has a greater effect on the loss modulus than on the modulus of elasticity. For the first time, it is shown that the flux density B = 0.6 T of the control magnetic field causes a 25 % increase in the stiffness coefficient (and modulus of elasticity), which causes an increase in the frequency of natural oscillations from 2.5 to 2.7 Hz (by 8 %). The damping factor increased by 118 % (from 0.038 to 0.083), i.e. 4.7 times higher than the stiffness coefficient.

3. In the course of dynamic tests on the developed stand, using manufactured modern measuring equipment, for the first time it is discovered that when the control magnetic field is switched on, the time constant of free oscillation of mass on elastic elements of magnetoreological elastomers decreased from 1.48 to 0.78 s. The transient was almost completed in 2.34 s. The amplitudes of the resonance vibrations of the mass on the elastic elements of the magnetoreological elastomers, when the control magnetic field B = 0.6 T is switched on, are halved in 2.34 s.

4. The original designs of the controlled elastic hinge of magnetoreological elastomers and the device for creation of the control magnetic field are developed and patented. The parameters that provided a uniform (within 10 %) distribution of magnetic flux density in the sections of the hinges were determined. In order to achieve magnetic flux density in the magnetoreological elastomer at the level of 0.6 T, the value of the magnetomotive force (15 kA) is determined, the current density in the coil of the device ≤ 10 A/mm^2 is selected, with operation time of up to 10 s.

5. Requirements for control laws are formulated, which allow to increase the smooth of running of vehicles depending on speed and length of bumps by more than 40 %.

6. For the first time, it has been found that the control of the loss modulus of hinges of the magnetorheological elastomers of the vehicle suspension has a greater effect on improving the smooth of running than the control of their modulus of elasticity.

7. The rational limits of the relative change of the loss modules of the hinges of the magnetoreological elastomers (not more than 5 times) during their control are determined; it is recommended to use them in formulating the requirements for magnetoreological elastomers, and to develop designs of controlled nodes of the cushioning systems.

8. According to the results of the research carried out, 4 patents of Ukraine were obtained for the method of control, the design of the hinges of magnetoreological elastomers and the suspension.

REFERENCES

1. Ginder J.M., Nichols M.E., Elie L.D., Tardiff J.L. Magnetorheological elastomers: properties and applications. *Proceeding of SPIE*, 1999, vol.3675, pp. 131-138.

2. Lokander M., Stenberg B. Performance of isotropic magnetorheological rubber materials. *Polymer Testing*, 2003, vol.22, no.3, pp. 245-251. **doi: 10.1016/s0142-9418(02)00043-0**.

3. Jolly M.R., Carlson J.D., Muñoz B.C., Bullions T.A. The magnetoviscoelastic response of elastomer composites consisting of ferrous particles embedded in a polymer matrix. *Journal of Intelligent Material Systems and Structures*, 1996, vol.7, no.6, pp. 613-622. **doi: 10.1177/1045389x9600700601**.

4. Li W.H., Zhang X.Z., Du H. Magnetorheological elastomers and their applications. *Book Chapter in Advanced Structured Materials*, 2013, vol.I, pp. 357-374. **doi: 10.1007/978-3-642-20925-3_12**.

5. Böse H., Röder R. Magnetorheological elastomers with high variability of their mechanical properties. *Journal of Physics: Conference Series*, 2009, vol.149, p. 012090. **doi: 10.1088/1742-6596/149/1/012090**.

6. Gorbunov A.I., Mikhailov V.P., Stepanov G.V., Borin D.Yu., Adrianov A.A., Temnov D.V., Semerenko D.A. Investigation of properties and new application of magnetic silicon composites. *Herald of the Bauman Moscow State Technical University. Series Mechanical Engineering*, 2008, no.1(70), pp. 90-107. (Rus).

7. Mihailov V.P., Shakov K.G, Selivanonko A.S., Bazinenkov A.M. Vibration isolation control in precision equipment. *Science and Education of the Bauman MSTU*, 2012, vol.12, no.9, pp. 1-12. (Rus). **doi: 10.7463/0912.0454475**.

8. Chen L., Gong X.L., Li W.H. Microstructures and viscoelastic properties of anisotropic magnetorheological elastomers. *Smart Materials and Structures*, 2007, vol.16, no.6, pp. 2645-2650. **doi: 10.1088/0964-1726/16/6/069**.

9. Gong X.L., Chen L., Li J.F. Study of utilizable magnetorheological elastomers. *International Journal of Modern Physics B*, 2007, vol.21, no.28n29, pp. 4875-4882. **doi: 10.1142/s0217979207045785**.

10. Duschenko V.V., Masliev A.O. Research of the magnetic field and the choice of the construction of an elastic joint with the sleeve of the magnetorheological elastomer suspension of wheeled armored vehicle. *Bulletin of NTU «KhPI». Series: Transport machine building*. – 2017. – no.5(1227). – pp. 173-178. (Ukr).

11. Available at: https://www.google.com/search?q=кривые+намагничивания+ферромагнитных+материалов&rlz=1C2JZAP_ruUA747UA755 (accessed 20 May 2018).

12. Krautz M., Werner D., Schrödner M., Funk A., Jantz A., Popp J., Eckert J., Waske A. Hysteretic behavior of soft magnetic elastomer composites. *Journal of Magnetism and Magnetic Materials*, 2017, vol.426, pp. 60-63. **doi: 10.1016/j.jmmm.2016.11.048**.

13. Dushhenko V.V, Masliev A.O. Improvement of the construction of hinge using magnetorheological elastomers of lever of controled suspension of the vehicle. *Mechanics and mechanical engineering*, 2017, no.1, pp. 90-97. (Ukr).

14. Dushhenko V.V, Masliev A.O. *Pidviska z regulyuvannyam zhorstkosti ta dempfiruvannya* [Suspension with adjustable stiffness and damping]. Patent UA, no.110476, 2016. (Ukr).

15. Masliev A.O., Dushhenko V.V., Ljubarskij B.G., Masliev V.G. *Pidviska transportnogo zasobu* [Vehicle suspension]. Patent UA, no.115131, 2017. (Ukr).

16. Duschenko V.V., Masliev A.O. Stand for experimental study of the effect of magnetic field on the elastic modulus and a module of losses of magnetorheological elastomers. *Bulletin of NTU «KhPI». Series: Transport machine building*, 2018, no.29(1305), pp. 46-50. (Ukr).

17. Masliev A.O., Dushhenko V.V., Masliev V.G. *Stend dlia doslidzhennia vplyvu mahnitnoho polia na kharakterystyky zhorstkosti, dempfiruvannia ta modul pruzhnosti mahnitoreolohichnykh elastomeriv* [A stand for studying the influence of a magnetic field on the characteristics of stiffness, damping, and the elastic modulus of magnetorheological elastomers]. Patent UA, no.128767, 2018. (Ukr).

18. Kallio M. *The elastic and damping properties of magnetorheological elastomers*. VTT Publications, 2005. 149 pp.

19. Pankov A.A. Magnetodeformation effect of an elastomer with magnetized polydisperse spherical inclusions. *Journal of Radio Electronics*, 2015, no.4, 15 p. (Rus).

20. Dushhenko V.V., Masliev A.O., Masliev V.G. *Sposib polipshennia plavnosti rukhu transportnoho zasobu* [A method for improving the smoothness of the vehicle]. Patent UA, no.128458, 2018. (Ukr).

21. Aleksandrov E.E., Volontsevich D.O., Dushhenko V.V. *Matematicheskoe modelirovanie processov vozmushhennogo dvizhenija agregatov i sistem bronetankovoj tehniki* [Mathematical modeling of processes of disturbed movement of units and systems of armored vehicles]. Kharkiv, «KhPI» Publ., 2012. 354 p. (Rus).

Received 11.04.2019

V.V. Dushchenko[1], *Doctor of Technical Science, Professor,*
V.G. Masliev[1], *Doctor of Technical Science, Professor,*
R.A. Nanivskyi[2], *Candidate of Technical Science, Senior Instructor,*
A.O. Masliev[1], *Postgraduate Student,*
[1] National Technical University «Kharkiv Polytechnic Institute», 2, Kyrpychova Str., Kharkiv, 61002, Ukraine,
phone +380 57 7076355,
e-mail: dushchenko@ukr.net
[2] Hetman Petro Sahaidachnyi National Army Academy, 32, Heroes of Maidan Str., Lviv, 79026, Ukraine,
phone +380 96 9409559,
e-mail: roman_nani@ukr.net

How to cite this article:
Dushchenko V.V., Masliev V.G., Nanivskyi R.A., Masliev A.O. Application of magnetorheological elastomers for performance control of cushioning systems for wheeled vehicles. *Electrical engineering & electromechanics*, 2019, no.5, pp. 50-59. **doi: 10.20998/2074-272X.2019.5.09.**

UDC 621.3 **doi: 10.20998/2074-272X.2019.5.10**

S. Belakehal, A. Djellad, R. Chenni

PERFORMANCE COMPARISON OF MULTICELL SERIES AND NPC MULTILEVEL CONVERTERS FOR A STATCOM

Abstract. In this paper, we present a comparative study of the performances of the multicells series and the Neutral-Point-Clamped (NPC) three-level converters used at synchronous static compensators (STATCOM) for the control of the voltage at a point of the network. The analysis consists on a mathematical modeling, a pulse width modulation (PWM) control algorithm application and a simulation using the Matlab Simulink environment. The simulation results obtained show that the STATCOM allows the regulation of the voltage at the point of common coupling (PCC) by acting the reactive energy that it can supply or absorb. References 22, tables 4, figures 24.
Key words: **STATCOM, VSC, NPC converter, multicell series converter, modeling, control.**

В статье представлено сравнительное исследование характеристик многоэлементных последовательных и трехуровневых преобразователей со связанной нейтральной точкой, используемых в синхронных статических компенсаторах (STATCOM) для управления напряжением в точке сети. Анализ основан на математическом моделировании, алгоритме управления с широтно-импульсной модуляцией (ШИМ) и моделировании с использованием среды Matlab Simulink. Полученные результаты моделирования показывают, что STATCOM позволяет регулировать напряжение в точке общей связи действием реактивной энергии, которую он способен подавать или поглощать. Библ. 22, табл. 4, рис. 24.
Ключевые слова: **синхронный статический компенсатор, преобразователь источника напряжения, преобразователь со связанной нейтральной точкой, многоэлементный последовательный преобразователь, моделирование, управление.**

Introduction. To improve the power quality, Flexible AC Transmission Systems (FACTS) devices have received widespread interest for high voltage power systems control. They are faster and more flexible of compared with mechanically switched control of the transmission system [1, 2]. Among the FACTs compensators that offer this possibility, the synchronous static compensators «STATCOM» are connected in parallel at sensitive points of the network. The STATCOM is the first FACTS using the Voltage Source Converter (VSC). It uses high power gate turn-off (GTO) thyristors or insulated gate bipolar transistors (IGBT). Highly efficient, this device is characterized by the robust support of the voltage in the presence of strong disturbances, the balancing of asymmetric and fluctuating loads and the damping of power oscillations [3, 4]. The design of VSC can be realized in several ways. It can be modeled using the conventional (two-level) or multilevel three-phase bridge converter. However, multi-level converter offers a wide variety of advantages over conventional converter such as lower harmonic content, reduced stress on switches and decreased switching loss [5]. Currently used STATCOM based on multilevel converters are very popular in medium-voltage networks, including flying-capacitor multilevel converters (FCMC), diode-clamped multilevel converters (DCMC) and cascaded H-bridge multilevel converters (CHMC) [6].

Cascaded H-Bridge Converters (CHBs) are the most common topologies in STATCOM applications. The advantages of CHB converters include low switching loss, modularity and lack of holding diodes. However there disadvantage resides is the fact that one cannot get a negative output voltage and an isolated power supply for each module [7, 8].

The Neutral-Point-Clamped (NPC) converters are the first practical topology for multi-level voltage converters. The advantage of this topology is generalizable so as to obtain a greater number of output voltage levels, all the phases are connected to the same common DC bus and the number of capacitors used is limited. The disadvantage of this structure is when the number of levels becomes high, the balance of the voltages across the capacitors quickly becomes complex to control [8-10].

The multi-cell series converters or floating capacitors is an energy conversion topology that relies on the series setting of controlled switches. The advantage of this topology is that it eliminates the problem of loopback diodes present in the topologies of multi-level NPC inverters. In addition, the voltage stresses imposed on the power components are naturally limited. Thus, by phase, only one DC source is needed. The disadvantage of this structure is that the need to balance the voltages across the floating capacitors adds complexity to the converter [11].

From the description of the different converters we can deduce that the voltage of the output is more sinusoidal and the harmonic distortion rate will be low if the number of levels is high but the structure of the converter becomes complicated. Its cost and the complexity of its order are increased its reliability is reduced.

The focus in this paper is on using the converters multi-cells and NPC three level as a shunt connected STATCOM for the regulation of the voltage profile along the line, so as to avoid fluctuations between the voltage at the source and the voltage at the load. For a DC input voltage source supplied by the charged capacitor, the converter produces a set of controllable three-phase output voltages with the frequency of the AC power system. These voltages on the alternating side of the converter are in phase with that of the network so as to exchange only the reactive energy with the latter. The value of the current and the direction of the reactive power exchanged are set by the value of the voltage of the converter. The setting principle is described in the following paragraph.

Description of the studied network. In this study, we used a conventional three-phase network composed of a three-phase power source that is variable in amplitude, in phase and in frequency. It supplies three-phase electric charges through a three-phase line. The diagram per phase is illustrated in Fig. 1.

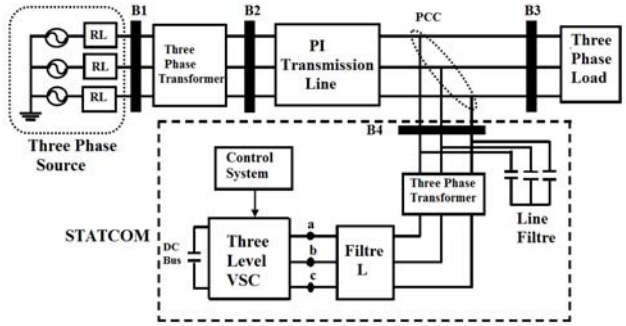

Fig. 1. Basic circuit of a STATCOM

The other major component of the system is the STATCOM which permits the regulation of the voltage at the Common Connection Point (PCC) between the network and the loads. It is composed of a continuous energy source or a capacitor associated with a static converter based on semiconductors of the IGBT type and a transformer T that has always a certain leakage reactance. The transformer plays a dual role: it transforms the voltage and offers the reactance required by the compensation.

The operating principle of the STATCOM is simple. By varying the magnitude of the output voltages produced, the reactive power exchange between the STATCOM and the network can be adjusted [1, 12]

- if the amplitude of the voltage V_{Kn} ($K = a, b, c$) is greater than the amplitude of the voltage E_K, the current I_K is advance of $\pi/2$ on E_K (Fig. 2,*b*), the compensator provides reactive power to the transmission line and the compensator behaves like a huge capacitor;
- if the amplitude of the voltage V_{Kn} is lower than the amplitude of the voltage E_K, the current I_K is $\pi/2$ behind E_K (Fig. 2,*a*), the compensator absorbs reactive power at the transmission line and the compensator behaves like an immense inductor;
- if the amplitude of the voltage V_{Kn} is equal to the amplitude of the voltage E_K, (Fig. 2,*c*), the current I_K is zero and therefore the compensation is zero.

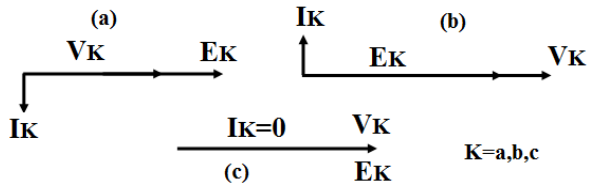

Fig. 2. STATCOM operating modes

STATCOM modeling. The equivalent circuit of the STATCOM is shown in Fig. 3. In this power system, the resistance r in series with the voltage source inverter represents the sum of the transformer winding resistance losses and the inverter conduction losses. The inductance L represents the leakage inductance of the transformer. In Fig. 3 the instantaneous value of system bus phase voltage are E_a, E_b, E_c, the instantaneous current the system inject into the STATCOM are I_a, I_b, I_c, the instantaneous value of converter's AC side phase voltage are V_a, V_b, V_c, the DC bus voltage is V_{dc}.

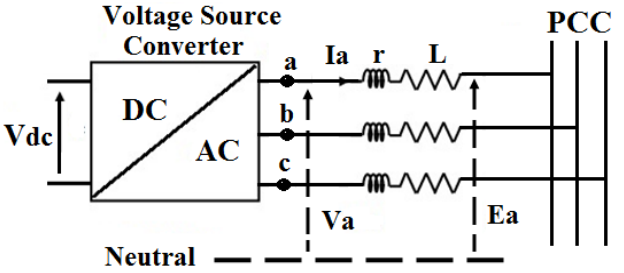

Fig. 3. Schematic diagram of the grid connection of a converter

Two Cell Converter Model. The two cells converter with three voltage levels is shown in Fig. 4. It consists of three arms, where each one consists of two cells. Each cell consists of two switches and a voltage source. The switches work in a complementary way, when one is passing the other is blocked.

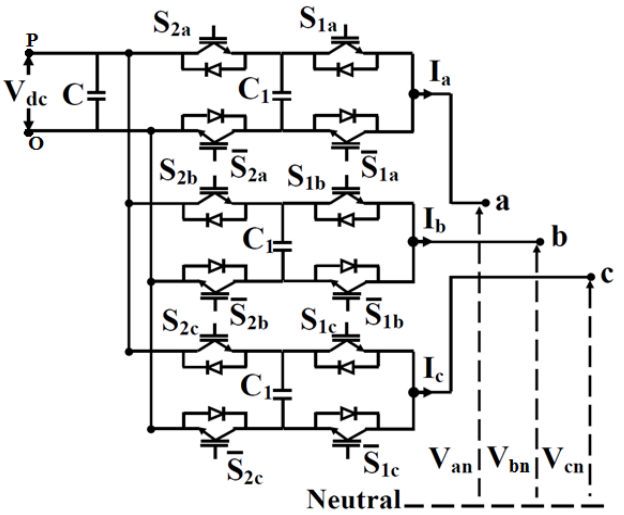

Fig. 4. Multi-cell series converter

To model the multi-cell converter, the following simplifying assumptions are used: perfect switches, perfect sources and neglected idle time [13, 15].

The converter is controlled by the switching functions S_{iK} whose value lies be hour 0 and 1 ($K = a, b$ or c designates the phase and $i = 1$ or 2 the relevant cell) whose value lies between 0 and 1. The Table 1 shows the different voltage levels V_{KO} obtained according to the control states of the switches. Each arm can release three levels of tension.

Table 1

Switching logic and output voltage

S_{1K}	S_{2K}	V_{KO}
0	0	0
1	0	$V_{dc}/2$
0	1	$V_{dc}/2$
1	1	V_{dc}

The output voltage of the converter can be expressed according to S_{iK} control commands:

$$V_{KO} = \frac{V_{dc}}{P} \times \sum_{i=1}^{p} S_{iK} \ . \qquad (1)$$

The output voltages of the converter with respect to the negative terminal (point O) of the DC bus will be:

$$V_{aO} = \frac{V_{dc}}{2}(S_{1a} + S_{2a}); \quad (2)$$

$$V_{bO} = \frac{V_{dc}}{2}(S_{1b} + S_{2b}); \quad (3)$$

$$V_{cO} = \frac{V_{dc}}{2}(S_{1c} + S_{2c}). \quad (4)$$

With O-neutral voltage $V_{On} = -(V_{aO} + V_{bO} + V_{cO})/3$.

The equation which lends the voltage of the continuous node to the voltages on the alternative side V_{an}, V_{bn} and V_{cn} is:

$$\begin{bmatrix} V_{an} \\ V_{bn} \\ V_{cn} \end{bmatrix} = \frac{V_{dc}}{6}\begin{bmatrix} 2S_{1a} & -S_{1b} & -S_{1c} \\ -S_{1a} & 2S_{1b} & -S_{1c} \\ -S_{1a} & -S_{1b} & 2S_{1c} \end{bmatrix} + \frac{V_{dc}}{6}\begin{bmatrix} 2S_{2a} & -S_{2b} & -S_{2c} \\ -S_{2a} & 2S_{2b} & -S_{2c} \\ -S_{2a} & -S_{2b} & 2S_{2c} \end{bmatrix} \quad (5)$$

Three-level NPC converter Model. The three-level NPC converter is shown in Fig. 5. The DC input bus is composed of two capacitors in series (C_1 and C_2) forming a midpoint noted (O) which allows the inverter to access an additional voltage level with respect to the conventional two levels converters. The total voltage of the DC bus is V_{dc}. Under normal operating conditions, it is uniformly distributed over the two capacitors which have a voltage $V_{dc}/2$ at their terminals. Each of the three arms of the converter is composed of four controlled switches S_{iK} (K = a, b, c and i = 1, 2, 3, 4) and two clamped diodes connected to the midpoint of the DC bus [10, 16, 17].

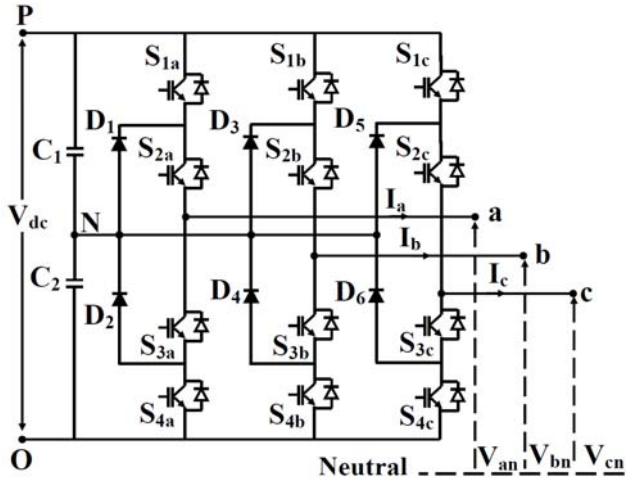

Fig. 5. Three level NPC converter

There are three possible sequences for this converter according to the different possible states for the switches (see Table 2).

Table 2

Switching logic and output voltage

S_{1K}	S_{2K}	S_{3K}	S_{4K}	V_{OK}
1	1	0	0	$V_{dc}/2$
0	0	1	1	$-V_{dc}/2$
0	1	1	0	0

The objective of the modeling is to find a relation between the control variables and the electrical quantities of the alternative and continuous part of the inverter. Thus, the pairs of switches S_{1K}, S_{3K} and S_{2K}, S_{4K} are controlled in a complementary manner.

The following expressions shows the relationship between the voltages V_{aO}, V_{bO}, V_{cO} the states of the switches and the DC voltage V_{dc}:

$$V_{aO} = \frac{V_{dc}}{2}(S_{1a} + S_{2a} - 1); \quad (6)$$

$$V_{bO} = \frac{V_{dc}}{2}(S_{1b} + S_{2b} - 1); \quad (7)$$

$$V_{cO} = \frac{V_{dc}}{2}(S_{1c} + S_{2c} - 1). \quad (8)$$

The relationships of the phase-neutral output voltages V_{an}, V_{bn}, V_{cn} of the converter according to the states of the switches S_{iK} are given by the equation:

$$\begin{bmatrix} V_{an} \\ V_{bn} \\ V_{cn} \end{bmatrix} = \frac{V_{dc}}{6}\begin{bmatrix} 2S_{1a} & 2S_{2a} & -S_{1b} & -S_{2b} & -S_{1c} & -S_{2c} \\ -S_{1a} & -S_{2a} & 2S_{1b} & 2S_{2b} & -S_{1c} & -S_{2c} \\ -S_{1a} & -S_{2a} & -S_{1b} & -S_{2b} & 2S_{1c} & 2S_{2c} \end{bmatrix}. \quad (9)$$

The model of STATCOM. The dynamics equations governing the instantaneous values of the three-phase output voltages in the AC side of the STATCOM exchanged with the utility grid are given by:

$$E_a = V_{an} + rI_a + L\frac{dI_a}{dt}; \quad (10)$$

$$E_b = V_{bn} + rI_b + L\frac{dI_b}{dt}; \quad (11)$$

$$E_c = V_{cn} + rI_c + L\frac{dI_c}{dt}. \quad (12)$$

Equations (10-12) describe the system in differential equations in *abc* frame. Transforming these equations to synchronous reference frame using Park's transformation the equations becomes:

$$E_d = V_d + rI_d + L\frac{dI_d}{dt} - \omega LI_q; \quad (13)$$

$$E_q = V_q + rI_q + L\frac{dI_q}{dt} + \omega LI_d. \quad (14)$$

The instantaneous output power of STATCOM is given by:

$$P = \frac{3}{2}\cdot(V_d I_d + V_q I_q); \quad (15)$$

$$Q = \frac{3}{2}.(V_q I_d - V_d I_q). \quad (16)$$

Within the synchronous rotating frame $V_s = V_d$ and $V_q = 0$, the instantaneous active and reactive power is given by

$$P = \frac{3}{2}\cdot V_d I_d; \quad (17)$$

$$Q = -\frac{3}{2}.V_d I_q. \quad (18)$$

STATCOM Control. The detailed control system of STATCOM is shown in Fig. 6. In this system the error signal between the rms measured and the rms AC voltage reference values is given to a PI regulator which produces a reference current I_{q_ref}. Similarly to the AC voltage regulator the error between the measured and the DC

voltage reference values is given to a PI regulator that produces a reference current I_{d_ref}. The three-phase mains currents at the PCC are transformed into *dq* reference frame to create, I_d and I_q. These currents are then compared to the corresponding reference values to create error signals (ΔI_{Sd} et ΔI_{Sq}) which are transmitted to the PI controller in order to create the vectors of the reference voltages (V_{Sdref} and V_{Sqref}). Through Park's inverse transformation, the voltages V_{Sdref} and V_{Sqref} are converted to V_{Saref}, V_{Sbref} and V_{Scref} that are required by the SPWM generator [17-19].

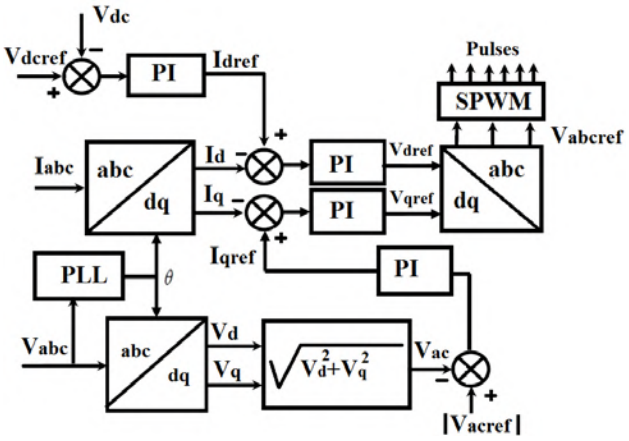

Fig. 6. STATCOM control system

The SPWM technique is one of the most popular modulation techniques applied to multi-level NPC and multi cells converters.

SPWM for two cells converters. The command of this converter is quite simple (Fig. 7). Each switching cell has its own carrier. To have a voltage of three levels, the carriers are phase shifted by $\left(\frac{2\pi}{N-1}\right)$ and therefore by 180° in this case. If these are not out of phase, the switches S_{1a} and S_{2a} or $\overline{S}_{1a}$ and $\overline{S}_{2a}$ switch at the same time, and the voltage is only of two levels (0 and V_{dc}).

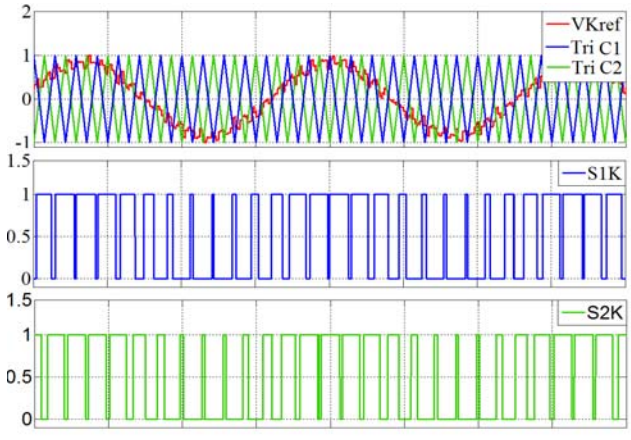

Fig. 7. Sine pulse width modulation for three two cells converter

SPWM for three level NPC converters. To generate the PWM control pulses of the three level voltage converter, two triangular carriers are required (one positive and the other negative). These carriers have the same frequency and amplitude (Fig. 8). They are then compared to the reference signal (sinus). Each comparison gives 1 if a carrier is greater than or equal to the reference, 0 otherwise. Thus for the NPC case, the control signals of the switches S_{1K} and S_{3K} are complementary and the switches S_{2K} and S_{4K} are also complementary.

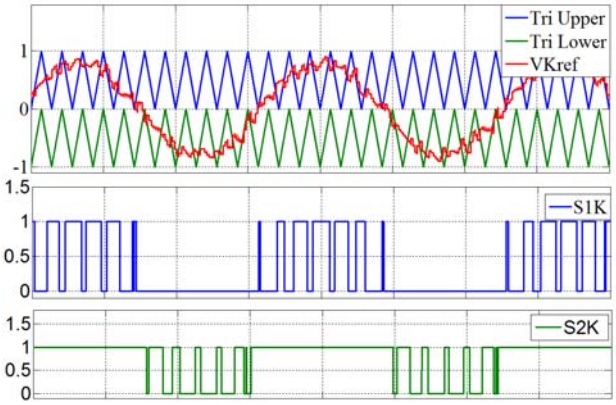

Fig. 8. Sine pulse width modulation for three level NPC converter

Simulation results. To demonstrate the efficiency of the STATCOM in the field of reactive energy compensation and voltage regulation in power grids, simulations have been carried out using Neutral-Point-Clamped (NPC) multilevel converters and multi-cells series based on Pulse Width Modulation Control (SPWM). For this, we applied two types of tests for the considered. The first concerns the presence of a voltage dip and a voltage drop at the source and the second the connection of additional inductive load. The entire system is simulated in MATLAB / Simulink with the parameters shown in Table 3.

Table 3

System parameters

Parameter name	Symbol	Value	Unit
AC Source	U_n	110	kV
	S_n	2258	MVA
	f	60	Hz
Transformer	S_n	40	MVA
	T1	110/26.7	kV
STATCOM	S	3	MVAR
	T2	27.6/0.6	kV
	V_{ac}	0.6	kV
	V_{dc}	1.4	kV
Line	l	45	km
Load	R	254	Ω
	L	1.34	H

Case 1. A voltage dip of 4 % is applied at the three-phase source during the interval (0.15-0.25) s and then a voltage drop of the order of 4 % during the interval (0.35-0.45) s. The Fig. 9 and 10 show respectively the three-phase voltages and the rms voltage per phase at the PCC without STATCOM. The positive reaction of the STATCOM which manages to maintain the variable voltage to the PCC by controlling the quantity of reactive power injected or absorbed in the network as shown in the Fig. 11 and 12. In the interval of t = (0.15-0.25) s the STATCOM injects a quantity of reactive power (2.075 MVAR) to maintain voltage levels in the line in where compensator operates in the capacitive mode and in

the interval of t = (0.35-0.45) s the STATCOM absorbs a quantity of reactive power (2.075 MVAR) to maintain voltage levels in the line where the compensator operates in the inductive mode (see Fig. 13). This reactive power exchange is achieved through the transformer leakage inductance which helps to smooth currents in advance or behind the angle with the primary voltages that are imposed on the secondary of the transformer by the controlled voltage source as shown in the Fig. 14. As show in Fig. 15 it is very clear that the voltage regulating loop continues to prove its effectiveness in maintaining constant voltage at the terminal of the capacitor. Figures 16 and 17 respectively show the output phase voltage of the STATCOM converter and the output line to line voltage of the STATCOM converter.

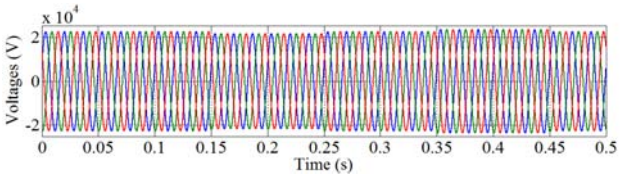

Fig. 9. Three-phase voltage *abc* at PCC without STATCOM

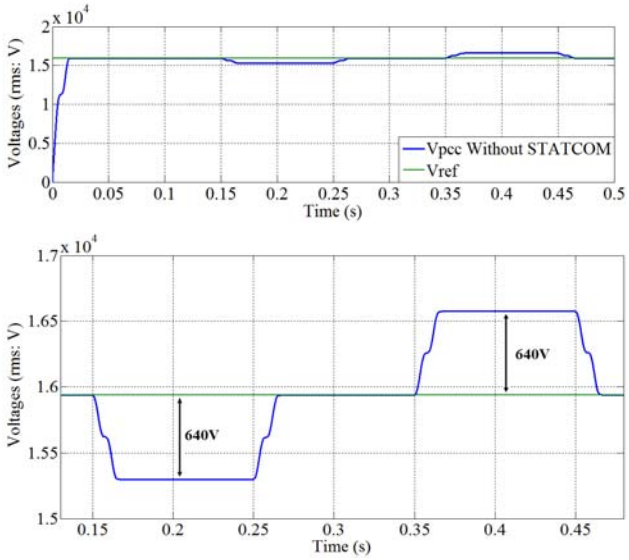

Fig. 10. Results of rms voltage phase at PCC without STATCOM

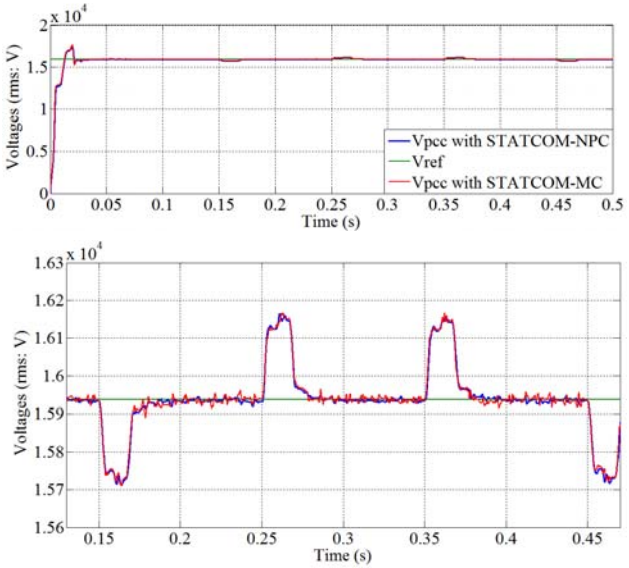

Fig. 11. Results of rms voltage phase at PCC with STATCOM

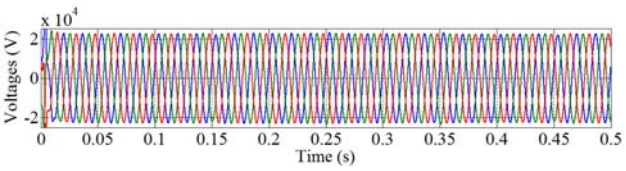

Fig. 12. Three-phase voltage *abc* at PCC with STATCOM

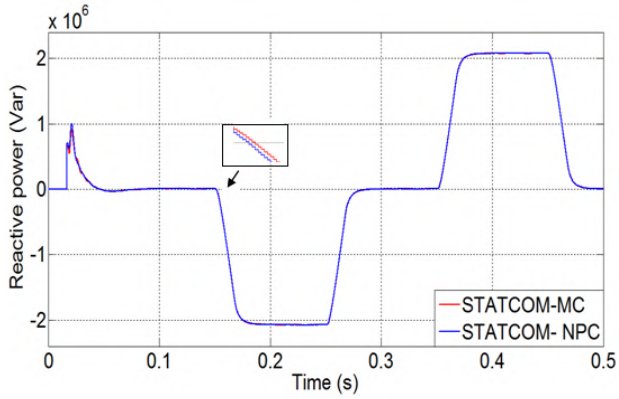

Fig. 13. Reactive power supplied and absorbed by STATCOM

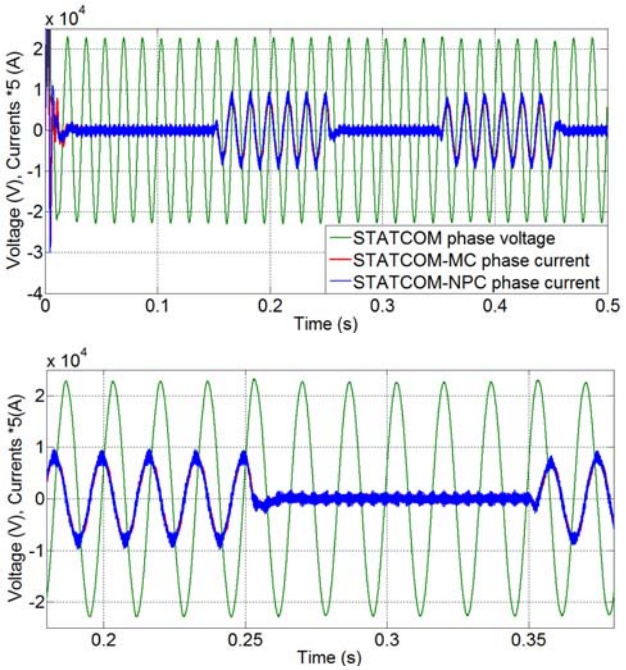

Fig. 14. Voltage and current of phase *a* at the PCC

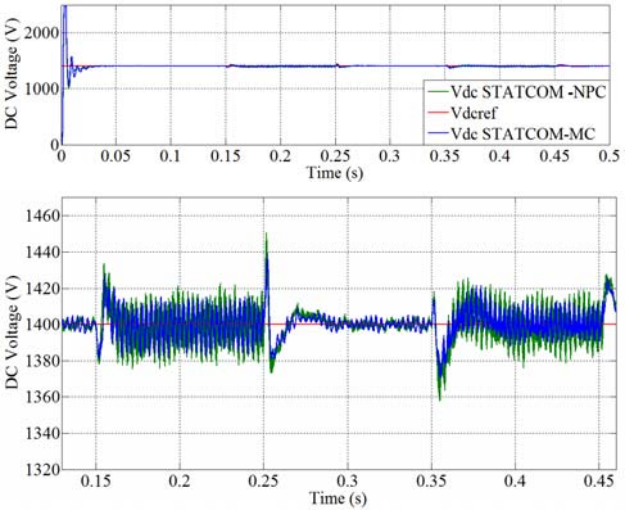

Fig. 15. Response curves of DC voltage

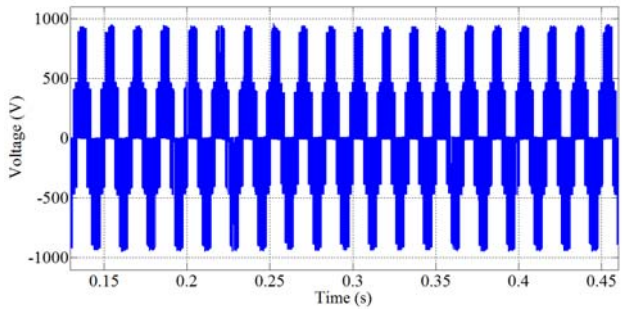

(*a*) Multi-cell converter

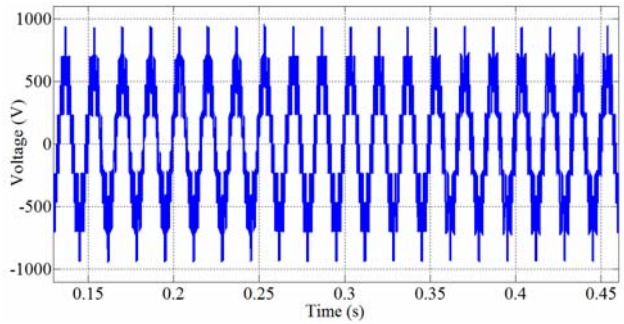

(*b*) NPC converter

Fig. 16. Output phase voltage of the STATCOM converter

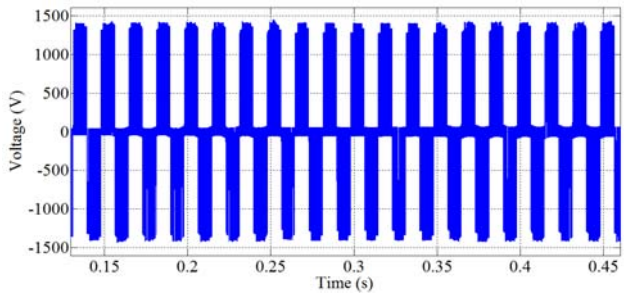

(*a*) Multi-cell converter

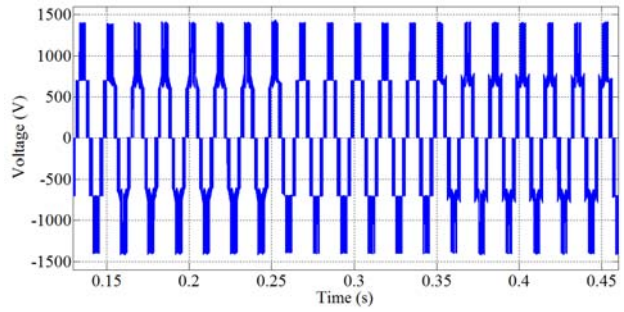

(*b*) NPC converter

Fig. 17. Output line voltage of the STATCOM converter

Case 2. A balanced three-phase inductive load is applied during the interval (0.25-0.35) s. Figures 18 and 19 shows the voltage drop caused by the inductive load at the period t = (0.25-0.35) s. The STATCOM injects the reactive power (2.25 MVAR) into the line to maintain the voltage at the PCC connection point as shown in Fig. 20 and 21 in this case it operates in the capacitive mode as shown in Fig. 22. The reactive power exchange is achieved through the transformer leakage inductance which helps to smooth currents in advance of 90° on the PCC common point voltages (see Fig. 23). Figure 24 shows the voltage across the dc capacitor.

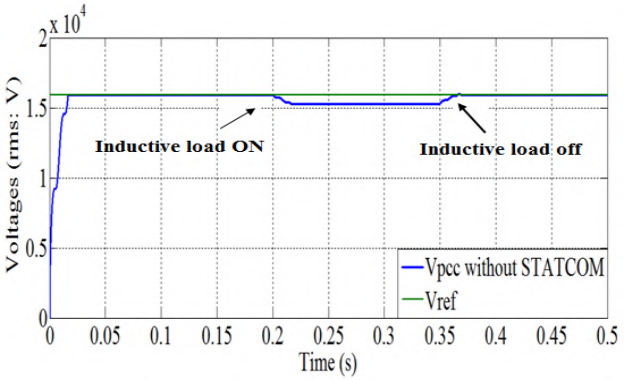

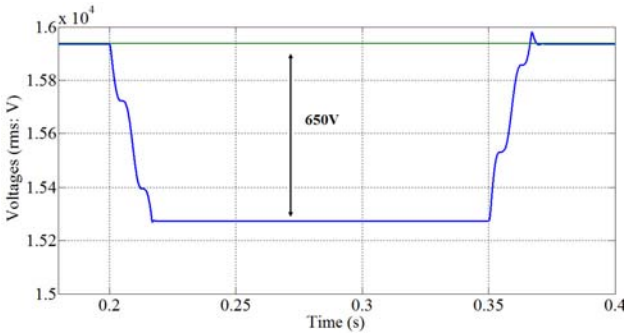

Fig. 18. Results of rms voltage phase to line at PCC without STATCOM

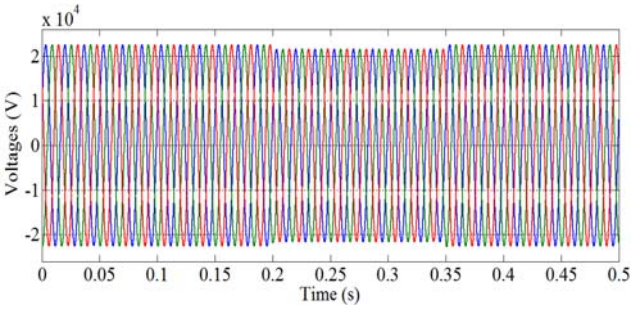

Fig. 19. Three-phase voltage *abc* at PCC without STATCOM

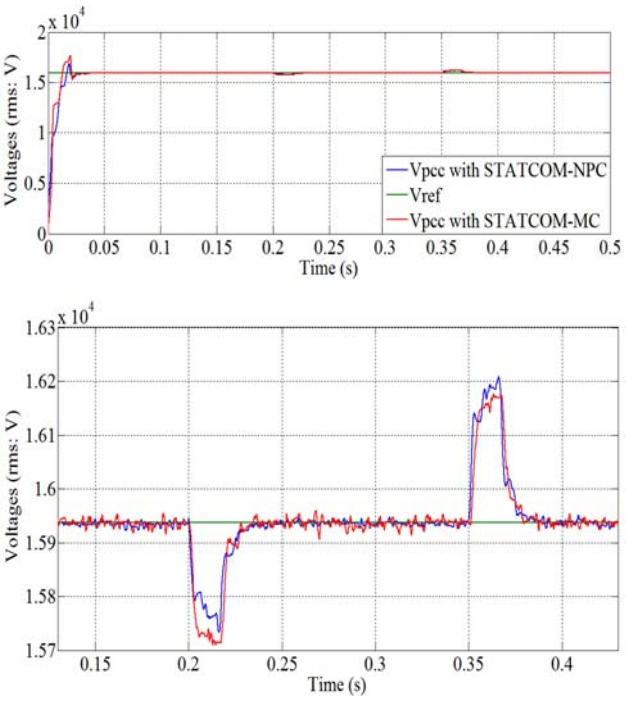

Fig. 20. Results of rms voltage phase at PCC with STATCOM

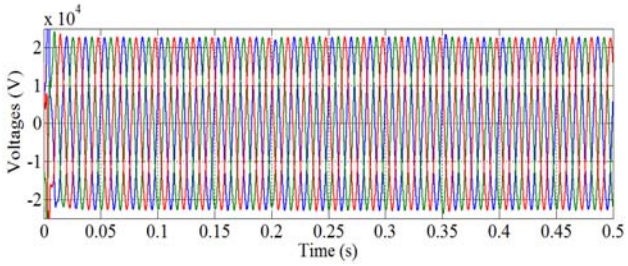

Fig. 21. Three-phase voltage *abc* at PCC with STATCOM

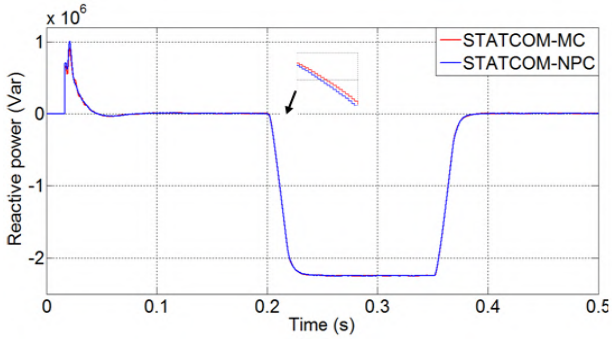

Fig. 22. Reactive power supplied and absorbed by STATCOM

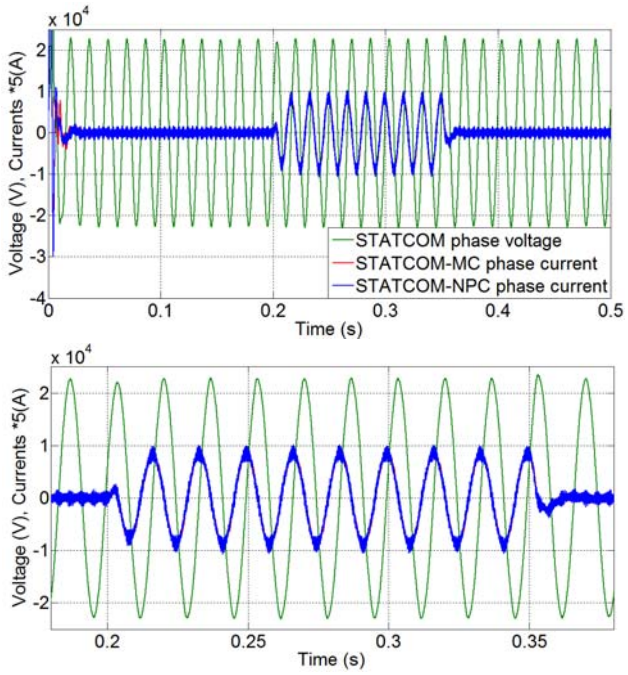

Fig. 23. Voltage and current of phase *a* at the PCC

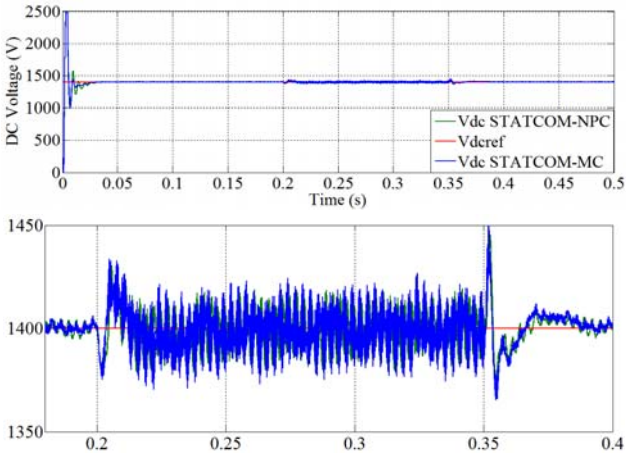

Fig. 24. Response curves of DC voltage

Case 3. A Fast Fourier Transform (FFT) analysis in MATLAB is used to conduct the harmonic analysis for multi-cells converter and multilevel NPC converter. It is summarized in Table 4. Using PWM technique, the THD% values of the three level NPC STATCOM and three level multi-cells STATCOM can be satisfied under IEEE Std. 519-1992 [22].

Table 4

Comparison of performance of MC-VSC and NPC-VSC

	Total Harmonic Distortion THD (%) Vabc at PCC	Fundamental Vabc at PCC
	Capacitive Mode	
NPC-VSC	1.12	2.54e4
MC-VSC	1.46	2.54e4
	Floating Mode	
NPC-VSC	0.81	2.55e4
MC-VSC	1.44	2.55e4
	Inductive Mode	
NPC-VSC	1	2.59e4
MC-VSC	1.43	2.59e4

Conclusion. This article presents a performance analysis of three-level NPC and multi-cell converters used in STATCOM applications for voltage regulation and reactive energy compensation in an electrical grid. The STATCOM model and the proposed control are implemented on SIMULINK / MATLAB to check steady state and dynamic performance. The simulation tests carried out have shown that the STATCOM with the proposed control is capable of supplying or absorbing the reactive energy to maintain the stable voltage at the common connection point (PCC) and whatever the type of disturbance (voltage drop or voltage dip). Finally, the two converters give almost identical output voltage values, so the values of the reactive powers are identical. But the voltage THD (1.12 %) is better for the NPC case. But against the point of view components used and the cost, the multi-cell converter is more interesting.

REFERENCES

1. Hingorani N.G, Gyugyi L. *Understanding FACTS. Concepts and technology of Flexible AC Transmission Systems*. IEEE Press, New York, 2000.

2. Kouro S., Malinowski M., Gopakumar K., Pou J., Franquelo L.G., Bin Wu., Rodriguez J., Pérez M.A., Leon J.I. Recent advances and industrial applications of multilevel converters. *IEEE Transactions on Industrial Electronics*, 2010, vol.57, no.8, pp. 2553-2580. **doi: 10.1109/tie.2010.2049719**.

3. Chetan E. Morkhade, Bhushan S. Rakhonde. Improvement in voltage profile using FACT device. *International Journal of Scientific & Engineering Research*, 2013, vol.4, iss.6, pp. 27-32.

4. Huang Z., Shengzhen Y., Hongyan Y., Xingming F. A control method for SVPWM-based STATCOM using active-reactive current decouple under dq coordinate system. *International Conference and Exposition on Electrical and Power Engineering, EPE, Iasi, Romania*, 2012, pp. 191-196. **doi: 10.1109/icepe.2012.6463929**.

5. Barik S.R, Nayak B., Dash S. A comparative analysis of three level VSC based multi-pulse STATCOM. *International Journal of Engineering and Technology*, 2014, vol.6, no.3, pp. 1550-1563.

6. Liu X., Lv J., Gao G., Chen Z., Chen S. A novel STATCOM based on diode-clamped modular multilevel converters. *IEEE Transactions on Power Electronics*, 2017, vol.32, no.8, pp. 5964-5977. **doi: 10.1109/tpel.2016.2616495**.

7. Malinowski M., Gopakumar K., Rodriguez J., Perez M.A. A survey on cascaded multilevel inverters. *IEEE Transactions on Industrial Electronics*, 2010, vol.57, no.7, pp. 2197-2206. **doi: 10.1109/tie.2009.2030767**.

8. Becker F. *Contribution à la continuité de service des convertisseurs statiques multiniveaux*. Phd de L'Université de Lorraine, 2017. (Fra).

9. Jones M., Satiawan I.N.W., Bodo N., Levi E. A dual five-phase space-vector modulation algorithm based on the decomposition method. *IEEE Transactions on Industry Applications*, 2012, vol.48, no.6, pp. 2110-2120. **doi: 10.1109/tia.2012.2226422**.

10. Baldés M. *Etude d'un compensateur statique pour éoliennes à vitesse fixe à base de génératrice asynchrone à cage*. Mémoire de Maitrise, Université du Québec, Canada, 2010. (Fra).

11. Berkoune K. *Approche Mathématique pour la Modulation de Largeur d'Impulsion pour la conversion statique de l''energie électrique: Application aux onduleurs multiniveaux*. Doctorat de l'université de Toulouse, France, 2016. (Fra).

12. Crappe M. *Exploitation des Réseaux Electriques avec L'électronique de Puissance*. Lavoisier, 2006. (Fra).

13. Hanafi S., Fellah M.K., Guebli A., Chiali E. Commande du convertisseur multicellulaire série (7 cellules) par SVM avec régulation des tensions flottantes. *The 2nd International Conference on Power Electronics and Electrical Drives*, Oran, Algeria, 2012. (Fra).

14. Defay F., Llor A.-M., Fadel M. A predictive control with flying capacitor balancing of a multicell active power filter. *IEEE Transactions on Industrial Electronics*, 2008, vol.55, no.9, pp. 3212-3220. **doi: 10.1109/tie.2008.927989**.

15. Defay F., Llor A.M., Fadel M. A direct predictive control of shunt active power filters using multicell converter. *2007 European Conference on Power Electronics and Applications*, 2007, pp. 1-9. **doi: 10.1109/epe.2007.4417411**.

16. Darshan P., Vineetha R., Jil S., Pratik P. A comparative study of three phase 2-level VSI with 3-level and 5-level diode clamped multilevel inverter. *International Journal of Emerging Technology and Advanced Engineering*, 2014, vol.4, no.4, pp. 708-713.

17. Wanchai S. Design and analysis three phase three level diode-clamped grid connected inverter. *Energy Procedia*, 2016, vol.89, pp. 130-136. **doi: 10.1016/j.egypro.2016.05.019**.

18. Murugesan K., Muthu R. Modeling and simulation of D-STATCOM for voltage regulations. *2011 1st International Conference on Electrical Energy Systems*, 2011. **doi: 10.1109/icees.2011.5727975.**

19. Giroux P., Sybille G, Le-Huy H. Modeling and simulation of a distribution STATCOM using Simulink's power system blockset. *IECON'01. The 27th Annual Conference of the IEEE Industrial Electronics Society*, 2001, pp. 990-994. **doi: 10.1109/iecon.2001.975905.**

20. Saha A., Ahmad S., Soma A.A., Chowdhury M.Z.A., Hossain A.A. Modelling and control of STATCOM to ensure stable power system operation. 2017 4th International Conference on Advances in Electrical Engineering (ICAEE), Sep. 2017, pp. 12-17. **doi: 10.1109/icaee.2017.8255318**.

21. Blažič B., Herman L., Božiček A., Papič I. Mathematical modeling and control algorithms of STATCOMs. *Book chapter in Static Compensators (STATCOMs) in Power Systems*, Dec. 2014, pp. 111-145. **doi: 10.1007/978-981-287-281-4_4**.

22. *IEEE Standard 519-1992. IEEE Recommended Practices and Requirements for Harmonic Control in Electrical Power Systems*. IEEE Inc., New York, 1992.

Received 24.06.2019

Soltane Belakehal[1], *Doctor of Electrotechnic, Associate Professor,*
Abed el hak Djellad[1], *Doctor of Electrotechnic, Associate Professor,*
Rachid Chenni[1], *Doctor of Electrotechnic, Professor,*
[1] Department of Electrical Engineering,
University of Constantine 1,
Constantine, Algeria.
e-mail: bel_soltane@yahoo.fr,
djellad.abedelhak@gmail.com,
rachid.chenni@caramail.com

How to cite this article:
Belakehal S., Djellad A., Chenni R. Performance comparison of multicell series and NPC multilevel converters for a STATCOM. *Electrical engineering & electromechanics*, 2019, no.5, pp. 60-67. **doi: 10.20998/2074-272X.2019.5.10.**

UDC 621.3 **doi: 10.20998/2074-272X.2019.5.11**

A. Moghayadniya, E. Razavi

REACTIVE POWER CONTROL IN MICRO-GRID NETWORKS USING ADAPTIVE CONTROL

Purpose. Despite their economic and environmental benefits, distributed products in power systems have caused problems in power systems. One of the most important issues in this regard is voltage fluctuations and frequencies in Micro-grids, which depends on several factors, such as variable consumption load and errors in power systems. One of the main challenges associated with the use of Micro-grids is power management among distributed generation sources. Power management plays a pivotal role in numerous Micro-grids and may ensure the stable and improved performance of Micro-grids in the permanent status of the system. The present study aimed to examine the power control in Micro-grids by proposing an adaptive control method along with the PID controller for power management and coordination in Micro-grids. This coordination system operates between production sources and controlling the voltage and frequency levels against the possible disturbances occurring anywhere in the system loop. The results of the simulation of the proposed algorithm in MATLAB software environment exhibited a high success rate (i.e., proper response to the fluctuations in the Micro-grid) and extremely low error rate (i.e., proper reactive power in the grid). References 17, tables 3, figures 12.

Key words: **Micro-grid, control parameters, online parameter setting, proportional-integral-derivative controller (PID), adaptive control.**

Цель. Несмотря на их экономические и экологические преимущества, распределенные продукты в энергосистемах приводят к возникновению проблем в последних. Одним из наиболее важных вопросов в этой связи являются колебания напряжения и частоты в микросетях, которые зависят от нескольких факторов, таких как переменная нагрузка потребления и ошибки в энергосистемах. Одной из основных проблем, связанных с использованием микросетей, является энергоменеджмент источников распределенной генерации. Энергоменеджмент играет ключевую роль во многих микросетях и может обеспечить стабильную и улучшенную работу микросетей при постоянном состоянии системы. Настоящее исследование направлено на исследование энергоменеджмента в микросетях путем предложения адаптивного метода управления вместе с ПИД-контроллером для энергоменеджмента и координации в микросетях. Эта система координации функционирует между источниками производимой энергии и контролирует уровни напряжения и частоты в отношении возможных помех, возникающих в любом месте контура системы. Результаты моделирования предложенного алгоритма в программной среде MATLAB показали высокую степень успеха (то есть правильную реакцию на колебания в микросети) и чрезвычайно низкую частоту ошибок (то есть надлежащую реактивную мощность в сети). Библ. 17, табл. 3, рис. 12.

Ключевые слова: **микросеть, параметры управления, онлайн настройка параметров, пропорционально-интегрально-дифференцирующий (ПИД) контроллер, адаптивное управление.**

Introduction. The structure of the power industry consists of producers, transmission lines and electrical equipment; the operators of this industry are still monitoring the state of the system with delays, which is about 10 sec behind the actual time.

The above grid should use a wide range of sensors, communications and control techniques to improve the performance of production, transmission and distribution systems of electric power, and move towards a more reliable and an optimized power system, cost effective and eco-friendly system by providing a ground for distributed production and using renewable sources [1]. A Micro-grid typically consists of a set of distributed sources, a power storage system, and loads which may be used via connecting to the global power grid or via the island function (independent). Distributed generation refers to cases where electricity is produced at the same place of consumption or near the place of consumption [2].

From the perspective of consumers, Micro-grid is capable of providing increased reliability, improved power quality and reduced consumption costs. From the point of view of the power companies, the use of Micro-grid has the potential to reduce consumption and thus reduce the facilities required for the development of transmission lines, and in addition to eliminating peak consumption points, it reduces grid losses.

The topic of frequency and voltage stability is one of the significant factors that should be taken into account in the planning and exploitation of Micro-grid in order to avoid the collapse of voltage and off in system. Regarding the fact that there are not an infinite number of Micro-grid buses, and most power supply sources have power interfaces, the main concern in controlling Micro-grid is the control of electronic power converters [4]. In connected state, the Micro-grid does not have many problems with voltage and frequency stability. This is due to the fact that it is connected to system with far higher inertia than itself, and if it has a shortage of production, it will be distributed from the larger system [5]. But in the island state, the worst problem deals with the instability of the voltage and frequency of the Micro-grid, and in many cases, it deals with the voltage and frequency drop. The overall Micro-grid inertia is low, and as a result of sudden changes in loads or faults, if there is no effective protection and control system, Micro-grid will quickly undergo instability and collapse.

Different structures have been developed to control Micro-grid in recent years. But in 2012, a relatively good initial structure for standardization was presented by Prof. Guererro, in which a PID Controller (hierarchical control) inspired from traditional and old power control system, which included: local control (primary), supplemental control (secondary) and Micro-grid power control (third) [6]. Prof. Beaverani has improved this hierarchical

structure by modifying the three levels and adding a new loop to the structure. This new loop is Emergency Control of Micro-grid [7]. In Micro-grid, both the frequency and voltage parameters are simultaneously dependent on both the actual power and reactive power parameters. Even to improve this, other loops such as Loop Impedance have been established [8].

In a PID Controller, the loop of local control (primary) prevents the permanent drop but does not necessarily return it to the nominal values. The secondary control loop includes two voltage control and frequency control units, and consists of two loops with two regular PID controllers. The Micro-grid power control loop (third), which is the frequency synchronization, allows the loop to only connect the Micro-grid to the main grid when the phase difference of both systems is less than (low), so that the micro-grid is interrupted by transient disturbances. The synchronization operation is performed by the PID controllers [9].

At the island state, the third control loop can determine the amount of power generated by each distributed source, and in the connected state, it can take the amount of power imported or exported from the grid to the main grid. At the island state, the nominal values of the grid (ex. 220 V and 50 Hz), and in connection state, the instant values of the voltage and frequency of the main grid will be the reference values. Among the controversial topics, we may point to the presence of virtual impedance and how to set these control factors. The reason for using a comparative controller is the simplicity of control in terms of performance as well as implementation [10].

Materials and methods. Micro-grid is part of a power system that includes distributed generation sources that operate as a load or power source and must be operational after being disconnected from the main grid.

The Micro-grid is connected to the distribution network in normal mode. If a fault or short circuit occurs in the distribution system, the fault detection system commands breaker and that the Micro-grid goes to autonomous or islanding mode. We have the highest number of frequency instability and voltage problems in islanding mode, and in most cases, we observe voltage and frequency drops. The overall Micro-grid inertia is low; therefore, sudden changes in load or faults in absence of an effective protection and control system, the Micro-grid experiences instant instability and collapse. In result, we need a controller that can stabilize the system.

Controlling distributed sources in Micro-grids bears high importance in optimizing and increasing the reliability and stability of power network. The PID controller is one of the most commonly used feedback controllers that has been used in a wide range of controlling processes such as DC motor speed control, pressure control, and temperature control, etc. The PID controller computes the «error» value between the process output and the desired input value. The goal of controller is to minimize error via adjusting process control inputs.

In fact, the PID controller is used to control the frequency and stability of the system and thus the power control. An example of controllers that are widely used in controlling industrial processes is called a Proportional–Integral–Derivative controller or PID. Figure 1 shows block diagram of Unity Feedback System with controller.

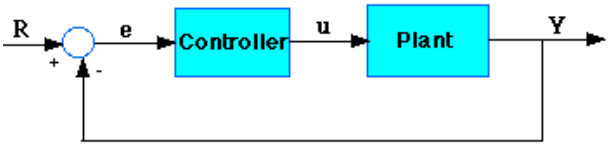

Fig. 1. Unity Feedback System

The transfer function of the PID controller appears as follows

$$K_P + \frac{K_I}{s} + K_D s = \frac{K_D s^2 + K_P s + K_I}{s}, \qquad (1)$$

where K_P – proportional gain, K_I – integral gain, K_D – derivative gain.

First, it is necessary to look at how the PID controller works in a closed-loop system using the schematic shown above. The variable (e) represents the tracking error, the difference between the desired input value (R) and the actual output (Y). This error signal (e) is sent to the PID controller, which computes both the derivative and the integral of this error signal. The signal (u), just past the controller, is now equal to the proportional gain (K_P) times the magnitude of the error plus the integral gain (K_I) times the integral of the error plus the derivative gain (K_D) times the derivative of the error

$$U = K_P e + K_I \int e dt + K_D \frac{de}{dt}. \qquad (2)$$

The signal (u) is sent to the plant. The new output (Y) returns again to the sensor to find the new error signal (e). The proportional controller (K_P) affects the on reduction of the rise time and the integral controller (K_I) affects the elimination of the steady-state error. The derivative control (K_D) affects the increase the stability of the system, reduce the overshoot, and improve the transient response. The effects of each of the Controllers K_P, K_D, and K_I on a closed-loop system are summarized in the table below. Table 1 shows the effect of change in the coefficient of PID Controllers on rise time and steady state error in closed-loop system.

Table 1

Effect of PID controllers on a closed-loop system

CL response	Rise time	Overshoot	Settling time	S-S error
K_P	Decrease	Increase	Small change	Decrease
K_I	Decrease	Increase	Increase	Eliminate
K_D	Small change	Decrease	Decrease	Small change

In the Table 1 CL is closed-loop system, overshoot is the occurrence of a signal or function exceeding its target, rise time is the time taken by a signal to change from a specified low value to a specified high value, settling time includes a propagation delay, plus the time required for the output to slew to the vicinity of the final value, recover from the overload condition associated with slew, and finally settle to within the specified error,

S-S error is: steady state error. Steady-state error is defined as the difference between the input (command) and the output of a system in the limit as time goes to infinity (i.e. when the response has reached steady state).

In this section, an adaptive control is proposed in order to determine the parameters of the PID controller to deal with complex and uncertain conditions, which is due to reduced computations.

It is supposed that the PID controlling method determines the optimal optimization parameters based on adaptive control. This method applies an adaptive control method to find the optimal parameters. Therefore, the quality of detecting the range of optimal domain extracted for algorithm operation. The order of the effect of the suggested method is in extracting the best range of values; so that, it provides the closest PID controller values.

Adaptive control. In control of power systems, the dynamics of the system may be fully apparent at the start of operation, but its parameters face unpredictable changes through the control process. Therefore, the initially designed controller, which was initially appropriate, may not be able to control the changing system without the redesign of the controller. In general, the main purpose of the adaptive control is to consistently maintain the system's operation against parametric uncertainty or their uncertain changes. Regarding that such a parametric uncertainty and/or their variation may occur in many practical problems, adaptive control is useful in a number of industrial situations.

In existing adaptive methods in nonlinear systems, it is generally required to make the planetary dynamics linearly parametric, i.e. parametric uncertainty is functionally expressed as a line of an uncertain set of parameter. Linear parameterization and in result, adaptive control cannot be reached in some cases, but resistant control (or adaptive control with semi resistant sentences) may be possible.

An adaptive controller differs with a regular controller from the point that the controller parameters are changeable in it and that there is a mechanism based on system signals used for timely adjustment of such parameters. In the design of non-adaptive controllers, the structure (such as the polarity determination) is firstly determined, and then the controller parameters are computed based on the system parameters. In the adaptive control, the essential difference is that the system parameters are uncertain; so, the controller parameters should be obtained by an adaptive law. Consequently, adaptive control design is more complicated because of the additional requirements of the selecting adaptation law and proving system stability against adaptation.

The basis of adaptive control is the parameter estimation that is a branch of system identification. Common estimation methods include recursive least squares and descending gradients.

In fact, adaptive control systems are often used to control time variable parameters. The design of a comparative controller usually involves the following three steps:

- selecting a control law that includes variable parameters;
- selecting an adaption law to set these parameters;
- analyzing the properties of the convergence of the resulting control systems.

Many distributed generation sources, such as fuel cells, photovoltaic cells and microturbines, are connected through a grid voltage source inverter. Therefore, in order to control power, distributed generation sources are connected as a DC voltage source and through the inverter to the grid (Fig. 2).

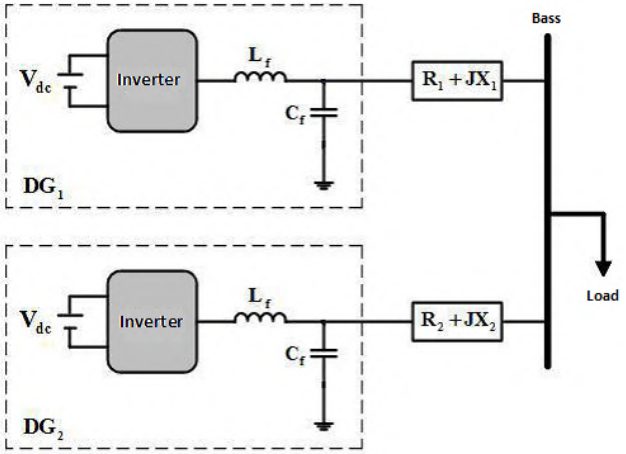

Fig. 2. The structure of the network studied

Tiny network structure studied. Distribution sources can be an island for some reason, such as error or planning, to maintain their goals. In this state of operation, the distributed generation sources have no connection to the main grid. Therefore, the power control strategy of this state of operation should meet the following objectives:

- adjusting frequency;
- maintaining and adjusting voltage;
- managing the distribution of active and reactive powers between distributed island sources;
- performing proper distribution of power between sources when changing loads.

Figure 3 shows the controller in island state. The controller constitutes of three main components of power control, voltage control and current control, which are described below.

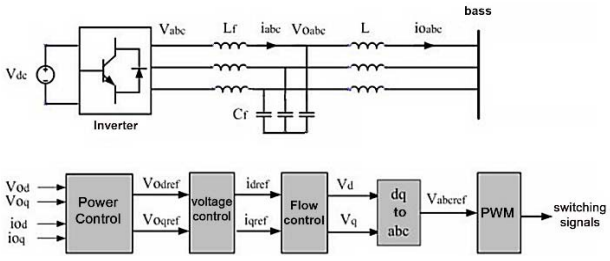

Fig. 3. Controller in the island fashion

Reactive power control. In the control of reactive power, the Droop method has been used to calculate the active and reactive power of the inverter output using the measured values of the current and the inverter output voltage. It also uses a low pass filter whose off frequency is 10 % of the nominal frequency of the system, to eliminate oscillations and obtain essential output power content.

Equations (3) and (4) indicate the power computation method.

$$P = \frac{3}{2} \cdot \frac{\omega_C}{S + \omega_C} \left(V_{od} I_{od} + V_{oq} I_{oq} \right); \quad (3)$$

$$Q = \frac{3}{2} \cdot \frac{\omega_C}{S + \omega_C} \left(V_{oq} I_{od} + V_{od} I_{oq} \right). \quad (4)$$

The Drop features are used up to the provision of a drop in the range and frequency of the output voltage, as follows

$$\omega = \omega_n - mP; \quad (5)$$

$$V = V_n - nQ. \quad (6)$$

Finally, the controller is designed in a way to allocate the reference voltage, obtained by the Droop method, to the *d*-axis and set the reference *q* to zero. These reference values are voltage control inputs (Fig.4-6).

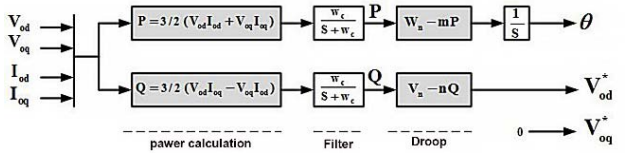

Fig. 4. Reactive power controller in the island fashion

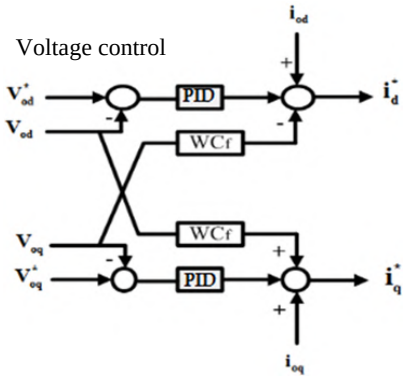

Fig. 5. Voltage controller in the island fashion

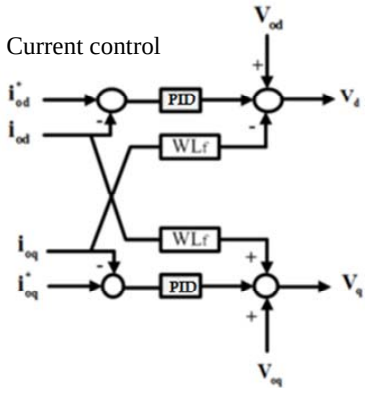

Fig. 6. Current controller in the island fashion

Optimization method for PID controller parameters with adaptive control. The parameters considered in the optimization of the coefficients are IIK, PIK, IVK, and PVK. The optimization goal is to minimize current and voltage errors according to the Fig. 7.

The considered Micro-grid parameters are simulated in MATLAB software and the results of their optimization by adoptive control method are presented in the following Tables 2, 3.

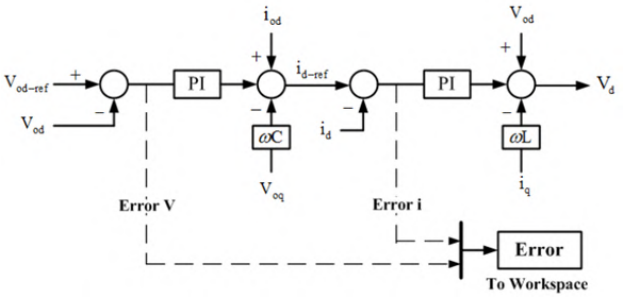

Fig. 7. Optimization of controller parameters by minimizing voltage and current errors

Table 2

Network parameters studied

Parameter		Value
DG_1, DG_2	Source voltage V_{DC}	580 V
	Inductance filter inverter (L_f)	1 mH
	Capricanticism filter inverter (C_f)	50 μF
	Frequency switching inverter (f_s)	8 kHz
	m	$6.25 \cdot 10^{-5}$
	n	$1.8 \cdot 10^{-3}$
	f_n	50 Hz
	V_n	$220\sqrt{2}$
Z_1, Z_2		$0.424j\Omega$
Power		6 kW
Voltage effective line		$220\sqrt{3}$

Table 2

Results obtained from optimization

	K_P	K_I	K_D
Normal PID control	0.13034	10.418	0.63969
Adaptive PID control	0.32987	39.962	1.0926

To check the performance of the controller, the load at the instant of t = 0.6 s is changed from 6 kW to 10 kW. The following is the simulation's output with parameters optimized by comparative control.

According to the obtained forms:

- power is divided between units in proper mode;
- frequency drops are within permissible range.

Simulation outputs are desirable. Although there are overshoot in outputs, but its value is ignorable. Also, the output speed is desired. Simulation outputs with parameters optimized by adoptive control method are also given below. With regard to the output figures with optimized parameters, the following results are achievable:

- power is divided between units;
- frequency drops are in the allowed range.

Simulation outputs are desirable in terms of speed and overshoot and there is no overshoot and undershoot in the responses (Fig. 8).

In this Fig. 8 distributed generation (DG) is an approach that employs small-scale technologies to produce electricity close to the end users of power. DG technologies often consist of modular (and sometimes renewable-energy) generators, and they offer a number of potential benefits.

As a result, it is notable that the optimization of the adoptive control is done correctly and the system has optimal response with these optimal parameters.

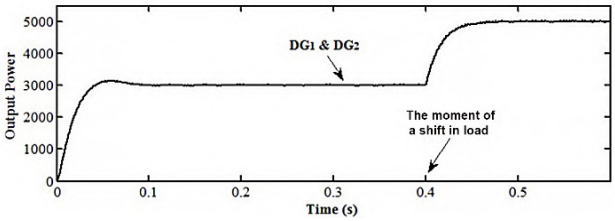

Fig. 8. Output power of DGs with parameters optimized by adaptive control

Stability analysis method for determining the function of converting voltage and current controllers. Block current controller diagram in island state shown in Fig. 9, where V_0 is the disturbance input.

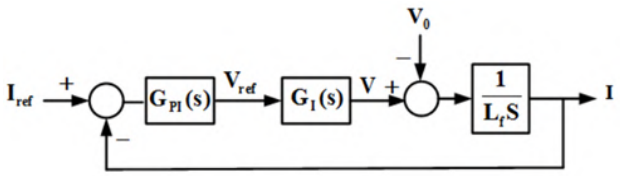

Fig. 9. Block current controller diagram in island state

The inverter conversion function is $G_I(S) = 1$ and $G_{PI}(S)$ is PID controller conversion function, expressed as

$$G_{PI}(S) = K_{PID} + \frac{K_{II}}{S}. \quad (7)$$

Block diagram of voltage controller in island state shown in Fig. 10, where I_0 is the disturbance input.

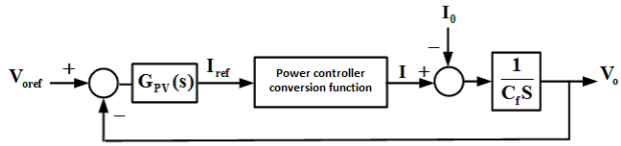

Fig.10. Block Diagram of Voltage Controller in Island State

$G_{PV}(S)$ is the PID controller conversion function, as follows

$$G_{PV}(S) = K_{PV} + \frac{K_{IV}}{S}. \quad (8)$$

In order to obtain the voltage controller conversion function, firstly obtain the current controller conversion function and then, the conversion function obtained will be considered in the voltage controller. The stability of the controller can be checked upon obtaining the open loop and closed loop function and having parameters. In order to analyze the stability of the optimal comparator control, first, the stability of the current controller and then the stability of the voltage controller must be checked. These analyses are performed according to the parameters optimized by comparative control.

The current controller conversion function is

$$T_{I-Adaptive}(S) = \frac{1.3123 \cdot S + 309.08}{0.5 \cdot 10^{-3} \cdot S^2 + 1.3123 \cdot S + 309.08}. \quad (9)$$

The graph of these conversion functions is shown in the Fig. 11, 12. Considering the Figure it is founded that the margin of interest and the margin of the controller phase are positive; therefore, the system is stable.

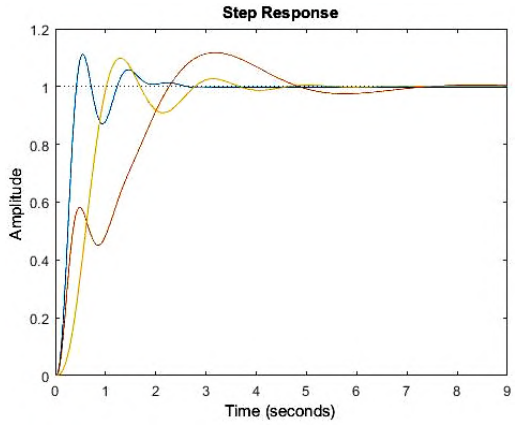

Fig. 11. Voltage controller stage response in island state with parameters optimized by adaptive control

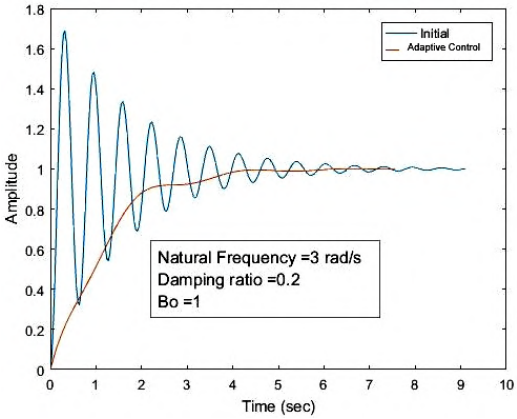

Fig. 12. Controller stage response in island state with parameters optimized by adaptive control

Conclusion. The adoptive control method was used to select the optimal PID controller parameters in Micro-grid. The sample grid and the adoptive control used for finding the most optimal response were implemented in MATLAB software. The simulation results show the correct control of the reactive power between the Micro-grids distributed generation sources. These simulation results also indicate that the optimization of the parameters is done correctly and the system responses are desirable. These responses were evaluated in terms of the speed and error of the steady state.

Sustainability analysis was performed with optimized parameters and the stability of the systems with bad graphs and their performance and speed were investigated with step responses. The performance of these systems was also investigated against step type turbulence. The results of this thesis once again indicate the requirement of proper selection of correct controller coefficients, because the lack of proper selection may lead to undesirable and oscillatory responses of the system.

REFERENCES

1. Elkhatib M.E., El-Shatshat R., Salama M.M.A. Novel Coordinated Voltage Control for Smart Distribution Networks with DG. *IEEE Transactions on Smart Grid*, 2011, vol.2, no.4, pp. 598-605. **doi: 10.1109/TSG.2011.2162083**.

2. Pepermans G., Driesen J., Haeseldonckx G., Belmans R., D'haeseleer W. Distributed generation: definition, benefits and issues. *Energy Policy*, 2005, vol.33, no.6, pp. 787-798. **doi: 10.1016/j.enpol.2003.10.004**.

3. Mandis A.C., Manoloiu A., StefanaNeagoe A.G., Leonida T., Neagoe A.C. Impact of distributed generation on steady state of electrical networks. *Proceedings of ISFEE '2014 – International Symposium on Fundamentals of Electrical Engineering.* **doi: 10.1109/ISFEE.2014.7050605.**

4. Rezaei N., Haghifam M-R. Protection scheme for a distribution system with distributed generation using neural networks. *International Journal of Electrical Power & Energy Systems*, 2008, vol.30, no.4, pp. 235-241. **doi: 10.1016/j.ijepes.2007.07.006**.

5. Poornazaryan B., Karimyan P., Gharehpetian G.B., Abedi M. Optimal allocation and sizing of DG units considering voltage stability, losses and load variations. *International Journal of Electrical Power & Energy Systems*, 2016, vol.79, pp. 42-52. **doi: 10.1016/j.ijepes.2015.12.034**.

6. Sheng W., Meng X., Zhao S., Song X. Maximum penetration level of distributed generation in consideration of voltage fluctuations based on multi-resolution model. *IET Generation, Transmission & Distribution*, 2015, vol.9, no.3, pp. 241-248. **doi: 10.1049/iet-gtd.2013.0883**.

7. Pandi V.R., Zeineldin H.H., Xiao W. Determining Optimal Location and Size of Distributed Generation Resources Considering Harmonic and Protection Coordination Limits. *IEEE Transactions on Power Systems*, 2013, vol.28, no.2, pp. 1245-1254. **doi: 10.1109/TPWRS.2012.2209687**.

8. Bevrani H., Ghosh A., Ledwich G. Renewable energy sources and frequency regulation: survey and new perspectives. *IET Renewable Power Generation*, 2010, vol.4, no.5, pp. 438-457. **doi: 10.1049/iet-rpg.2009.0049**.

9. Shiva C.K., Mukherjee V. Automatic generation control of interconnected power system for robust decentralized random load disturbances using a novel quasioppositional harmony search algorithm. *International Journal of Electrical Power & Energy Systems*, 2015, vol.73, pp. 991-1001. **doi: 10.1016/j.ijepes.2015.06.016**.

10. Rerkpreedapong D., Hasanovic A., Feliachi A. Robust load frequency control using genetic algorithms and linear matrix inequalities. *IEEE Transactions on Power Systems*, 2003, vol.18, no.2, pp. 855-861. **doi: 10.1109/TPWRS.2003.811005.**

11. Esmaeli A. Stability analysis and control of microgrids by sliding mode control. *International Journal of Electrical Power & Energy Systems*, 2016. vol.78, pp. 22-28. **doi: 10.1016/j.ijepes.2015.11.068.**

12. Miveh M.R., Rahmat M.F., Ghadimi A.A., Mustafa M.W. Control techniques for three-phase four-leg voltage source inverters in autonomous Micro-grids: A review. *Renewable and Sustainable Energy Reviews*, 2016, vol.54, pp. 1592-1610. **doi: 10.1016/j.rser.2015.10.079**.

13. Khalghani M.R., Khooban M.H., Mahboubi-Moghaddam E., Vafamand V., Goodarzi M. A self-tuning load frequency control strategy for Micro-grids: Human brain emotional learning. *International Journal of Electrical Power & Energy Systems*, 2016, vol.75, pp. 311-319. **doi: 10.1016/j.ijepes.2015.08.026**.

14. Ghanbarian M.M., Nayeripour M., Rajaei A., Mansouri M.M. Design and implementation of a new modified sliding mode controller for grid connected inverter to controlling the voltage and frequency. *ISA Transactions*, 2016, vol.61, pp. 179-187. **doi: 10.1016/j.isatra.2015.11.023.**

15. Mahmoud M.S., Alyazidi N.M., Abouheaf M.I. Adaptive intelligent techniques for Micro-grid control systems: A survey. *International Journal of Electrical Power & Energy Systems*, 2017, vol.90, pp. 292-305. **doi: 10.1016/j.ijepes.2017.02.008**.

16. Shariatzadeh F., Kumar N., Srivastava A.K. Optimal Control Algorithms for Reconfiguration of Shipboard Micro-grid Distribution System Using Intelligent Techniques. *IEEE Transactions on Industry Applications*, 2017, vol.53, no.1, pp. 474-482. **doi: 10.1109/TIA.2016.2601558**.

17. Sedighizadeha M., Esmaili M., Eisapour-Moarref A. Voltage and frequency regulation in autonomous Micro-grids using Hybrid Big Bang-Big Crunch algorithm. *Applied Soft Computing*, 2017, vol.52, pp. 176-189. **doi: 10.1016/j.asoc.2016.12.031**.

Received 07.05.2019

Amin Moghayadniya[1], *Candidate of Power Engineering, M.Sc. Student,*
S. Ehsan Razavi[1], *Doctor of Control Engineering, Assistant Professor,*
[1] Department of Electrical Engineering,
Mashhad Branch, Islamic Azad University,
Ostad Yusofi Str., Emamieh Boulevard, GhasemAbad,
Mashhad, Iran.
e-mail: ehsanrazavi@mshdiau.ac.ir,
e_razavi_control@yahoo.com

How to cite this article:
Moghayadniya A., Razavi E. Reactive power control in micro-grid networks using adaptive control. *Electrical engineering & electromechanics*, 2019, no.5, pp. 68-73. **doi: 10.20998/2074-272X.2019.5.11.**

Матеріали приймаються за адресою:
Кафедра "Електричні апарати", НТУ "ХПИ", вул. Кирпичова, 21, м. Харків, 61002, Україна
Електронні варіанти матеріалів по e-mail: a.m.grechko@gmail.com

Довідки за телефонами: +38 050 653 49 82 Клименко Борис Володимирович
+38 067 359 46 96 Гречко Олександр Михайлович

Передплатний індекс: 01216